Ph.D. Thesis
Ingeniería Industrial

Contributions to Control of Electronic Power Converters

Author: Antonio Ventosa Cutillas
Advisors: Francisco Gordillo Álvarez
Francisco Salas Gómez

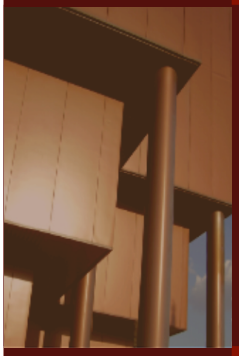

Departamento de Ingeniería de Sistemas y Automática
Escuela Técnica Superior de Ingeniería
Universidad de Sevilla

Sevilla, 2019

UNIVERSIDAD DE SEVILLA

Ph.D. Thesis
Ingeniería Industrial

Contributions to Control of Electronic Power Converters

Author:

Antonio Ventosa Cutillas

Advisors:

Francisco Gordillo Álvarez

Catedrático de Universidad

Francisco Salas Gómez

Profesor Titular de Universidad

Departamento de Ingeniería de Sistemas y Automática
Escuela Técnica Superior de Ingeniería
Universidad de Sevilla

2019

Tesis Doctoral: Contributions to Control of Electronic Power Converters

Autor: Antonio Ventosa Cutillas
Directores: Francisco Gordillo Álvarez
Francisco Salas Gómez

El tribunal nombrado para juzgar la Tesis arriba indicada, compuesto por los siguientes doctores:

Presidente:

Vocales:

Secretario:

acuerdan otorgarle la calificación de:

El Secretario del Tribunal

Fecha:

A María José
A Nicolás
A mi familia

Acknowledgements

El trabajo que aquí se presenta es el resultado de varios años de esfuerzo y dedicación en los que he contado con el apoyo y la ayuda de numerosas personas. Aunque aquí sólo pueda mostrar mi gratitud a una parte de ellas, quiero dar las gracias a todos los que habéis estado involucrados.

Las primeras personas a las que quiero dar las gracias son mis directores de tesis, Francisco Gordillo y Francisco Salas, por haberme dado la oportunidad de formar parte de su grupo de investigación y haberme guiado y ayudado durante el transcurso de mi beca y la escritura de esta tesis.

También quisiera agradecer al resto de profesores del grupo, Federico Cuesta y Fabio Gómez-Stern, por su ayuda, colaboración en varios artículos y sus valiosos comentarios en nuestras, en algunos casos interminables, reuniones. Cada una de ellas ha sido una clase magistral sobre ingeniería.

Agradecer también a los Profesores Carolina Albea y Alexandre Seuret por mi estancia en el Laboratoire d'analyse et d'architecture des systèmes (LASS) en Toulouse. Sin duda una de las experiencias más interesantes durante la realización de esta tesis.

Se merecen un agradecimiento especial mis compañeros becarios del Departamento de Automática y de Sistemas de la Universidad de Sevilla, Pablo, Manu, Marta, Ramón, José Enrique, David y Guille, por su ayuda, consejos, apoyos y por todos los "descansitos" en las máquinas de los laboratorios.

También quiero agradecer a los miembros del Departamento de Electrónica su ayuda, principalmente en la puesta en marcha y experimentos con los equipos de pruebas, y en

especial a Enrique Moreno.

Desde un punto de vista más personal, quiero agradecer a María José su enorme apoyo y su cariño, por estar a mi lado, por hacerme feliz y por compartir conmigo los buenos y malos momentos por los que hemos pasado en el desarrollo de este trabajo. Sin duda, ella ha hecho mucho más llevadero todo este esfuerzo.

A mi hijo, Nicolás, porque con sólo cinco meses, su sonrisa y su alegría me han dado ánimos para seguir trabajando cuando más lo he necesitado.

A mi familia, por estar siempre disponibles, por escucharme, por preocuparse por mí, por ser el apoyo incondicional que en ocasiones he buscado.

Por último, quisiera mencionar que este trabajo ha sido posible gracias a la ayuda del Ministerio de Economía y Competitividad y a los proyectos DPI2013-41891-R y DPI2016-75294-C2-1-R.

Daría todo lo que sé por la mitad de lo que ignoro

DESCARTES

Antonio Ventosa Cutillas

Sevilla, 2019

Resumen

La presente tesis trata sobre el control de convertidores electrónicos de potencia. En su desarrollo se han diferenciado dos partes principales. Por un lado, se trata el problema del balance de tensiones en los condensadores que forman el dc-link en un convertidor NPC de tres niveles. Por otro lado, dado que las técnicas utilizadas en la primera parte para modelar los convertidores necesitan realizar determinadas suposiciones y, con la intención de evitar modelos promediados, en la segunda parte se han desarrollado modelos afines conmutados para diseñar el control de la tensión de salida en convertidores DC-DC tipo boost.

De esta forma, en la primera parte se han desarrollado varias leyes de control utilizando un modelo promediado formulado mediante ciclos de trabajo para cada nivel en cada fase. Esta formulación permite considerar en la fase de diseño de los controladores, un grado de libertad asociado a la inyección de tensión homopolar. Por lo tanto, se diseñan los controladores a la vez que una parte de la modulación, de forma que se integra control y modulación en una misma fase. De esta forma, se han diseñado tres controladores donde, a parte del objetivo de balancear la tensión de los condensadores, se ha ido buscando mejorar también otros objetivos como el número de conmutaciones o la calidad de la señal de salida.

En la segunda parte de la tesis, se han desarrollado cuatro leyes de control aprovechando el modelado de convertidores como sistemas afines conmutados dada su naturaleza híbrida. De esta forma, las dos primeras leyes, aprovechan dicho modelado usando el operador delta para evitar problemas numéricos al utilizar sistemas donde el tiempo de muestreo es muy bajo. El primero de dichos controladores está basado en la función de Lyapunov

mientras que el segundo es independiente de dicha función obteniendo así resultados menos conservadores.

Las otras dos leyes desarrolladas para sistemas afines conmutados utilizan un modelado alternativo al realizado en las dos primeras, de forma que se evitan ciertas desventajas existentes y mantienen un diseño no basado en la función de Lyapunov. Así, la primera ley presenta un control más básico pero que, aun así, mejora los resultados de otras leyes existentes en la literatura. Por último, se ha presentado un procedimiento de diseño que hace frente a sistemas con variaciones en sus parámetros.

Abstract

This thesis deals with the control of electronic power converters. In its development two main parts have been differentiated. On the one hand, the problem of the voltage balance in the capacitors of the dc-link in a three-level NPC converter is addressed. On the other hand, given that the techniques used in the first part to model the converters need to make certain assumptions and, with the intention of avoiding averaged models, in the second part, switched affine models have been developed to design the control of the output voltage in DC-DC boost type converters.

In this way, in the first part several control laws have been developed using an averaged model formulated by duty cycles for each level in each phase. This formulation allows to consider, in the controllers design stage, the degree of freedom associated with the homopolar voltage injection. Therefore, the controllers are designed as well as a part of the modulation, so that control and modulation are integrated in the same stage. In this way, three controllers have been designed where, apart from the objective of the voltage balance of the capacitors, other objectives such as the number of commutations or the quality of the output signal have also been improved.

In the second part of the thesis, four methods have been developed for the design of control laws taking advantage of the modeling of converters as switched affine systems given their hybrid behaviour. Thus, the first two laws take advantage of this modeling using the delta operator to avoid numerical problems when using systems where the sampling time is very low. The first of these controllers is based on Lyapunov's function while the second is independent of this function, thus obtaining less conservative results.

The other two laws developed for switched affine systems use an alternative model to that performed in the first two controllers, so certain existing disadvantages are avoided using again a design not based on Lyapunov's function. Thus, the first law presents a basic control but, even so, improves the results of other existing laws in the literature. Finally, a design method to deal with systems with variations in their parameters has been presented.

Contents

Acronyms

AC	Alternative Current
AF	Active Filter
CB-PWM	Carrier Based Pulse Width Modulation
CHB	Cascade H-Brigde
DC	Direct Current
DCC	Diode Clamped Converter
DPC	Direct Power Control
DTC	Direct Torque Control
DVR	Dynamic Voltage Restorer
FACTS	Flexible AC Transmission Systems
FC	Flying Capacitor
FS-MPC	Finite States Model Predictive Control
ICM	Integrated Control and Modulation
IGBT	Insulated Gate Bipolar Transistor
LMI	Linear Matrix Inequality
MPC	Model Predictive Control
NPC	Neutral Point-Clamped
NTV	Nearest Three Vectors
PI	Proportional Integral
PR	Proportional Resonant
PWM	Pulse-Width Modulation
STATCOM	Static Compensator

SHE-PWM	Selective Harmonic Elimination Pulse Width Modulation
SV-PWM	Space Vector Pulse Width Modulation
THD	Total Harmonic Distortion
UPFC	Unified Power Quality Conditioner
UPS	Uninterruptible Power Supply
VSVM	Virtual Space Vector Modulation

Notation

$\|a\|$	Absolute value of a
$\dot{a}$	Time derivative of a
$\widehat{a}$	Estimated value of a
A^{-1}	Inverse matrix of A
C	Capacitor [F]
$C(s)$	Continuous controller transfer function
$\boldsymbol{D}$	Linear reduced model input vector
d_i	Element {i} in vector $\boldsymbol{D}$
$det(A)$	Determinant of A
e	Error
$G(s)$	Continuous transfer function
I	Electric current [A]
K	Static gain
L	Inductance [H]
P	Active power [W]
Q	Reactive power [Var]
R	Electrical resistance [Ω]
T_D	Derivative time [s]
T_I	Integral time [s]
t	Time
t_r	Rise time [s]
V	Voltage [V]

$\boldsymbol{x}$	State vector
$\boldsymbol{y}$	Output vector
abc	abc coodinates
$\alpha\beta\gamma$	$\alpha\beta\gamma$ coodinates
τ	Time constant [s]
ω	Frequency [rad s^{-1}]

Subscripts and superscripts

max	maximum
min	minimum
ref	reference
u	input

1 Introduction

Sometimes it is the people no one can imagine anything of, who do the things no one can imagine.

ALAN TURING

Contents

The thesis presented here aims to control electronic power converters. Specifically, the objective is to improve the control on the one hand of multilevel converters and on the other hand of DC-DC converters. In the case of multilevel converters, apart from the usual control objectives in this type of power converters [1], namely reduced total harmonic distortion (THD), achieve total DC-link voltage reference, reduced number of commutations or achieve active and reactive powers reference, this thesis focuses, as a first goal, on the voltage balance between capacitors. In the case of DC-DC converters,

the objective focuses on minimizing the output voltage error or chattering [2], that is the second goal of this thesis. With this intention, an alternative modeling to that performed in the first part of the thesis has been applied, modeling this type of power converters as switched affine systems.

1.1 Multilevel Converters

The power converters most used nowadays are multilevel to the detriment of the classic two-level converters (2L). This is due to the fact that, for the same application, classic power converters topologies need high-voltage semiconductors and multilevel converter topologies can use medium-voltage devices. Multilevel topology offers some additional benefits, among which are an improved harmonic distortion for a given switching frequency, a lower overvoltage stress at cables and end windings of transformers/motors, a lower common-mode voltage and substantially lower semiconductor switching losses [3]. Multilevel voltage source converters also step in as an interesting alternative since they can achieve higher dynamic performance but without the voltage limit of the classic 2L [4]. Another advantage over two-level converters is that the peaks that occur in the switches when they open are much smaller, because these devices support less load due to be able to distribute it among more switches.

Generally, a larger number of voltage levels, applied to a given grid-filter, achieves a lower harmonic range of the current, obtaining a high power quality in the converter's AC-side. On the other hand, the increase in the number of levels increases the complexity of the control [5].

Multilevel converter technology started with the introduction of the multilevel stepped waveform concept with a series-connected H-bridge, which is also known as cascaded H-Bridge converter, in the late 1960s [6]. This same year, a Flying Capacitor topology was developed [7]. In the late 1970s, the diode-clamped converter (DCC) [8] was first introduced. The DCC concept evolved into the three-level NPC (3L-NPC) converter we know today as it was proposed in [9]. This converter was based on a modification of the classic two-level converter topology adding two new power semiconductors per phase. These three multilevel converter topologies, neutral-point-clamped (NPC), cascaded H-bridge (CHB) and flying-capacitor (FC), could be considered now as traditional multilevel topologies.

NPC converter is one of the most used multilevel converter topologies. Operating in

rectifier mode, the dc-link voltage is obtained as the addition of the voltage that drops across the capacitors. This voltage must be balanced between the capacitors, otherwise this can result in poor output voltage quality, affecting the performance of the control or even damaging the semiconductor devices.

Nowadays, multilevel converters are used in several industrial applications [10, 11]:

- Power distribution control and management: Flexible AC Transmission Systems (FACTS) as active filters (AFs), static compensators (STATCOM), dynamic voltage restorers (DVRs), unified power flow controllers (UPFCs), and unified power quality conditioners [12, 13].

- Distributed generation: The integration of several grids to interconnect and distribute power generated at a more local level by diverse renewable energy sources and even interconnect storage or grid compensation systems demands a smarter grid with new converter topologies that operate at higher voltages and power, with increased efficiency and power quality to ensure proper power management [14].

- Traction applications: Train Traction, Ship Propulsion, and Automotive Applications [15].

- Energy Generation, Conversion, and Transmission: In wind turbines the use of a reduced-capacity converter stage can reduce structural stress, reduce audible noise and increase power generation and efficiency in larger turbines [16]. Another use of multilevel converters is as power interface for large photovoltaic grid-connected systems or hydropumped energy storage system [17].

- Uninterruptible power supply (UPS) systems to provide a separate emergency supply of electric power to the connected equipment, when the utility mains are not available [18].

However, despite their good features, only the three-level converter is widely used in the industry. The converters with more than three levels have not been extended significantly at commercial level. This is probably due to problems such as reliability, efficiency or control complexity.

1.2 DC-DC Converters

DC-DC converters are some of the simplest power electronic circuits due to its advantageous features in terms of size, weight and reliable performance. Their applications are widely extended in the power supply equipment for most electronic instruments or in specialised high-power applications such as battery charging, hybrid vehicles, fuel cell vehicles or renewable energy as in photovoltaic systems [19, 20].

The DC-DC converter input is generally unregulated dc voltage and the required output should be a constant or fixed voltage so the scope is to achieve output voltage regulation in the presence of input voltage and output load variations.

There are various types of DC-DC converters required for particular purpose like the Buck converter, that is used to generate a lower voltage than the input, the Boost converter, that is used to generate a higher voltage than the input voltage and the Buck-Boost converter, where the output voltage can be increased or decreased than the input voltage. Other existing topologies are modifications of this three converters like the flyback topology. This converter works similar to the buck-boost converter in the isolating category. The difference is that the flyback uses a transformer to store the energy instead of an inductor [21].

If the switching frequency is much higher than the frequency of the grid, power converters can be modeled as continuous systems. In this way, the discrete signals used in the converter can be approximated by continuous signals in a sampling period. This offers an advantage when classic control theories are used. But they also have the disadvantage that some assumptions have to be made, such as assuming that certain signals are balanced [22]. As a solution to this, it is possible to use hybrid control theory, which is applied in the second part of this thesis. These theories allow modeling and designing controllers without making the previous assumptions. The use of these theories will be used to design control laws applied to DC-DC converters modeled as switched affine systems.

1.3 Objectives of the thesis

This thesis is mainly focused on two problems that appear in the control of power converters: on the one hand, in multilevel converters one of the control objectives is the capacitor voltage balance, proposing several methods to approach this problem, and on the other hand, in order to analyze and model rigorously power converters from the point of view of their hybrid behaviour, DC-DC converters are modeled as switched affine systems and several controllers are designed to reduce the problem of chattering in the output of these converters.

Regarding the first subject, this thesis presents a new approach to deal with the control of three-level NPC converters. The circuit model is formulated in terms of the duty ratios of each phase at each level. This formulation allows to explicitly consider, in the control design stage, the extra degree of freedom associated with the injection of homopolar component. The increase in the number of variables does not make the design significantly more difficult since, with an appropriate change of variables, the dc-link voltage and active and reactive power control problems can be formulated in a similar way to other usual approaches. As a result, the voltage balance controller can be easily designed at the same time that an important part of modulation is not needed. The main advantage of the proposed law is its simplicity in implementation compared with other reputable methods.

The drawback of the adopted formulation is that it may lead to an unnecessary increase in the number of commutations, which is the case of the first control law proposed. To overcome the large number of commutations, two new controllers are designed by exploiting some additional degrees of freedom in such a way that the resultant number of commutations is considerably reduced.

The second part focusses on the design of switching control laws for discrete-time switched affine systems. Two approaches are studied, the first one presents a novel formulation for systems where the sampling time is very low. In the second, an alternative model formulation is made to overcome some disadvantages of the previous model. For both types of systems a basic and a robust control law are developed where their parameters result from an optimization problem, aiming at reducing the volume of the attractive and invariant set, where the solutions of the closed-loop systems converge to. Furthermore, in the second case, in order to cope with model uncertainties, a novel control law is introduced where the design is based on a quadratic Lyapunov function and guarantees global practical stability and robustness with respect to parameter variations.

1.4 Thesis overview

This thesis is structured as follows:

- ***Chapter 2***:

  This chapter is dedicated to describe the fundamentals of operation and the mathematical model of the three-level converter. Also in this chapter there is an introduction of the control problems of the converter, focussed in the voltage balance problem.

- ***Chapter 3***:

  In this chapter, the solutions proposed for the voltage balance problem are addressed. A reminder is made to the original control law with the problem of excessive commutations and the improved control laws are introduced in which commutations are reduced significantly. The results of simulations and experiments in real systems are shown at the end of this chapter.

- ***Chapter 4***:

  The fourth chapter is oriented to present an introduction to the switched affine systems, showing the typical model of a DC-DC converter. This chapter will also show the necessary stability conditions in this kind of systems.

- ***Chapter 5***:

  This chapter details the design of several switching control laws for a discrete-time switched affine system. The results of simulations are shown at the end of this chapter.

- ***Chapter 6***:

  The last chapter summarizes the mains conclusions and contributions and proposes some future research lines.

- ***Appendix A***:

  The design and construction of a prototype converter to perform the experimental tests of chapter 3 is shown in the appendix. In this chapter the design of this converter is analyzed and the different components necessary for its construction are detailed.

1.5 List of publications

The following papers have been published during the elaboration of this Thesis:

Patent:

- Antonio Ventosa-Cutillas, Federico Cuesta, Fabio Gómez-Stern, Francisco Gordillo and Francisco Salas.
  Método de balance de tensiones para un convertidor NPC. Spain, Patent, ES 2708130 B2, PCT/ES2018/070638, 2018

Journal papers:

- [23] Antonio Ventosa-Cutillas, Pablo Montero-Robina, Francisco Umbría, Federico Cuesta and Francisco Gordillo.
  Integrated Control and Modulation for Three-Level NPC Rectifiers. *Energies*, 2019; 12(9):1641.

- [24] Antonio Ventosa-Cutillas, Pablo Montero-Robina, Francisco Umbría, Federico Cuesta and Francisco Gordillo.
  A Simplified and Integrated Control and Modulation for Three-Level NPC Rectifiers. Manuscript submitted to *Energy*, 2019. Status: Under revision

- [25] Carolina Albea Sánchez, Antonio Ventosa-Cutillas, Alexandre Seuret, Francisco Gordillo.
  Robust switching control design for uncertain discrete-time switched affine systems. Manuscript submitted to *International Journal of Robust and Nonlinear Control*, 2019. Status: Under revision

Conference papers:

- [26] Antonio Ventosa-Cutillas, Marta Gómez-Correa, Francisco Gordillo and Federico Cuesta.
  Diseño, construcción y control de un convertidor de potencia de cinco niveles. *Proceedings of the XXXVII Jornadas de Automática*, Madrid, 2016.

- [27] Antonio Ventosa-Cutillas, Carolina Albea Sanchez, Alexandre Seuret, Francisco Gordillo.
  Relaxed periodic switching controllers of high-frequency DC-DC converters using the δ-operator formulation. *Proceedings of the 57th IEEE Conference on Decision and Control (CDC'18)*, USA, 2018.

- [28] Antonio Ventosa-Cutillas, Francisco Gordillo and Francisco Salas.
  Contributions to Control of Electronic Power Converters. *Proceedings of the XVII Simposio CEA de Ingeniería de Control y V Seminario de Innovación Docente en Automática*, Sevilla, 2019.

2 Preliminaries

What we know is a drop, what we don't know is an ocean.

Sir Isaac Newton

Contents

This chapter is devoted to present the three-level NPC converter as well as its dynamic model and to introduce the voltage balance problem. In the first section of this chapter, a review of the modulation techniques will be done, since they are directly related to the approaches that will be presented later.

Some of the different types of topologies of multilevel converters are neutral-point-clamped (NPC), cascaded H-bridge (CHB) or flying-capacitor (FC) [29, 4, 30]. The NPC converter, which was proposed for the first time in [9], is one of the most used multilevel converter topologies. This is due to advantages like the lower current THD that reduces

the filtering effort or the possibility to use IGBTs and diodes with breakdown voltages that are lower than the actual dc-link voltage, producing lower losses and increasing the efficiency [31]. The usual variables to control in NPC converters are active and reactive powers, currents, total dc-link voltage or number of commutations among others [1], but NPC converters present an additional objective apart from these usual control objectives that is the voltage balance between capacitors. Operating in rectifier mode, the voltage that drops across each capacitor must be balanced, otherwise it can result in poor output voltage quality, affecting the performance of the control or even damaging the semiconductor devices.

Regarding the modelling, the model used in the first part of this thesis is an averaged model. The objective of this model in computing the averaged equations is to obtain a simpler model which retains the important properties of the original. The resulting equivalent circuit is much easier to solve, and allows insight to be gained into the important functional properties of the converter. Additionally, since averaged models are time-invariant, they can be linearized about any desired operating point for small-signal analysis, i.e., obtaining local transfer functions. It is usual to work with averaged models when the switching frequency is much faster than the frequency range of the system. In that situation, the discrete values of the gating elements can be replaced by their averaged values in a switching period and can be considered as continuous signals [29, 32]. This assumption yields that other signals, such as voltage, can also be considered as averaged signals, resulting that the system can be modeled as a continuous system.

2.1 Modulation Techniques

In order to implement the control laws obtained with the models commented before, a discretization stage, usually called modulation, needs to be accomplished [33]. Modulation plays an important role in the overall system performance since properties such as number of commutations and harmonic distortion of currents and voltages are affected by the way modulation is carried out. It should be remembered that increasing the number of commutations also increases losses. Modulation methods can be classified in three main groups [34]:

- Pseudo-modulation [35]: In this method, a simple comparison of the reference voltage is used. One way to do this is to choose the voltage level closest to the desired voltage. The same principle can be used in the nearest vector control technique, applying the nearest space vector to the reference vector. The simplest

form of pseudomodulation is the square-wave modulation, comparing the reference voltage with zero.

- Closed-loop control methods with implicit modulator [36, 37, 38]: In this method, control techniques are used that directly generate the switching signals of the converter switches. Among the techniques used in this method are the Hysteresis Current Control, the Direct Torque Control (DTC), the Direct Power Control (DPC) and the Finite-States Model-Predictive Control (FS-MPC).

- Pulse width modulation (PWM) [39, 40]: As mentioned before, the three approaches presented in this thesis are closely related to PWM modulation techniques. Hence, this section will be devoted to explain this type of modulation.

  There are two main methods of modulation by PWM that use high switching frequency [29]: the carrier-based modulation (CB-PWM) and the space vector modulation (SV-PWM).

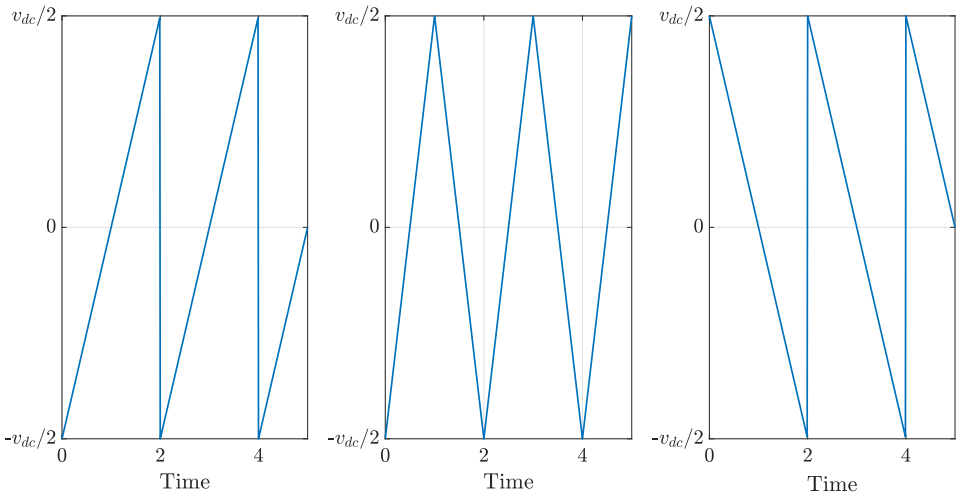

Figure 2.1 Carrier signals: Trailing edge (left), triangular (center) and leading edge (right).

In carrier-based modulation, the activation signals of the switches are obtained by comparing the amplitudes of a high-frequency signal called carrier and a low-frequency signal called modulator. The most common forms of the carrier signal are the triangular, the leading edge (when the mounting slope is infinite) and the trailing edge (when descendant slope is infinite) [41]. A graph with carrier signals

can be observed in Fig. 2.1. On the other hand, the modulator or reference signal can have different forms such as sinusoidal or discontinuous or forms characteristic of the method used to obtain it, such as Carrier based Space Vector Pulse Width Modulation (CB-SVPWM) or injection of the third harmonic among others [42].

In Fig.2.2 it is possible to observe the operation of the modulation by PWM. If the value of the reference signal (triangle signal) is more than the value of the modulation waveform (sinusoidal signal), the resultant PWM signal is a high signal, Otherwise, the resultant waveform is in the low state.

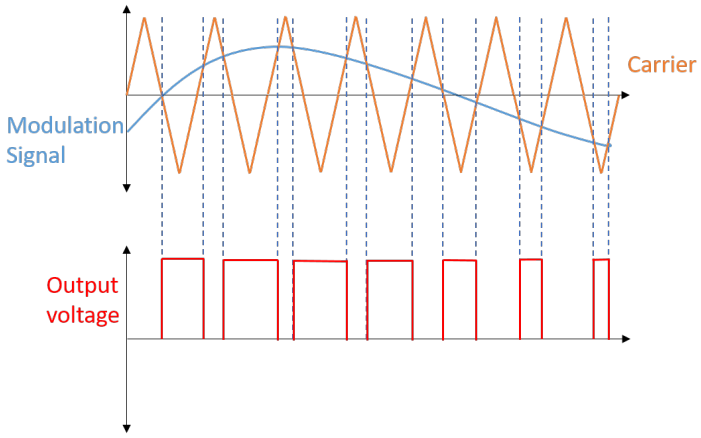

Figure 2.2 Output voltage generated by PWM.

An important characteristic in modulation techniques, which affects the PWM modulation, is the level of DC bus utilization. This can be measured by the modulation index, which is defined as the amplitude of the modulating signal, normalized with respect to the maximum amplitude of the carrier:

$$M = \frac{A}{v_{dc}/2} \tag{2.1}$$

where A is the maximum amplitude of the carrier signal and (v_{dc}) is the total dc-link voltage.

If this index is less than or equal to one, the peak of the modulating signal is less than or equal to the peak of the carrier signal and the converter will be in the linear mode

of operation. On the other hand, if the opposite occurs and the index is greater than one, the converter will be in a non-linear mode of operation called overmodulation. In this mode, the intersections between carrier and modulator disappear and the pulses generated in the comparison remain at a single level. The output voltage does not reach to equal the reference value, generating non-linear relationships between the amplitudes and the phase angles of the reference signal and the output signal of the inverter.

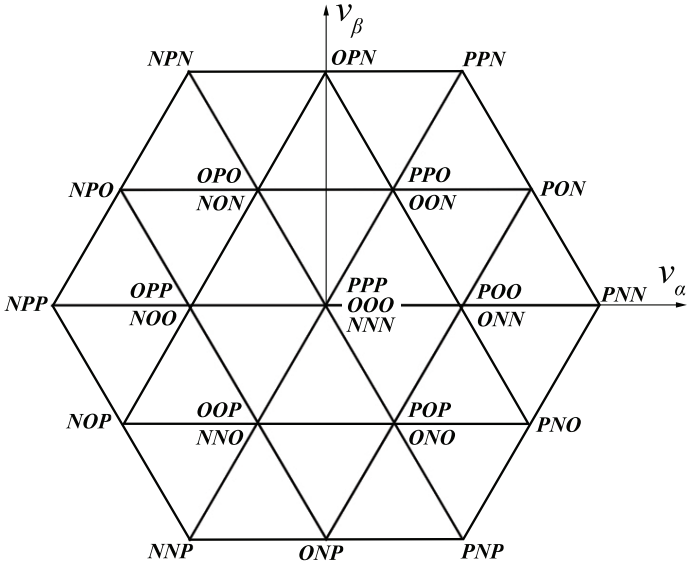

Figure 2.3 Space Vector hexagon.

In the Space Vector Modulation (SV-PWM), the Clarke transformation is applied on the three-phase set of modulating signals to create a space vector reference in $\alpha\beta$ coordinates. In balanced systems, this vector has constant amplitude and rotates in the $\alpha\beta$ plane following a circular path. In this $\alpha\beta$ plane, the different switching states of the converter can be represented by vectors that give rise to a so-called space vector hexagon represented in Fig. 2.3. The reference vector is obtained by lineal combination of this vectors. The way to obtain this combination can be reduced to two techniques [43]. Although there are numerous techniques that use space vector, most of them use variations of these two. The first one is called Nearest Three Vectors (NTV). In this technique, the hexagon is divided into six sectors formed by four triangles each in a three-level converter. Once the sector and the triangle where the reference vector is located are identified, the three closest vectors are

chosen and the switching states are computed. In the second technique, the hexagon is decomposed into six smaller hexagons. In this way, each hexagon is considered as the hexagon of a two-level converter. The new reference vector is calculated based on the original vector and the sector where it is located within this new hexagon is calculated. The switching states are computed based on the two closest vectors in each sector. In Fig. 2.4 it is possible to observe the space vector hexagon divided in the six small hexagons.

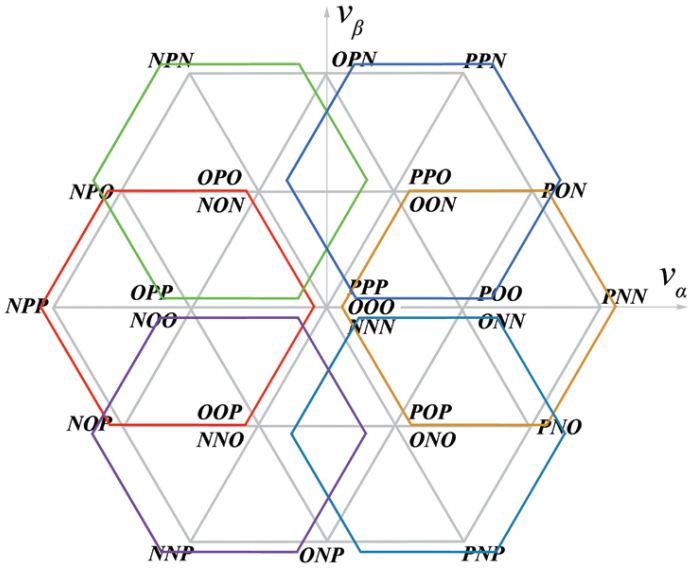

Figure 2.4 Simplification of the three-level Space Vector hexagon diagram.

2.2 Dynamic Model of the System

The three-level converter circuit is shown in Fig. 2.5. In this figure, the converter is in rectifier mode, where the electrical power grid is considered as a three-phase voltage source, and where the phase voltages are represented by v_{sa}, v_{sb} and v_{sc}. The converter is connected to the grid through an inductive filter where inductances have the same value L.

On the dc-link side, capacitors have the same value C and their voltages are denoted by v_{c1} and v_{c2}. Connected to the converter terminals there is a resistive load R. The total dc-link voltage is defined as $v_{dc} = v_{c1} + v_{c2}$.

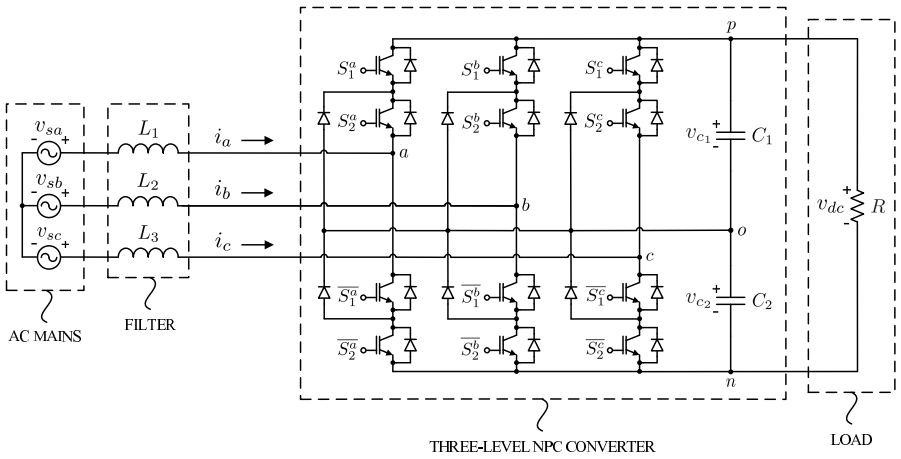

Figure 2.5 Squematic diagram of the three-phase three-level NPC rectifier.

The switches S_j^i, are Insulated Gate Bipolar Transistors (IGBTs), where i indicates each of the three phases and j indicates the switch number. $\overline{S_j^i}$ represents the inverted signal of S_j^i. Due to this configuration, there are only some allowed combinations of the states of each switch, the rest are destructive or potentially destructive. Table 2.1 and Fig. 2.6 shows the permitted combinations of the switches for phase a and represents the current flow associated with each state, respectively. The phases b and c have the same possible combinations. The signals that control the positions of the switches are represented by the control signals δ_a^*, δ_b^* and δ_c^*, as can be seen in that table. As mentioned before, the circuit has been modeled as an averaged model, so that these control signals can be expressed as averaged duty cycles (d_a, d_b and d_c) for each level in each phase. In this way, the value of the signals varies from zero to one as a percentage of the time the switches have to be

open or closed. Thus, if the duty of phase a at positive level (d_{ap}) has a value of 0.4, the switches of leg a will be in the position represented by figure 2.6a during 40 percent of the sampling time. Taking this into account, the circuit model is formulated in terms of nine duty cycle variables (three duty cycles per phase) instead of just three (one duty cycle per phase) as in the traditional model, where the duty cycles only takes three possible values (-1, 0, 1) to assign the positions of the switches. It is shown that the formulation used in this thesis allows to explicitly consider, in the control design stage, the extra degree of freedom associated with the injection of homopolar component. The increase in the number of variables does not make the design significantly more difficult since, with an appropriate change of variables, the dc-link voltage and active and reactive power control problems can be formulated with the same facility of other usual approaches.

Table 2.1 Switching states of the three-level NPC converter.

S_a^1	S_a^2	$\overline{S_a^1}$	$\overline{S_a^2}$	v_a	δ_a^*	Figure
Closed	Closed	Open	Open	v_{c1}	1	2.6a
Open	Closed	Closed	Open	0	0	2.6b
Open	Open	Closed	Closed	$-v_{c2}$	-1	2.6c

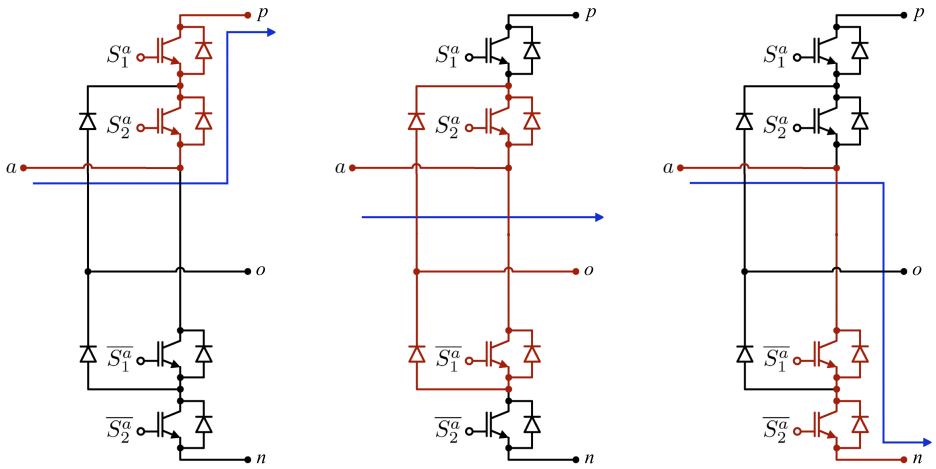

(a) Positive level. (b) Zero level. (c) Negative level.

Figure 2.6 Switching states for phase a.

The model considered in this thesis is described in [44], which is based on a model presented in [45], assuming a symmetric and balanced system without losses. Using abc coordinates:

$$\begin{aligned} L\frac{di_a}{dt} &= v_{sa} + \left[-\frac{1}{3}(d_{ap}+d_{an}) + \frac{1}{6}(d_{bp}+d_{bn}) + \frac{1}{6}(d_{cp}+d_{cn})\right] v_{dc} \\ &\quad + \left[-\frac{1}{3}(d_{ap}-d_{an}) + \frac{1}{6}(d_{bp}-d_{bn}) + \frac{1}{6}(d_{cp}-d_{cn})\right] v_d \end{aligned} \tag{2.2}$$

$$\begin{aligned} L\frac{di_b}{dt} &= v_{sb} + \left[\frac{1}{6}(d_{ap}+d_{an}) - \frac{1}{3}(d_{bp}+d_{bn}) + \frac{1}{6}(d_{cp}+d_{cn})\right] v_{dc} \\ &\quad + \left[\frac{1}{6}(d_{ap}-d_{an}) - \frac{1}{3}(d_{bp}-d_{bn}) + \frac{1}{6}(d_{cp}-d_{cn})\right] v_d \end{aligned} \tag{2.3}$$

$$\begin{aligned} L\frac{di_c}{dt} &= v_{sc} + \left[\frac{1}{6}(d_{ap}+d_{an}) + \frac{1}{6}(d_{bp}+d_{bn}) - \frac{1}{3}(d_{cp}+d_{cn})\right] v_{dc} \\ &\quad + \left[\frac{1}{6}(d_{ap}-d_{an}) + \frac{1}{6}(d_{bp}-d_{bn}) - \frac{1}{3}(d_{cp}-d_{cn})\right] v_d \end{aligned} \tag{2.4}$$

$$C\frac{dv_{dc}}{dt} = (d_{ap}-d_{an})i_a + (d_{bp}-d_{bn})i_b + (d_{cp}-d_{cn})i_c - 2\frac{v_{dc}}{R} \tag{2.5}$$

$$C\frac{dv_d}{dt} = (d_{ap}+d_{an})i_a + (d_{bp}+d_{bn})i_b + (d_{cp}+d_{cn})i_c, \tag{2.6}$$

where v_d is the dc-link capacitor voltage difference defined by $v_d = v_{c1} - v_{c2}$ and the control inputs d_{ap}, d_{an}, d_{bp}, d_{bn}, d_{cp} and d_{cn} are the duty ratios in abc coordinates.

It should be remarked that the duty ratios in abc coordinates are subject to the following constraints

$$d_{ap} + d_{ao} + d_{an} = 1 \tag{2.7}$$

$$d_{bp} + d_{bo} + d_{bn} = 1 \tag{2.8}$$

$$d_{cp} + d_{co} + d_{cn} = 1 \tag{2.9}$$

$$d_{ij} \in [0,1], \text{ for } i = a,b,c \text{ and } j = p,o,n. \tag{2.10}$$

Introducing the power-invariant form of the Clarke Transform in (2.2)–(2.6), the next equations are obtained in $\alpha\beta\gamma$ coordinates.

$$L\frac{di_\alpha}{dt} = v_{s\alpha} - (d_{\alpha p} - d_{\alpha n})\frac{v_{dc}}{2} - (d_{\alpha p} + d_{\alpha n})\frac{v_d}{2} \tag{2.11}$$

$$L\frac{di_\beta}{dt} = v_{s\beta} - (d_{\beta p} - d_{\beta n})\frac{v_{dc}}{2} - (d_{\beta p} + d_{\beta n})\frac{v_d}{2} \tag{2.12}$$

$$C\frac{dv_{dc}}{dt} = (d_{\alpha p} - d_{\alpha n})i_\alpha + (d_{\beta p} - d_{\beta n})i_\beta - 2\frac{v_{dc}}{R} \tag{2.13}$$

$$C\frac{dv_d}{dt} = (d_{\alpha p} + d_{\alpha n})i_\alpha + (d_{\beta p} + d_{\beta n})i_\beta, \tag{2.14}$$

where the control inputs $d_{\alpha p}$, $d_{\alpha n}$, $d_{\beta p}$ and $d_{\beta n}$ are the duty ratios in $\alpha\beta\gamma$ coordinates. Remaining control inputs $d_{\gamma p}$ and $d_{\gamma n}$ do not appear in the model, as mentioned in [44], because they are multiplied by i_γ, whose value is assumed to be zero, thus the equation of the derivative of i_γ with respect to time does not appear either.

Phase currents i_α and i_β can be expressed in terms of powers as

$$i_\alpha = \frac{1}{v_{s\alpha}^2 + v_{s\beta}^2}\left(v_{s\alpha}p - v_{s\beta}q\right) \tag{2.15}$$

$$i_\beta = \frac{1}{v_{s\alpha}^2 + v_{s\beta}^2}\left(v_{s\beta}p + v_{s\alpha}q\right), \tag{2.16}$$

where p and q are the instantaneous active and reactive powers of the system, respectively. Introducing (2.15)–(2.16) into (2.11)–(2.14) and denoting f as the frequency of the grid and $Z_L = 2\pi f L$ as the inductive reactance, the following equations are obtained, which represent the system model in terms of instantaneous powers.

$$L\frac{dp}{dt} = v_{s\alpha}^2 + v_{s\beta}^2 + Z_L\, q - \left(\left(d_{\alpha p} - d_{\alpha n}\right) v_{s\alpha} + \left(d_{\beta p} - d_{\beta n}\right) v_{s\beta}\right) \frac{v_{dc}}{2} - \left(\left(d_{\alpha p} + d_{\alpha n}\right) v_{s\alpha} + \left(d_{\beta p} + d_{\beta n}\right) v_{s\beta}\right) \frac{v_d}{2} \tag{2.17}$$

$$L\frac{dq}{dt} = -Z_L\, p + \left(\left(d_{\alpha p} - d_{\alpha n}\right) v_{s\beta} - \left(d_{\beta p} - d_{\beta n}\right) v_{s\alpha}\right) \frac{v_{dc}}{2} + \left(\left(d_{\alpha p} + d_{\alpha n}\right) v_{s\beta} - \left(d_{\beta p} + d_{\beta n}\right) v_{s\alpha}\right) \frac{v_d}{2} \tag{2.18}$$

$$C\frac{dv_{dc}}{dt} = \frac{1}{v_{s\alpha}^2 + v_{s\beta}^2} \left(d_{\alpha p} - d_{\alpha n}\right) \left(v_{s\alpha} p - v_{s\beta} q\right) + \frac{1}{v_{s\alpha}^2 + v_{s\beta}^2} \left(d_{\beta p} - d_{\beta n}\right) \left(v_{s\beta} p + v_{s\alpha} q\right) - 2\,\frac{v_{dc}}{R} \tag{2.19}$$

$$C\frac{dv_d}{dt} = \frac{1}{v_{s\alpha}^2 + v_{s\beta}^2} \left(d_{\alpha p} + d_{\alpha n}\right) \left(v_{s\alpha} p - v_{s\beta} q\right) + \frac{1}{v_{s\alpha}^2 + v_{s\beta}^2} \left(d_{\beta p} + d_{\beta n}\right) \left(v_{s\beta} p + v_{s\alpha} q\right). \tag{2.20}$$

2.2.1 Alternative Model of the System

An alternative way of obtaining the converter model, is using $dq0$ coordinates instead of $\alpha\beta\gamma$. To do so, the Park's transformation, represented by the following relationship, is used.

$$\begin{bmatrix} x_d \\ x_q \\ x_0 \end{bmatrix} = \frac{2}{3} \begin{bmatrix} \cos(wt) & \cos\left(wt - \frac{2\pi}{3}\right) & \cos\left(wt + \frac{2\pi}{3}\right) \\ -\sin(wt) & -\sin\left(wt - \frac{2\pi}{3}\right) & -\sin\left(wt + \frac{2\pi}{3}\right) \\ \frac{1}{2} & \frac{1}{2} & \frac{1}{2} \end{bmatrix} \begin{bmatrix} x_a \\ x_b \\ x_c \end{bmatrix}, \tag{2.21}$$

where the subscripts d, q, and 0 represent the direct, quadrature and zero components and w represents the frequency of the grid.

A fundamental property of the $dq0$ transformation is that it maps symmetric ac signals to constants because the coordinate system $dq0$ rotates at the frequency of the grid instead of being fixed as in the $\alpha\beta\gamma$ system. This has the disadvantage that it is necessary to

calculate precisely the angle of rotation.

Therefore, using Park's transformation in the equations (2.2)–(2.6), the system model in $dq0$ coordinates is represented by

$$L\frac{di_d}{dt} = Lwi_q + (d_{dp} + d_{dn})\frac{v_{dc}}{2} + (d_{dp} - d_{dn})\frac{v_d}{2} \tag{2.22}$$

$$L\frac{di_q}{dt} = -Lwi_d + (d_{qp} + d_{qn})\frac{v_{dc}}{2} + (d_{qp} - d_{qn})\frac{v_d}{2} \tag{2.23}$$

$$C\frac{dv_{dc}}{dt} = -(d_{dp} + d_{dn})i_d - (d_{qp} + d_{qn})i_q \tag{2.24}$$

$$C\frac{dv_d}{dt} = -(d_{dp} - d_{dn})i_d - (d_{qp} - d_{qn})i_q, \tag{2.25}$$

where the control inputs d_{dp}, d_{dn}, d_{qp} and d_{qn} are the duty ratios in $dq0$ coordinates.

2.3 Voltage Balance Problem

As mentioned in the introductory chapter, three level NPC converters have numerous advantages over the classic two levels converters. However, this type of converters present some problems that must be addressed in order to implement them practically. One of those problems is that the voltages that drop across the capacitors must be balanced. This problem appears because the values of the capacitors are not identical or also to the presence of asymmetrical load conditions. On the one hand, due to this problem, the capacitors can work outside their operating range limiting their useful life and even causing their destruction and therefore the malfunction of the complete converter. On the other hand, the imbalance deteriorates the ac-side voltage waveforms by making them to contain second or higher-order even harmonics [46].

Over the last few years numerous techniques have been developed to correct the voltage unbalance. Some of them use additional circuitry, but this leads to an increase in cost, losses and complexity in hardware.

In [47], a circuit with two additional switches is added to control the voltage balance in a three-level boost NPC inverter. The possible combinations of these switches generate four possible states. To control the voltage balance, a PI controller is used, which together with the duty ratio value, define a table of ten possible cases where the four states of the switches are used in a certain sequence.

In [48], a circuit based on adding a boost and a buck converter to a three-level NPC inverter is used. In this way, when it is desired to modify the voltage in one of the capacitors, the buck converter is activated ($v_{c1} > v_{c2}$) and when it is desired to modify the voltage in the other, the boost converter is used ($v_{c2} > v_{c1}$).

In [49], a circuit with four switches and two inductances is used for the voltage balance of a five-level DCC converter. Using a cascaded PI controller, they minimize the number of components added by the additional circuit to allow the use of conventional PWM techniques.

Other authors use different control techniques with algorithms of varying difficulty. Many of them, use modifications of the well-known Space Vector Modulation (SVM). Basically, it consists, by means of some type of algorithm, of calculating the time that it is necessary to be in a switching state to make the voltage in the capacitors to be balanced. Techniques that use redundant switching states, like [50], are often used to achieve voltage balance among capacitors. Using these techniques, it is possible to use states where the

same reference vectors are generated but the charge or discharge of a given capacitor is encouraged.

In [51], a modification of SVM for the voltage balance problem in a three-level inverter is used. The method uses an observer to estimate the value of the voltage in the capacitors and corrects the unbalance of these by modifying the times of the middle voltage vectors.

Among these methods, it is worth highlighting the modification done in [52] of the virtual space vector modulation (VSVM) [53]. In this method, virtual vectors, formed with the original vectors of the space vector hexagon, are calculated where the possible switching states are weighted to generate currents that benefit the voltage balance, charging or discharging each capacitor as needed. This method will be used in the next chapter for comparison with the methods proposed in this thesis.

In [54], the voltage balance problem is addressed using Selective Harmonic Elimination Pulsewidth Modulation (SHE-PWM) in a three-level NPC converter. The control modifies the duty cycle of the zero level to control the current at the neutral point, thus modifying its voltage as well. This algorithm bases its strategy on the polarity of the output current and the voltage of the lower dc-link capacitor.

In [55], A Direct Power Control (DPC) is used to control a three-level NPC rectifier. In this paper, the model equations for the voltage balance include a nonlinear term that is estimated by a Luenberger observer to be used in the controller.

The authors of [56] use a long-horizon predictive control for current control in an NPC inverter. In addition, they use a control by redundant states, based on this prediction, to carry out the voltage balance in the capacitors.

3 Three-Level Converter Control

You cannot teach a man anything; you can only help him discover it in himself.

GALILEO GALILEI

Contents

In this chapter, the proposed approaches for the capacitor voltage balance problem in a three-level converter are presented. Although the voltage balance is the main objective, it should be noted that in power converters it is necessary to control other variables such as currents, powers, dc-link voltage, among others. For this, contrasted controllers in the literature can be used, which will be commented in the first sections of this chapter. Although several of them are described, for the development of the thesis an instantaneous power control and a total dc-link voltage control will be used. It is important to note that although a formulation with averaged duties is being used, the design of the controllers is not difficult and it is possible to use traditional techniques such as those shown in the next sections.

In the previous chapter it was possible to observe as modeling in terms of duty ratios is used to explicitly consider, in the control design stage, an extra degree of freedom. In the following, this degree of freedom will be used to formulate, with an appropriate change of variables, the dc-link voltage and active and reactive power control problems in a similar way to other usual approaches. The voltage balance controller can be easily designed at the same time that an important part of modulation is not needed. For this, the proposed approach can be considered as a control method with implicit modulator [34], and in what follows it is called “Integrated Control and Modulation” (ICM). The main advantage of the proposed law is its simplicity in implementation compared with Space Vector Modulation (SV-PWM) [53] and that presents some advantages with respect to CB-PWM. This is because the modulation stage is simplified without loosing part of the flexibility of SV-PWM [57, 58].

The drawback of the adopted formulation is that it may lead to an unnecessary increase in the number of commutations. This is due to the fact that, unless some of the duty cycle variables turn out to be zero, the resultant switching signals will commute among all the levels for the three phases every sampling period, which is the case of the first control law proposed (ICM1) whereas the dc-link voltage, current or power control can be accomplished by switching each phase between two levels [59] when the voltage balance problem is not considered. When the degree of freedom associated with the injection of homopolar component is used for the voltage balance control, some additional commutations are needed but not as much as in ICM1. To overcome the large number of commutations, a new control (ICM2) is designed by exploiting some additional degrees of freedom in such a way that the resultant number of commutations is considerably reduced.

A third variant is proposed in order to achieve the voltage balance in the capacitors. As has been used in the first two approaches, the balancing task can be carried out in the modulation stage. In carrier-based pulse width modulation (CBPWM), there exists a common component that can be added/subtracted to the three reference signals simultaneously without affecting the overall performance but allowing the control to modify the levels used like in ICM1 and ICM2. Considering this common component and using the nearest-two-level modulation, the minimum amount of commutations is achieved by keeping one phase at one level while the other two commute between two levels each. This is the case of this last variant, where this common component is calculated by solving an optimization problem.

3.1 Current and Power Controllers

Current and power controllers are not the main goal in this thesis, but they are necessary to control the converter. Even so, the formulation used here is a novelty since it uses the averaged model described in the previous section. In this way making a change of variables, as will be seen later, the usual method to design controllers can be used. Therefore, any current control of the many existing in the literature can be used. This section shows two of them. It should be noted that the control used in the development of this thesis is the power control although a current control can be used.

3.1.1 Current Control 1

The first current control is based on [60], where assuming balanced the voltage in the capacitors it is possible to simplify the dynamic equations of the model (2.11) – (2.12) by

$$L\frac{di_\alpha}{dt} = v_{s\alpha} - (d_{\alpha p} - d_{\alpha n})\frac{v_{dc}}{2} = v_{s\alpha} - u_1\frac{v_{dc}}{2} \tag{3.1}$$

$$L\frac{di_\beta}{dt} = v_{s\beta} - (d_{\beta p} - d_{\beta n})\frac{v_{dc}}{2} = v_{s\beta} - u_2\frac{v_{dc}}{2}, \tag{3.2}$$

where the next definition of the control variables u_1 and u_2 has been used,

$$u_1 \doteq d_{\alpha p} - d_{\alpha n} \tag{3.3}$$

$$u_2 \doteq d_{\beta p} - d_{\beta n}. \tag{3.4}$$

Taking into account this model equations, it is possible to define the next control signals,

$$u_1 = \frac{2}{v_{dc}} \left(v_{s\alpha} + k_p \left(i_\alpha - i_\alpha^r \right) + k_{pi} \int_0^t \left(i_\alpha - i_\alpha^r \right) d\tau \right) \tag{3.5}$$

$$u_2 = \frac{2}{v_{dc}} \left(v_{s\beta} + k_p \left(i_\beta - i_\beta^r \right) + k_{pi} \int_0^t \left(i_\beta - i_\beta^r \right) d\tau \right), \tag{3.6}$$

where design parameters k_p and k_{pi} are the proportional and integral gains of the controller. The currents references are defined, respectively, by i_α^r and i_β^r, whose expressions are

$$i_\alpha^r = \frac{1}{v_{s\alpha}^2 + v_{s\beta}^2} \left(v_{s\alpha} p^r - v_{s\beta} q^r \right) \tag{3.7}$$

$$i_\beta^r = \frac{1}{v_{s\alpha}^2 + v_{s\beta}^2} \left(v_{s\beta} p^r + v_{s\alpha} q^r \right). \tag{3.8}$$

3.1.2 Current Control 2

Computing $\{i_\alpha^r, i_\beta^r\}$ as in (3.7)–(3.8), another current controller can be implemented such as to reduce the current tracking error $\{\widehat{i_\alpha}, \widehat{i_\beta}\} = \{i_\alpha^r - i_\alpha, i_\beta^r - i_\beta\}$ as much as possible. In this way, a non-ideal proportional-resonant controller [61] tuned at the grid frequency is implemented. The basic functionality of the PR controller is to introduce an infinite gain at a selected resonant frequency for eliminating steady-state error at that frequency, and is therefore conceptually similar to an integrator whose infinite DC gain forces the DC steady-state error to zero.

$$G_{PR_\omega}(s) \;=\; k_p + \frac{2k_r\omega_c s}{s^2+2\omega_c s+\omega^2} \tag{3.9}$$

$$\begin{bmatrix} u_1 \\ u_2 \end{bmatrix} \;=\; \frac{2}{v_{dc}} \left(-G_{PR_{\omega_g}} \begin{bmatrix} \widehat{i_\alpha} \\ \widehat{i_\beta} \end{bmatrix} + \begin{bmatrix} v_{s\alpha} \\ v_{s\beta} \end{bmatrix} \right), \tag{3.10}$$

where $\{k_p, k_r\}$ are, respectively, the proportional and resonant control parameters, ω_c is the cut-off frequency of the low-pass filter implemented into the resonant part, ω is the resonant frequency—in this case, tuned at the grid one ($\omega_g = 2\pi f_{\text{grid}}$)—, and $\{v_{s\alpha}, v_{s\beta}\}$ are the grid voltages in the $\alpha\beta\gamma$ frame.

One disadvantage of the resonant control is that, being tuned to the frequency of the grid, if this frequency changes the control may stop working satisfactorily.

3.1.3 Instantaneous Power Controller

In this section an instantaneous power control is defined, as alternative to the current control, in order to transfer the desired amount of active power with a certain power factor. This is the controller used in the development of this thesis.

Using definitions (3.3)–(3.4) into the model equations and assuming that the value of variable v_d is small enough to be neglected, the active and reactive power dynamics can be expressed by

$$L\,\frac{dp}{dt} \simeq v_{s\alpha}^2 + v_{s\beta}^2 + Z_L\; q - \left(u_1 v_{s\alpha} + u_2 v_{s\beta}\right) \frac{v_{dc}}{2} \tag{3.11}$$

$$L\,\frac{dq}{dt} \simeq -Z_L\; p + \left(u_1 v_{s\beta} - u_2 v_{s\alpha}\right) \frac{v_{dc}}{2}. \tag{3.12}$$

These expressions are equivalent to the instantaneous power dynamics of the conventional two-level converter [44]. Therefore, by the use of the change of variables (3.3) - (3.4), the added difficulty inherent for the adopted formulation disappears, at least at this stage. Thus, implementing a DPC strategy [62, 63, 64], the virtual control variables are

defined by

$$\begin{aligned} u_1 &= u_1^z + k_p v_{s\alpha}(p-p^r) + k_{pi} v_{s\alpha} \int_0^t (p-p^r)\, d\tau \\ &\quad - k_q v_{s\beta}(q-q^r) - k_{qi} v_{s\beta} \int_0^t (q-q^r)\, d\tau \end{aligned} \tag{3.13}$$

$$\begin{aligned} u_2 &= u_2^z + k_p v_{s\beta}(p-p^r) + k_{pi} v_{s\beta} \int_0^t (p-p^r)\, d\tau \\ &\quad + k_q v_{s\alpha}(q-q^r) + k_{qi} v_{s\alpha} \int_0^t (q-q^r)\, d\tau, \end{aligned} \tag{3.14}$$

where design parameters k_p, k_q, k_{pi} and k_{qi} are the proportional and integral gains of the controller; the instantaneous active and reactive powers references are represented, respectively, by p^r and q^r, and terms u_1^z and u_2^z are defined by

$$u_1^z = \frac{2}{v_{dc}} \left(\left(1 + \frac{Z_L\, q}{v_{s\alpha}^2 + v_{s\beta}^2} \right) v_{s\alpha} + \frac{Z_L\, p}{v_{s\alpha}^2 + v_{s\beta}^2}\, v_{s\beta} \right) \tag{3.15}$$

$$u_2^z = \frac{2}{v_{dc}} \left(\left(1 + \frac{Z_L\, q}{v_{s\alpha}^2 + v_{s\beta}^2} \right) v_{s\beta} - \frac{Z_L\, p}{v_{s\alpha}^2 + v_{s\beta}^2}\, v_{s\alpha} \right). \tag{3.16}$$

These expressions have been obtained by equating the time derivatives in (3.11) – (3.12) to zero and isolating u_1 and u_2. Thus, they both represent the specific values of the virtual control variables such that, when they are applied to the system, that is, when $u_1 = u_1^z$ and $u_2 = u_2^z$, the instantaneous powers are constant.

3.2 Total DC-Link Voltage Controller

In order to maintain constant the dc-link voltage and close to its reference (v_{dc}^r), as usual, a specific PI controller is used [62, 65]. For this controller, the formulation made using averaged duties does not affect the design so traditional techniques can be used.

Notice that the instantaneous power dynamics are faster than those of the total dc-link voltage [44], so it is possible to assume that $p \simeq p^r$ and $q \simeq q^r$. Considering this and

expressions (3.13) – (3.14), equation (2.19) can be expressed as

$$C\frac{dv_{dc}^2}{dt} \simeq 4\left(p^r - \frac{v_{dc}^2}{R}\right). \tag{3.17}$$

This equation shows the relationship between p_r and v_{dc}, being able to define a usual PI controller

$$p^r = k_p^{dc}\left(v_{dc}^{r2} - v_{dc}^2\right) + k_i^{dc}\int_0^t \left(v_{dc}^{r2} - v_{dc}^2\right) d\tau, \tag{3.18}$$

where constants k_p^{dc} and k_i^{dc} are controller tuning parameters.

3.3 Voltage Balance Controller

The objective of the voltage balance controller is to keep the state variable v_d close to zero, avoiding the unbalance of the dc-link capacitor voltages. This controller is based on the definition of two new virtual control variables

$$u_3 \doteq d_{\alpha p} + d_{\alpha n} \tag{3.19}$$

$$u_4 \doteq d_{\beta p} + d_{\beta n}. \tag{3.20}$$

Introduction of (3.19) – (3.20) into (2.20) yields

$$C\frac{dv_d}{dt} = \frac{v_{s\alpha}p - v_{s\beta}q}{v_{s\alpha}^2 + v_{s\beta}^2}u_3 + \frac{v_{s\beta}p + v_{s\alpha}q}{v_{s\alpha}^2 + v_{s\beta}^2}u_4. \tag{3.21}$$

It is important to highlight that the definition of u_3 and u_4 causes a decoupling of the model equations for control purposes. Note that u_1 and u_2 are designed to regulate the state variables p and q (i_α and i_β in the case of using currents control), whereas u_3 and u_4 can be used to regulate v_d (3.21). This is an important benefit of the proposed control approach.

Taking into account (3.21), the following control laws were proposed in [44]

$$u_3 = k_d \frac{v_{s\alpha}p - v_{s\beta}q}{p^2+q^2}(v_d^r - v_d) + k_{di}\frac{v_{s\alpha}p - v_{s\beta}q}{p^2+q^2}\int_0^t (v_d^r - v_d)\,d\tau \tag{3.22}$$

$$u_4 = k_d \frac{v_{s\beta}p + v_{s\alpha}q}{p^2+q^2}(v_d^r - v_d) + k_{di}\frac{v_{s\beta}p + v_{s\alpha}q}{p^2+q^2}\int_0^t (v_d^r - v_d)\,d\tau, \tag{3.23}$$

where positive constants k_d and k_{di} are tuning parameters. The reference for v_d is denoted by v_d^r, which is set to zero to ensure a balanced distribution of the dc-link voltage across capacitors C_1 and C_2.

By introducing (3.22)–(3.23) into (3.21), the voltage balance dynamics become linear:

$$C\frac{d^2(v_d^r - v_d)}{dt^2} + k_d\frac{d(v_d^r - v_d)}{dt} + k_{d_i}(v_d^r - v_d) = 0, \tag{3.24}$$

whose stability is assured provided that parameters k_d and k_{d_i} are positive.

A complete schematic block diagram of all controllers is illustrated in Fig. 3.1. As stated above, in this case a power control has been chosen in addition to the total dc-link voltage and voltage balance control.

Using all these controllers, the control signals u_1, u_2, u_3 and u_4 are obtained. In the next section, several techniques to convert these control signals to duty values will be shown.

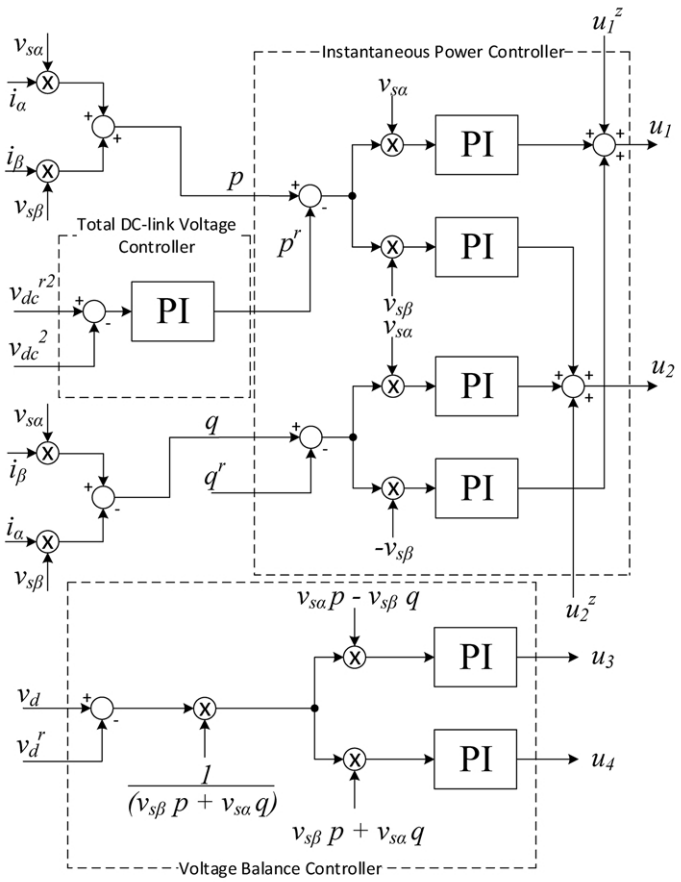

Figure 3.1 Complete schematic block diagram of the controllers.

3.4 Proposed approaches

The controller presented in the previous section provides, at each sampling time, the values for u_1, u_2, u_3 and u_4. The corresponding values for $d_{\alpha p}, d_{\alpha n}, d_{\beta p}$ and $d_{\beta n}$ can be obtained solving the system of equations (3.3)–(3.4) and (3.19)–(3.20) yielding

$$d_{\alpha p} = \frac{1}{2}(u_1 + u_3) \tag{3.25}$$

$$d_{\alpha n} = \frac{1}{2}(-u_1 + u_3) \tag{3.26}$$

$$d_{\beta p} = \frac{1}{2}(u_2 + u_4) \tag{3.27}$$

$$d_{\beta n} = \frac{1}{2}(-u_2 + u_4). \tag{3.28}$$

In order to compute the actual duty ratios $d_{ij}, i = a,b,c; j = p,n$, the Clarke transformation can be used

$$\begin{bmatrix} d_{aj} \\ d_{bj} \\ d_{cj} \end{bmatrix} = \sqrt{\frac{2}{3}} \begin{bmatrix} 1 & 0 & \frac{1}{\sqrt{2}} \\ -\frac{1}{2} & \frac{\sqrt{3}}{2} & \frac{1}{\sqrt{2}} \\ -\frac{1}{2} & -\frac{\sqrt{3}}{2} & \frac{1}{\sqrt{2}} \end{bmatrix} \begin{bmatrix} d_{\alpha j} \\ d_{\beta j} \\ d_{\gamma j} \end{bmatrix}, \quad j = p,n. \tag{3.29}$$

where $d_{\gamma p}$ and $d_{\gamma n}$ are remaining degrees of freedom. Obviously, the remaining duty ratios, d_{ao}, d_{bo} and d_{co} can be computed using (2.7)–(2.9).

As stated in the introduction to the chapter, the two first approaches that are going to be showed here can be considered as a control method with implicit modulator and are called “Integrated Control and Modulation” (ICM) because part of this modulation has been included in the design of the controllers.

In the third approach, the injection of a common component in the voltage output of the converter is used explicitly to achieve the voltage balance. This approach is proposed as an optimization problem based on the equation that controls the voltage balance. In this last variant, the control variables u_3 and u_4 are not used since the optimization problem is applied directly to the equation that governs the voltage balance in the capacitors.

3.4.1 ICM1

The first variant, ICM1, was proposed in [44]. In this variant, $d_{\gamma p}$ and $d_{\gamma n}$ are chosen to be constant and can be considered tuning parameters. To choose their values, it is necessary to express the control variables at steady state by

$$u_1 \simeq \frac{2}{v_{dc}^r} V_{\alpha\beta} cos(2\pi f t + \theta) \tag{3.30}$$

$$u_2 \simeq \frac{2}{v_{dc}^r} V_{\alpha\beta} sin(2\pi f t + \theta) \tag{3.31}$$

$$u_3 \simeq 0 \tag{3.32}$$

$$u_4 \simeq 0, \tag{3.33}$$

where θ and $V_{\alpha\beta}$ are the phase and amplitude of the voltages $v_{s\alpha}$ and $v_{s\beta}$ and f is the frequency of the grid.

From these expressions it is possible to calculate the duty ratios $d_{\alpha p}, d_{\alpha n}, d_{\beta p}$ and $d_{\beta n}$, in $\alpha\beta$ coordinates. Transforming these duties to abc coordinates, together with $d_{\gamma p}$ and $d_{\gamma n}$ and restrictions (2.7)–(2.10), gives the limits to choose these last variables, expressed by

$$d_{\gamma p} + d_{\gamma n} \leq \sqrt{3} \tag{3.34}$$

$$\sqrt{(2)}\frac{V_{\alpha\beta}}{v_{dc}^r} \leq d_{\gamma i} \leq \sqrt{3} - \sqrt{2}\frac{V_{\alpha\beta}}{v_{dc}^r}. \tag{3.35}$$

Notice that in the way in which these limits are obtained, very conservative results are obtained.

This approach is a simple way to accomplish the modulation but it presents an important drawback: except by chance, none of the d_{ij} will result in zero. This implies that, in each sampling time, each phase commutes among the three levels (positive (p), zero (o) and negative (n)) which can be considered too many commutations compared with other approaches, even those including voltage balancing. This fact could yield large switching losses.

3.4.2 ICM2

In order to avoid the large number of commutations, a new variant is proposed. This variant, takes advantage of the two degrees of freedom associated with $d_{\gamma p}$ and $d_{\gamma n}$ imposing, at each sampling period, one d_{ip} and one d_{in} $(i = a, b, c)$ to be zero. The two phases for which one of the duty ratios has to be zero need to be chosen carefully and taking into account that the duty cycles in abc coordinates have to be in the interval $[0,1]$. The result is that these two phases only switch between two levels. One of them only switches between zero and the positive level and the other one only switches between zero and the negative level. The remaining phase commutes among the three levels. This number of commutations is similar to the one in other control strategies that include voltage balance capabilities [66].

In order to select the phases that commute only between two levels, the following procedure is proposed: first of all, it is necessary to check if setting one of the $d_{ij}, i = a,b,c; j = p,n$ to zero yields to the fulfillment of the constraints $0 \leq d_{ij} \leq 1$ for the rest of duty cycle variables. Starting with the case $d_{ap} = 0$, Eq. (3.29) for $j = p$ can be considered as a set of equations, where $d_{\alpha p}, d_{\beta p}$ are known, $d_{ap} = 0$ and d_{bp}, d_{cp} and $d_{\gamma p}$ are the unknowns. The resultant system of equations can be solved in order to check if this case is feasible, that is, if d_{bp} and d_{cp} are in the interval $[0,1]$. Repeating for the other phases, three different cases have to be analyzed for $j = p$ and other three cases for $j = n$. The associated equations are

Case 1: $d_{aj} = 0$

$$d_{bj} = -\frac{\sqrt{6}}{2} d_{\alpha j} + \frac{\sqrt{2}}{2} d_{\beta j} \tag{3.36}$$

$$d_{cj} = -\frac{\sqrt{6}}{2} d_{\alpha j} - \frac{\sqrt{2}}{2} d_{\beta j}. \tag{3.37}$$

Case 2: $d_{bj} = 0$

$$d_{aj} = \frac{\sqrt{6}}{2} d_{\alpha j} - \frac{\sqrt{2}}{2} d_{\beta j} \tag{3.38}$$

$$d_{cj} = -\sqrt{2} d_{\beta j}. \tag{3.39}$$

Case 3: $d_{cj} = 0$

$$d_{aj} = \frac{\sqrt{6}}{2} d_{\alpha j} + \frac{\sqrt{2}}{2} d_{\beta j} \tag{3.40}$$

$$d_{bj} = \sqrt{2} d_{\beta j}, \tag{3.41}$$

where j = p,n. The resultant duty ratios for the considered sampling instant are the corresponding to one of the feasible cases, that is, cases where all the duty cycles are in the interval $[0,1]$. It will be shown below that, at every instant , there exist at least one (and apart from some border cases, only one) feasible case.

Regarding the computation, after computing (3.25)–(3.28), the calculation of the duty ratios $d_{ij}, i = a,b,c; j = p,n$ can be performed checking the constraints $d_{ij} \in [0,1]$ for the $3 \times 2 = 6$ cases. For this, (3.36)–(3.41) have to be used twice (for levels p and n). This last stage implies the computation of 20 multiplications and 8 sums as well as 24 comparisons.

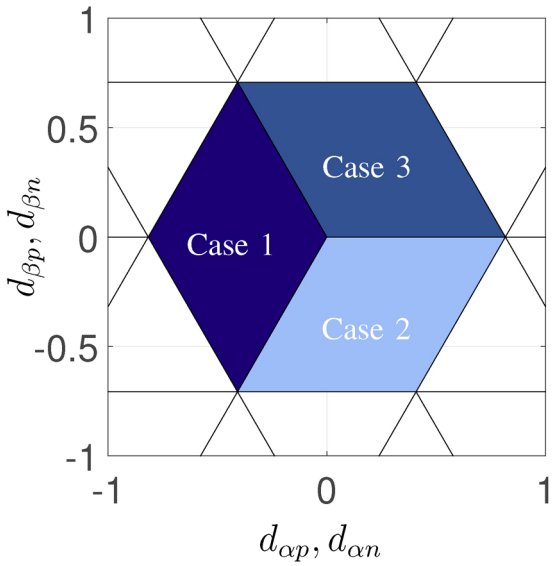

Figure 3.2 Graphical representation of the limits of each case.

Alternatively, a different approach can be used to choose the correct case at every sampling instant with the help of Fig. 3.2. The straight lines of this graph represent the borders for the fulfillment of constraints $0 \leq d_{ij} \leq 1$, as a function of $d_{\alpha j}$ and $d_{\beta j}$. As for

each level $j = p,n$ there is one d_{ij} that it is equal to zero, there are four of such lines for each case, instead of six. The shadowed areas represent the solution of the corresponding systems of inequalities. It can be seen that the three shadowed areas do not overlap (except at their borders) and that they cover a whole hexagon. An interesting fact is that this hexagon is related to the well-known hexagon of Space Vector Modulation (SVM), but in this case, there are two such hexagons (one for the positive level and other for the negative). The interest of this figure is twofold: 1) it shows that, provided the converter does not work in overmodulation region, one of the three cases is always feasible, and 2) Fig 3.2 can be used as an alternative method to choose the correct case: the working sector can be computed as usual in SVM and once the appropriate case is selected, the corresponding formulae can be applied.

In summary, the ICM2 algorithm, can be implemented in two alternative and equivalent ways that only differ in the computational burden, which in alternative B depends on the method used for the computation of the sextant:

Alternative A:

- Computation of u_3 and u_4 using (3.22) and (3.23).
- Computation of $d_{\alpha p}, d_{\alpha n}, d_{\beta p}, d_{\beta n}$ using (3.25)–(3.28).
- For levels p and n:
  - Computation of Eqs (3.36)–(3.41) and selection of the case that fulfills the constraints $0 \leq d_{ij} \leq 1$. This procedure gives directly the resultant duty cycles.

Alternative B:

- Computation of u_3 and u_4 using (3.22) and (3.23).
- Computation of $d_{\alpha p}, d_{\alpha n}, d_{\beta p}, d_{\beta n}$ (3.25)–(3.28).
- For levels p and n:
  - Computation of the sextant inside the hexagon of Fig. 3.2. This step is similar to the corresponding one in SVM (but it must be computed twice, one for level p and one for level n). The sextant gives the corresponding case.
  - Computation of the duties using the corresponding Eqs. of (3.36)–(3.41).

3.4.3 Variant 3

For this new variant, we again use the degree of freedom associated with component γ of the reference voltage, addressing the problem of the voltage balance from the modulation stage. The components u_1 and u_2 of the reference voltage are assumed to be known and calculated by an external controller as used in section 3.1.

$$\begin{bmatrix} u_a \\ u_b \\ u_c \end{bmatrix} = \sqrt{\frac{2}{3}} \begin{bmatrix} 1 & 0 & \frac{1}{\sqrt{2}} \\ -\frac{1}{2} & \frac{\sqrt{3}}{2} & \frac{1}{\sqrt{2}} \\ -\frac{1}{2} & -\frac{\sqrt{3}}{2} & \frac{1}{\sqrt{2}} \end{bmatrix} \begin{bmatrix} u_1 \\ u_2 \\ u_\gamma \end{bmatrix}, \tag{3.42}$$

Based on the inverse Clarke transformation of abc coordinates to $\alpha\beta\gamma$ expressed by (3.42) and known components u_1 and u_2, it is possible to calculate the components of the reference voltage in abc coordinates as a function of u_γ.

Using the transformation in (3.42), the following equations are obtained,

$$u_a = \sqrt{\frac{2}{3}} u_1 + \frac{1}{\sqrt{3}} u_\gamma \tag{3.43}$$

$$u_b = -\frac{1}{\sqrt{6}} u_1 + \frac{1}{\sqrt{2}} u_2 + \frac{1}{\sqrt{3}} u_\gamma \tag{3.44}$$

$$u_c = -\frac{1}{\sqrt{6}} u_1 - \frac{1}{\sqrt{2}} u_2 + \frac{1}{\sqrt{3}} u_\gamma. \tag{3.45}$$

Using the constant definitions:

$$x \doteq \frac{1}{\sqrt{3}} u_\gamma \tag{3.46}$$

$$\eta_a \doteq \sqrt{\frac{2}{3}} u_1 \tag{3.47}$$

$$\eta_b \doteq -\frac{1}{\sqrt{6}} u_1 + \frac{1}{\sqrt{2}} u_2 \tag{3.48}$$

$$\eta_c \doteq -\frac{1}{\sqrt{6}} u_1 - \frac{1}{\sqrt{2}} u_2, \tag{3.49}$$

the next equations are obtained,

$$u_a = \eta_a + x \tag{3.50}$$

$$u_b = \eta_b + x \tag{3.51}$$

$$u_c = \eta_c + x. \tag{3.52}$$

Notice that in these expressions, x depends only on u_γ, while η_a, η_b and η_c depend on u_1 and u_2.

Equations (3.50)–(3.52) correspond to the well-known fact that the homopolar component provides an associated degree of freedom [67, 68, 69]. These equations correspond to three parallel lines like those shown in Fig. 3.3. In this figure, the horizontal lines for u_{abc} = $\{-1,0,1\}$ represent the three implementable states for the case of a three-level converter. Also in this figure, it is possible to observe that the value of x will be between a minimum and maximum value. In this way, x_{min} corresponds to the maximum value of which one of the three lines corresponding to u_a, u_b or u_c crosses the line that passes through level -1, and x_{max} corresponds to the minimum value of which one of the three lines corresponding to u_a, u_b or u_c crosses the line that passes through level 1. In other words, $x \in [-1 - \min(\eta_a,\eta_b,\eta_c), 1 - \max(\eta_a,\eta_b,\eta_c)] \doteq [x_{min}, x_{max}]$.

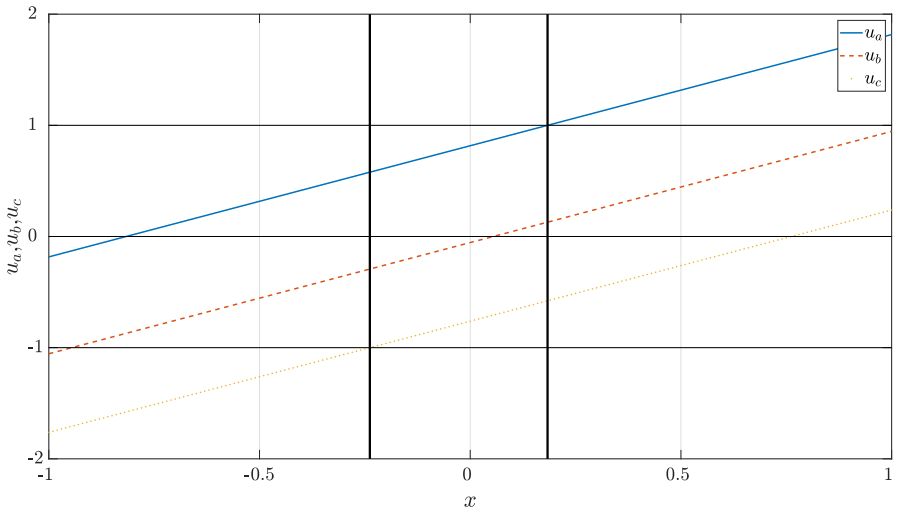

Figure 3.3 Instantaneous representation of u_a, u_b and u_c as a function of x value.

The feasibility condition of this method is that $x_{min} < x_{max}$. Notice that this condition is equivalent to the requirement that voltage reference vector (u_α, u_β) is inside the space vector hexagon, that is, there is no overmodulation.

Expressing equation (2.14), which governs the voltage difference between the capacitors, in abc coordinates, we obtain

$$C\frac{dv_d}{dt} = i_a(d_{ap}+d_{an})+i_b(d_{bp}+d_{bn})+i_c(d_{cp}+d_{cn}). \tag{3.53}$$

As can be seen, the right-hand side of this equation depends on the duty cycles of each phase at positive and negative level. To force the switching between only two levels, one of the duties of each phase is imposed to be zero and taking into account that the definition of the components of the reference voltage is expressed as $u_i = d_{ip} - d_{in}$ with $i = a, b, c$, equation (3.53) can be expressed as

$$C\frac{dv_d}{dt} = i_a\,|u_a| + i_b\,|u_b| + i_c\,|u_c|\,. \tag{3.54}$$

Based on this equation, this method focuses on minimizing the function sign(v_d)($i_a\,|u_a| + i_b\,|u_b| + i_c\,|u_c|$), where the function sign(v_d) is the standard sign function. In this way, the

voltage balance is being forced to be corrected as quickly as possible.

The proposed optimization problem turns out to be piecewise linear and depends on an only variable, x, so it is enough to evaluate the cost function 3.54 in a limited number of points and choose the one that makes it smaller. These points correspond to the limits x_{min} and x_{max} and the points where the three lines generated by (3.50)–(3.52) cross the horizontal axis.

Thus, the values of x that have to be analyzed are given by a set of points between the values x_{min} and x_{max}, according to table 3.1.

Table 3.1 Cost Function value.

x **value**	$f_{\textbf{cost}}(x)\textbf{sign}(v_d)$	**Condition**
$-\eta_a$	$i_b\lvert\eta_b-\eta_a\rvert+i_c\lvert\eta_c-\eta_a\rvert$	$x_{\text{min}}\leq-\eta_a\leq x_{\text{max}}$
$-\eta_b$	$i_a\lvert\eta_a-\eta_b\rvert+i_c\lvert\eta_c-\eta_b\rvert$	$x_{\text{min}}\leq-\eta_b\leq x_{\text{max}}$
$-\eta_c$	$i_a\lvert\eta_a-\eta_c\rvert+i_b\lvert\eta_b-\eta_c\rvert$	$x_{\text{min}}\leq-\eta_c\leq x_{\text{max}}$
x_{min}	$i_a\lvert\eta_a+x_{\text{min}}\rvert+i_b\lvert\eta_b+x_{\text{min}}\rvert+i_c\lvert\eta_c+x_{\text{min}}\rvert$	$--$
x_{max}	$i_a\lvert\eta_a+x_{\text{max}}\rvert+i_b\lvert\eta_b+x_{\text{max}}\rvert+i_c\lvert\eta_c+x_{\text{max}}\rvert$	$--$

With the optimal value x^*, that minimize the cost function, it is possible to obtain the components of the reference voltage in abc coordinates according to

$$u_a = \eta_a + x^* \tag{3.55}$$

$$u_b = \eta_b + x^* \tag{3.56}$$

$$u_c = \eta_c + x^*. \tag{3.57}$$

Initially, in order to reduce the number of commutations, it can be imposed the use of the nearest two levels modulation (NLM) to modulate the output. This is equivalent to make one of the duty ratios $\{d_{ip}, d_{in}\}$ of each phase equal to zero which results in the following constraint for the duty ratios

$$\begin{cases} d_{in} = 0 \quad \text{if} \quad u_i \geq 0 \\ d_{ip} = 0 \quad \text{if} \quad u_i < 0 \end{cases} \qquad i = \{a,b,c\}. \tag{3.58}$$

Also notice that $u_i = d_{ip} - d_{in}$ for $i = \{a,b,c\}$.

3.5 Simulation Results

In this section, the results of the simulations carried out on the circuit of Fig. 2.5, with the ICM1, ICM2 and Variant 3 control strategies, are shown. These simulations have been performed using PSCAD environment. The switching sequence has been generated following the implementation steps described in Section 3.4 and considering a PWM strategy with a triangular carrier where a typical stepped sequencing of levels, similar to CB-PWM [70], is implemented.

Circuit and control parameters for the simulations are shown in Table 3.2.

Table 3.2 Simulation Parameters.

Parameter	Value	Parameter	Value
f_{grid}	50 Hz	Sampling frequency (f_s)	10 kHz
v_{sa}, v_{sb}, v_{sc}	230 V_{RMS}	Switching frequency (f_{sw})	10 kHz
L	2 mH	k_p, k_q	$1.5 \cdot 10^{-7}$
C	3300 μF	k_{pi}, k_{qi}	$5 \cdot 10^{-5}$
R	$120 \rightarrow 60 \rightarrow 120\ \Omega$	k_d	0.1
v_{dc}^r	$700 \rightarrow 800$ V	k_{di}	$1 \cdot 10^{-2}$
k_p^{dc}	0.05	k_i^{dc}	1

In order to show the system behavior under different conditions, several stages with different resistive load values and reference voltages have been implemented. In this way, the different situations to which the converter is subjected are:

- $[I]\ v_{dc}^r = 700\ V,\ R = 120\ \Omega$: The values at the starting point are $R = 120\,\Omega$ and $v_{dc}^r =$ 700 V.
- $[II]\ v_{dc}^r = 700\ V,\ R = 60\ \Omega$: A step in the resistive load is applied to make $R = 60\,\Omega$ at t = 1s.
- $[III]\ v_{dc}^r = 700 \rightarrow 800\ V,\ R = 60\ \Omega$: The dc-link voltage reference is modified from 700 to 800 progressively from t = 1.8s to t = 2.45s.
- $[IV]\ v_{dc}^r = 800\ V,\ R = 60\ \Omega$: The dc-link voltage reference is maintained at 800 with $R = 60\,\Omega$ until t = 4s.
- $[V]\ v_{dc}^r = 800\ V,\ R = 120\ \Omega$: Finally the load is changed back to $120\,\Omega$.

Figure 3.4 represents the changes made in the reference voltage and the resistive load.

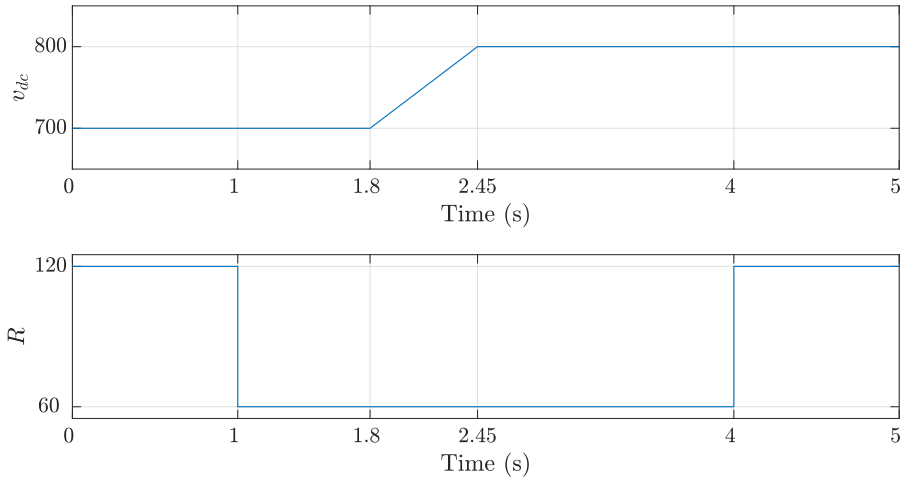

Figure 3.4 Evolution of the reference voltage (top) and the resistive load (bottom) under the simulations.

A low-pass filter has also been added to the proportional part of the total dc-link voltage controller as it is recommended in [71] in order to reduce the harmonics presence.

During the whole simulation, the instantaneous reactive power reference (q^r) has been assumed to be zero in order to guarantee unity power factor.

In this section, the simulation results of an existing method have been included in order to compare with the aproaches proposed in this thesis. This control technique [52] uses a modification of virtual space vector [53] (this modification will be denoted as mVSVPWM) to balance the voltage in the capacitors. In it, the voltage reference vector is obtained by creating virtual vectors where the possible switching states are weighted to generate currents that benefit the voltage balance.

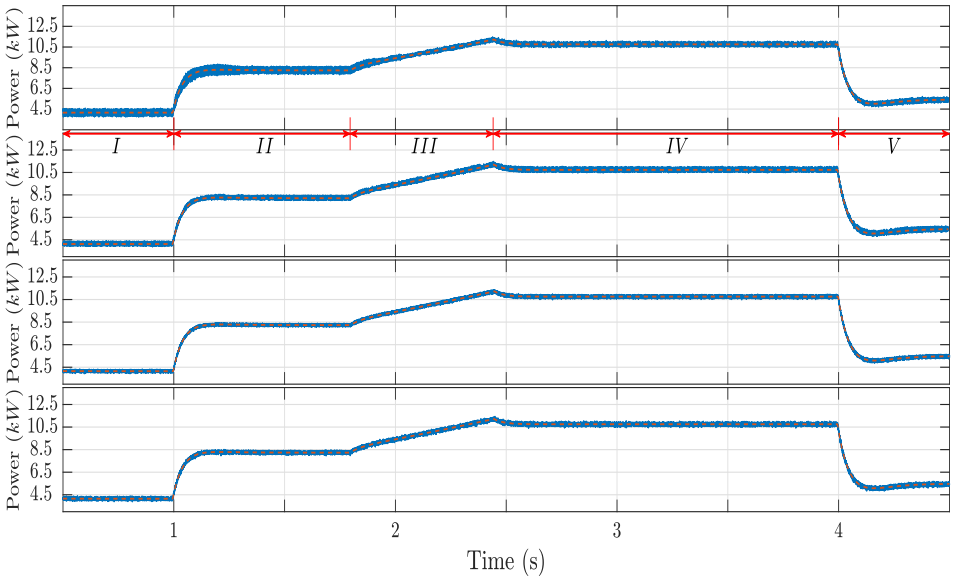

Figure 3.5 Simulation results: evolution of the instantaneous active power p (solid) and its reference value p^r (dashed), considering ICM1 (top), ICM2 (mid-up), Variant 3 (mid-down) and mVSVPWM (bottom) through the different stages of Fig. 3.4.

In Fig. 3.5 the instantaneous active power achieved for all the control laws and their references are shown. In this figure it is possible to observe how ICM2 presents a ripple smaller than ICM1, as well as Variant 3 with respect to ICM2. In fact, the Variant 3 approach presents a considerable improvement over the rest of the approaches. In the proposed approaches, the reference of active power is calculated by a PI controller from the reference voltage v_{dc}^r. This last variable can be seen, along with v_{dc}, in Fig. 3.6 where its tracking can be corroborated. As it is possible to see in this figure, the result in the control of the total dc-link voltage is similar in all the techniques used.

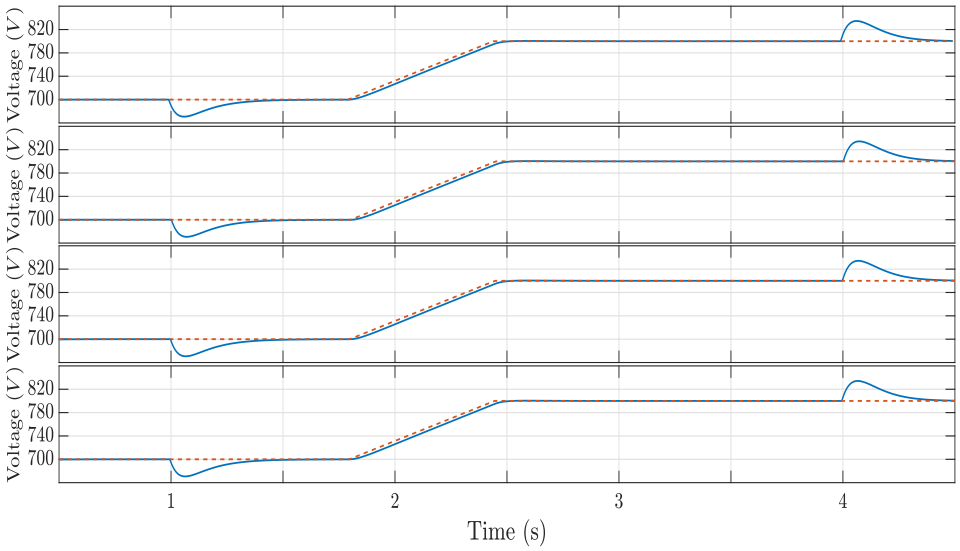

Figure 3.6 Simulation results: evolution of the total dc-link voltage v_{dc} (solid) and its reference value v_{dc}^r (dashed), considering ICM1 (top), ICM2 (mid-up), Variant 3 (mid-down) and mVSVPWM (bottom) through the different stages of Fig. 3.4.

Capacitor voltages are represented in Fig. 3.7, showing the behavior from an unbalanced condition with v_{dc}^r = 700 V and R = 120 Ω. In this figure it is possible to observe how the voltage is corrected much faster in Variant 3 than in the two previous proposed laws, reaching a convergence rate very close to mVSVPWM. In all of the laws, the voltage balance observed is much faster than the natural balance that can be obtained in the converter when connecting a purely resistive linear load. Notice that ICMs approaches have some tuning parameters (K_d and K_{di}) that could increase the speed on correcting the unbalance condition at the expenses of worsening the evolution of the currents during the transients because of saturation issues of the control variables u_3 and u_4. Therefore, there is a trade-off between balancing speed and transient behaviour in ICMs.

In Fig. 3.8, the grid currents are shown for the four algorithms where it can be seen a reduction in the ripple from ICM1 to ICM2 and to Variant 3, while mVSVPWM stays in the middle. This result is due to the presence of dead-times whose effect is lower when fewer commutations are implied. Furthermore, the unbalances are corrected even under non-symmetrical phase currents conditions. This fact is shown in Fig. 3.9 where the phase currents are unequal and the capacitor voltages are corrected from the same

initial condition as Fig. 3.7. Based on the currents showed in Fig. 3.8, the total harmonic distortion of all the approaches are obtained, yielding a THD of 5.6% in ICM1, 4.2% in ICM2, 3.9% in Variant 3 and 4.6% in mVSVPWM.

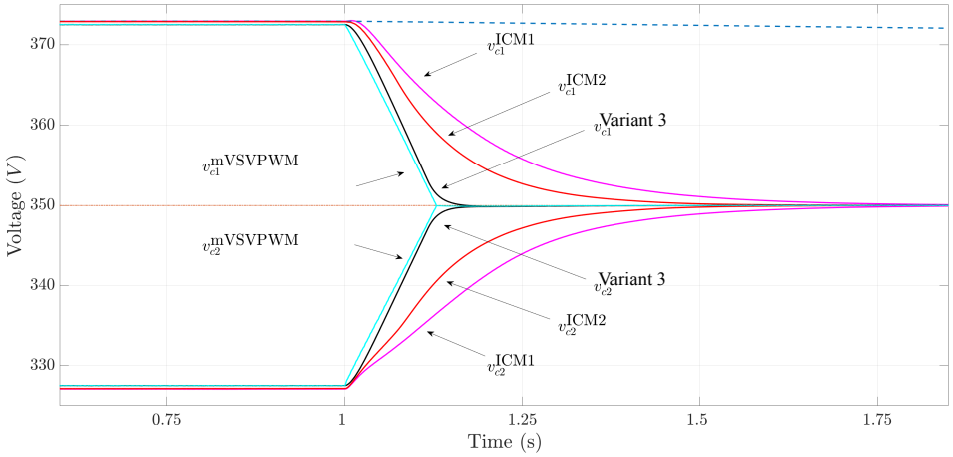

Figure 3.7 Simulation results: evolution of the capacitor voltages starting from an unbalanced condition, considering ICM1, ICM2, Variant 3 and mVSVPWM. (solid) balancing control activated; (dashed) no balancing control; (dash-dotted) reference voltage.

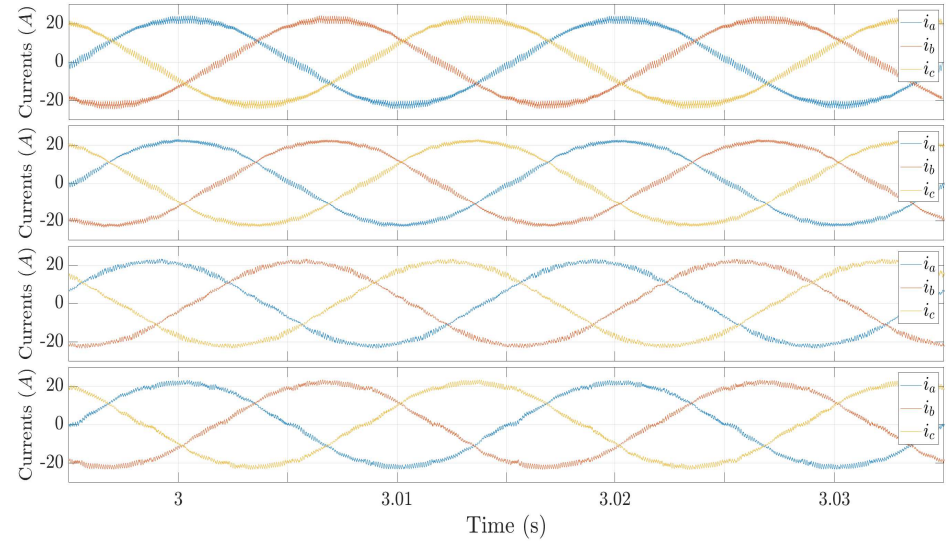

Figure 3.8 Simulation results: three-phase grid current considering ICM1 (top), ICM2 (mid-up), Variant 3 (mid-down) and mVSVPWM (bottom). $v_{dc}^{r} = 800$ V and $R = 60\,\Omega$.

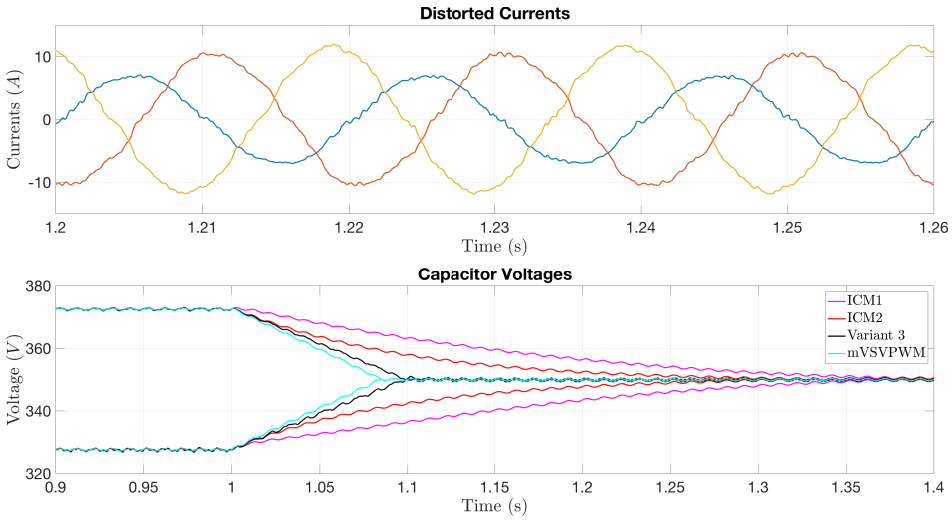

Figure 3.9 Simulation results: Capacitor voltages (bottom) starting from an unbalanced condition when phase currents (top) are distorted, considering ICM1, ICM2, Variant 3 and mVSVPWM.

Duty cycles and switching states for phase a in steady state are shown in Fig. 3.10 and 3.11 respectively. Notice that Fig. 3.11 also includes the switching state of the mVSVPWM approach which cannot be depicted similarly to Fig. 3.10 as the duty ratios for each level are not concern in this modulation approach. Figure 3.11 also includes its filtered signal in order to depict the output waveform. In this figure, state p refers to when both upper switching devices are closed; state o corresponds to both switching devices in the middle closed; and state n refers to lower switching devices closed according to Fig 2.6. Besides, it is possible to see that the commutations in phase a change among the three levels in ICM1 control law whereas, when using ICM2 and Variant 3, commutation between two levels is more frequent. Notice that shape of the output waveform of ICM2 is similar to those modulation approaches that inject a third-harmonic component to extend the fundamental frequency operative range which makes it possible to increase the modulation index without saturating the control signals. Therefore, this is another advantage of ICM2 when comparing with ICM1. This advantage can be corroborated when looking at figure 3.10 where the maximum values of signals d_{an} and d_{ap} are lower in the ICM2 approach. Based on Fig. 3.11 it is possible to obtain the numbers of commutations of the studied approaches, yielding 800 commutations per grid period at 10 KHz of switching frequency in ICM1, 522 in ICM2, 281 in Variant 3 and 412 in mVSVPWM.

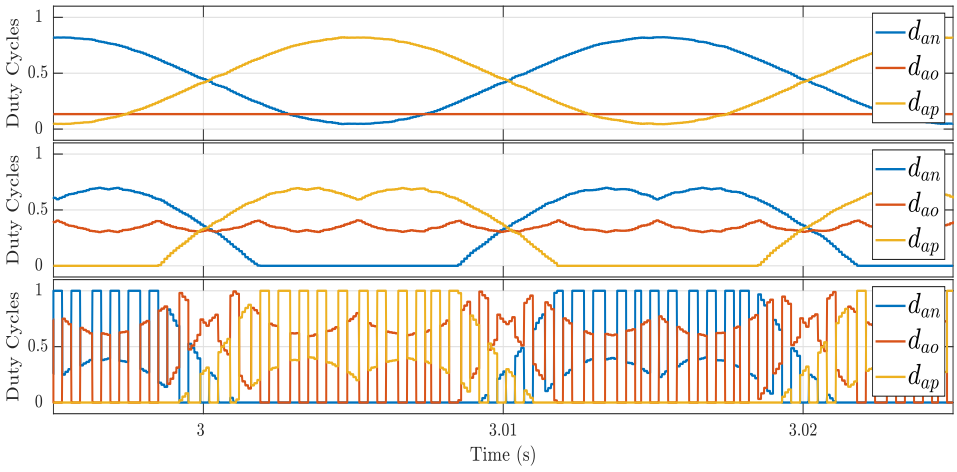

Figure 3.10 Simulation results: duty cycles of phase a considering ICM1 (top), ICM2 (mid) and Variant 3 (bottom).

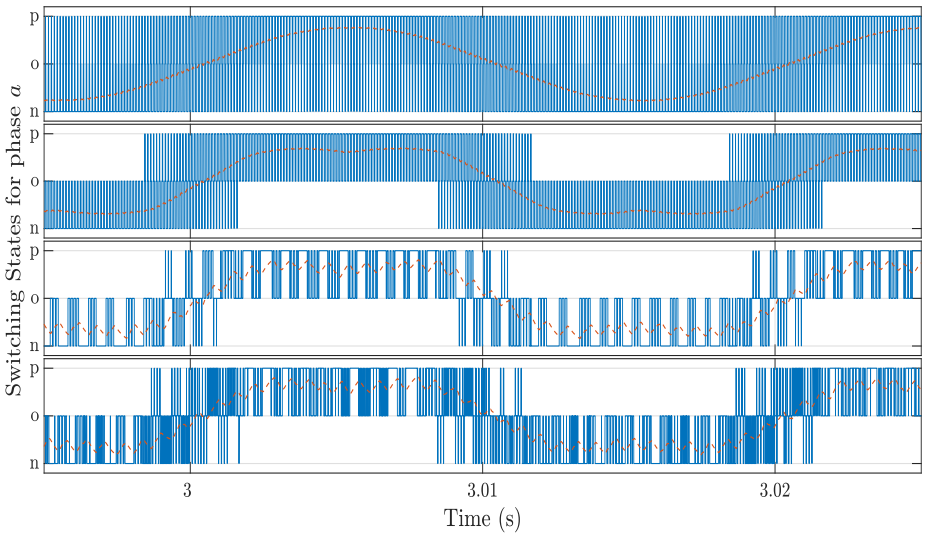

Figure 3.11 Simulation results: switching states of phase a and its averaged signal, considering ICM1 (top), ICM2 (mid-up), Variant 3 (mid-down) and mVSVPWM (bottom).

In conclusion, the results of the simulations performed with all the approaches are resumed in the table 3.3. In this table it is possible to observe the improvement in the THD, number of commutations and balance speed form Variant 3 to ICM2 and to ICM1.

Table 3.3 Simulations results of the considered approaches.

Approach	THD value	Number of commutations	Balancing time (Fig. 3.9)	Ripple
mVSVPWM	4.6%	412	0.17s	+
ICM1	5.6%	800	0.60s	++
ICM2	4.2%	522	0.5s	+
Variant 3	3.9%	281	0.2s	-

3.6 Experimental Results

This section presents the experimental results obtained in the laboratory. To this end, the three-level NPC converter shown in Fig. 3.12, has been used. It has been configured as rectifier and it has the same circuit and control parameters as those provided in Table 3.2. Appendix A shows the design and construction of this converter.

According to the simulations, similar changes in the load (R) and dc-link reference voltage (v_{dc}^{r}) are considered. The evolution of these two parameters was shown in Fig. 3.4.

In Fig. 3.13, the evolution of the instantaneous active power and its reference are shown for the proposed approaches and mVSVPWM. Notice a slight reduction in the power ripple

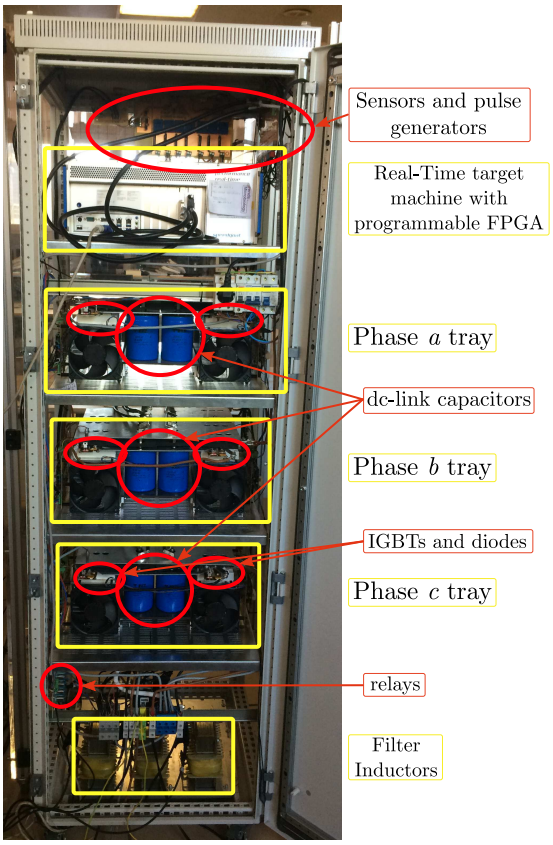

Figure 3.12 Experimental prototype of the three-level NPC rectifier.

from ICM1 to ICM2 that corresponds to a lower high-order harmonic component. This fact is due to the reduction in the total number of commutations that, given the presence of dead times, has also a direct effect on the low-order current harmonic components. In this figure it is also possible to observe how the Variant 3 approach has a ripple that is a little larger than the others. This is due to the fact that the control algorithm changes between x_{min} and x_{max} in a very repetitive way, thus introducing a lot of noise in the signals. This fact is not observed in Fig. 3.5 as the simulations do not take into account the electrical noise generated in the converter.

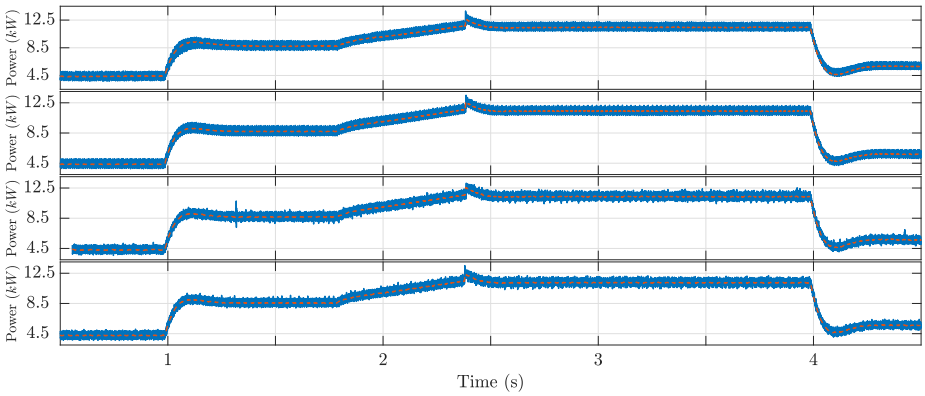

Figure 3.13 Experimental results: evolution of the instantaneous active power p (solid) and its reference value p^r (dashed), considering ICM1 (top), ICM2 (mid-up), Variant 3 (mid-down) and mVSVPWM (bottom) through the different stages of Fig. 3.4.

In Fig. 3.14, the evolution of the total dc-link voltage for all the control laws and their references are showed. As was observed in the simulations section (Fig. 3.6), the results of the dc-link voltage control are practically identical for all control laws.

In Fig. 3.15, the evolution of the capacitor voltages, starting from a situation of unbalance, is represented. This figure shows the effectiveness of the control law to balance the capacitor voltages compared with the same approach when the balancing control is deactivated. It can be easily seen that, when no balancing control is activated, the capacitors tend to equalize at a very slow rate which affects the current control performance during all this time period. Besides, consider that if the load is not balanced, only an active regulation, like the one used in this thesis, could correct this situation. In order to have a fair comparison, the result of applying the same voltage unbalance situation

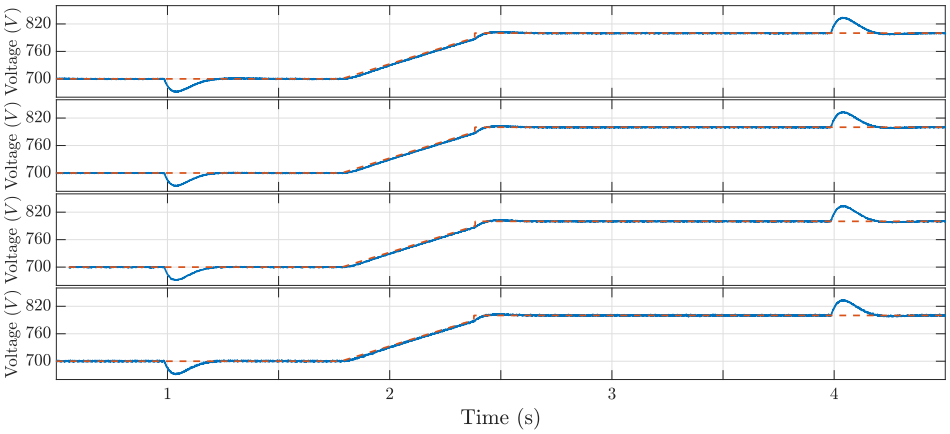

Figure 3.14 Experimental results: evolution of the total dc-link voltage v_{dc} (solid) and its reference value v_{dc}^{r} (dashed), considering ICM1 (top), ICM2 (mid-up), Variant 3 (mid-down) and mVSVPWM (bottom).

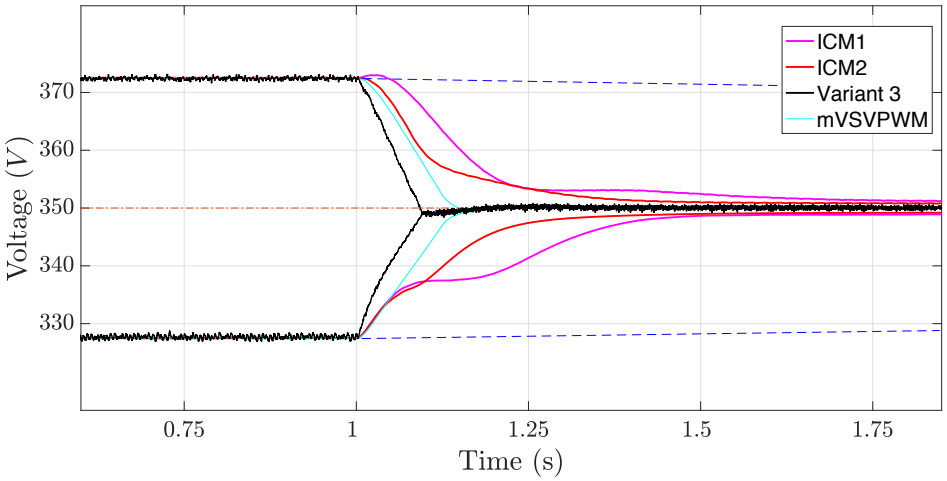

Figure 3.15 Experimental results: evolution of the capacitor voltages starting from an imbalanced condition, considering mVSVPWM, ICM1, ICM2 and Variant 3. The dashed lines refers to no-balancing control and the dash-dotted to the capacitor voltage reference.

to the mVSVPWM approach is also included in this figure. Under this conditions, the mVSVPWM approach corrects the unbalance faster than the ICM1 and ICM2 approaches. On the other hand, it can be observed that the Variant 3 approach corrects the imbalance faster than the other approaches, including mVSVPWM. Thus, the balance speed is quite

similar to that presented in Fig. 3.7, validating the model used to carry out the simulations.

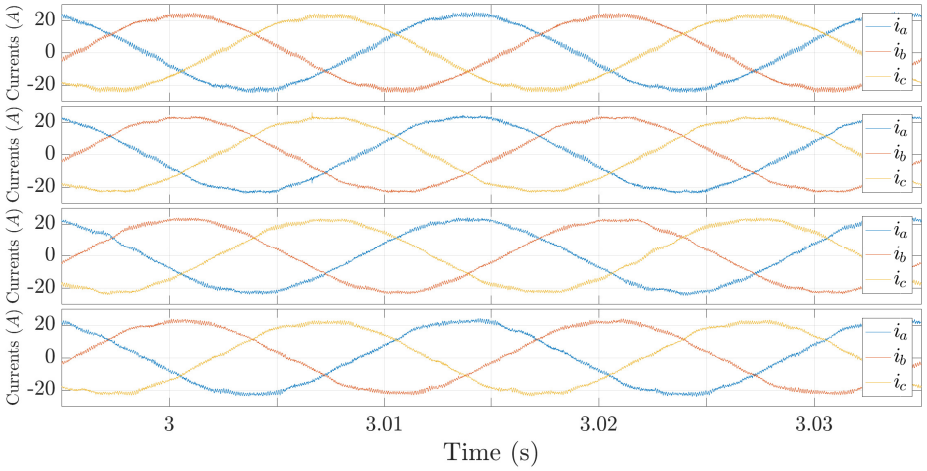

Figure 3.16 Experimental results: 3-phase grid currents considering ICM1 (top), ICM2 (mid-up), Variant 3 (mid-down) and mVSVPWM (bottom). $v_{dc}^{r} = 800$ V and $R = 60\,\Omega$.

In Fig. 3.16, the phase currents are shown for the proposed approaches and mVSVPWM. Total harmonic distortion (THD) values can also be retrieved from Fig. 3.16 along with the current harmonic spectrum and therefore they are depicted in Fig. 3.17. Notice that mVSVPWM and ICM1 presents a similar THD value (4.8% and 4.95% respectively), whereas ICM2 and Variant 3 have a considerably better result (4.19% and 4.37% respectively).

Applying the proposed approaches and mVSVPWM, the switching state of phase a can be obtained. These variables can be seen in Fig. 3.18. In this figure it is shown that, the ICM1 controller always switches among the three levels, positive (p), negative (n) and zero (o), while for ICM2 and Variant 3, this phase often only commutes between two levels. These data allow comparison of the number of commutations per period for each control law, yielding 800 commutations per grid period at 10 kHz of switching frequency in ICM1, 527 in ICM2, 265 in Variant 3 and 361 in mVSVPWM. As it is possible to see, the values of THD and the number of commutations obtained experimentally are very similar to those obtained in the simulation section.

Regarding the computational burden, the execution times for ICM1, ICM2 and Variant 3 are 67%, 61% and 40% faster respect of the time spent for the equivalent stage by mVSVPWM technique, showing the simplicity of the methods presented compared with

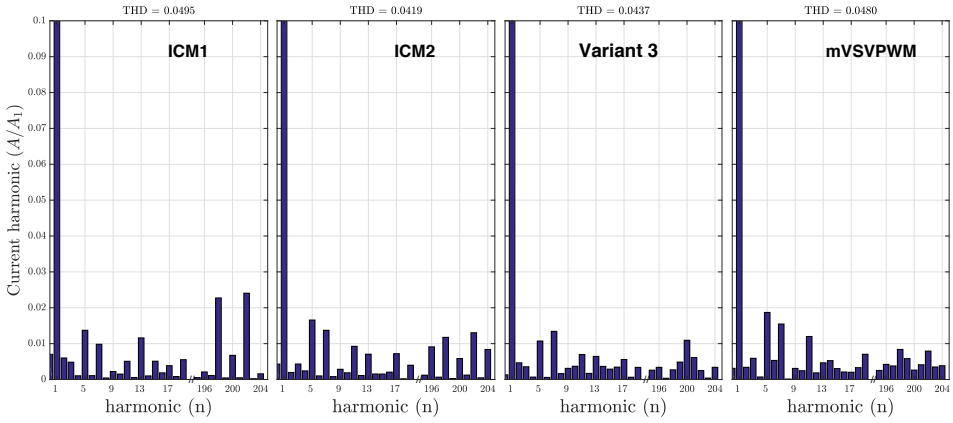

Figure 3.17 Experimental results: Harmonic spectrum of the current of phase a for the three approaches considered: ICM1, ICM2, Variant 3 and mVSVPWM .

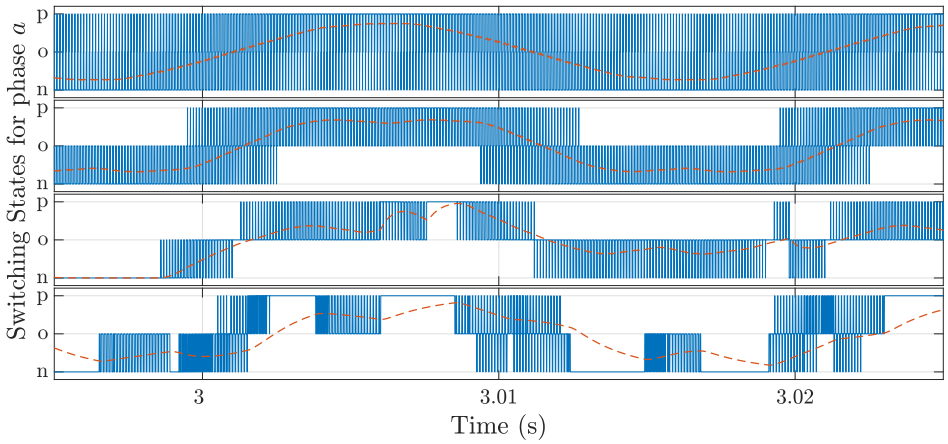

Figure 3.18 Experimental results: switching states of phase a (solid) and its averaged value (dashed), considering ICM1 (top), ICM2 (mid-up), Variant 3 (mid-down) and mVSVPWM (bottom).

mVSVPWM.

The duty cycles of the proposed control laws are shown in Figure 3.19. In this figure it is possible to observe, as indicated in the simulations section, how the duties of the ICM2 resemble those of an third-harmonic injection control law. In this way, it is possible to increase the modulation index without reaching saturation.

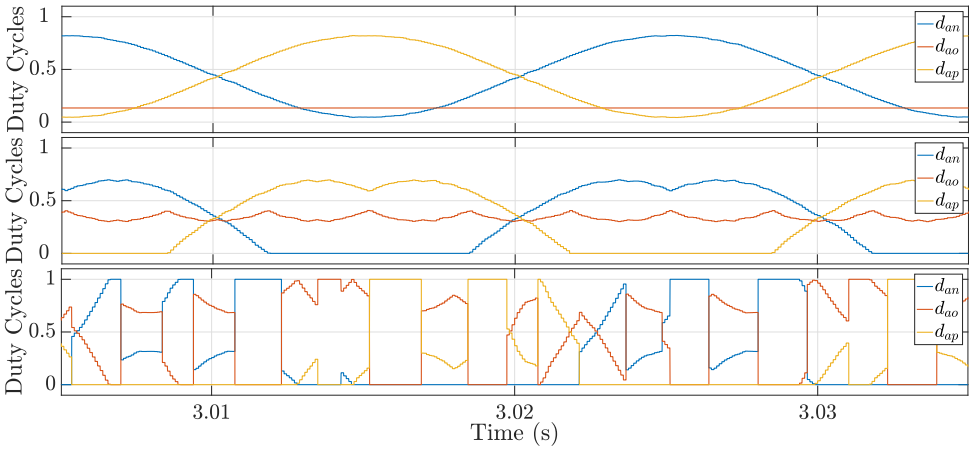

Figure 3.19 Experimental results: duty cycles of phase a considering ICM1 (top), ICM2 (mid) and Variant 3 (bottom).

3.7 Conclusions

In this chapter several control laws have been presented, the power or current controllers, total dc-link voltage and voltage balance, being this last one the main objective of control in this part of the thesis. Tacking into account this main objective, three approaches have been presented and compared with an existing technique. It is important to remember that the first approach (ICM1) was theoretically proposed in a previous work [44] and in this thesis it has been tested experimentally. The results of the comparison can be seen in table 3.4. In this table it is possible to observe that the THD values obtained in the three proposed variants are similar or better to the mVSVPWM technique. As discussed in this chapter, the first two variants improve the simplicity, expressed in the reduction of computational burden, at the cost of a higher number of commutations. This fact is solved in the third variant, where although the computational burden does not decrease so much, commutations are reduced considerably. Regarding the balancing time, again the first two variants are a bit slow achieving the voltage balance in the capacitors, being the third one even faster than mVSVPWM. It should be remembered that the first two variants have a trade-off between balancing speed and transient behaviour, expressed in the modification of some control parameters, which could improve the speed of the voltage balance.

As a final result of the comparison between all the techniques implemented, it can

Table 3.4 Main features of the considered approaches.

Approach	THD value	Number of commutations	Balancing time (Fig. 3.15)	Computational burden (% Reduction)
mVSVPWM	4.8%	361	0.15s	–
ICM1	4.95%	800	0.65s	67%
ICM2	4.19%	527	0.5s	61%
Variant 3	4.37%	265	0.10s	40%

be seen that the first proposed variant (ICM1), even though it is the simplest one, the worsening of THD, number of commutations and balance time is not compensated by the improvement in computational load. However, the modifications made from this technique in the second variant (ICM2) and the proposal of the third one (Variant 3), show very promising results with respect to the rest of the techniques.

4 Switched Affine Systems Modelling

If everything seems under control, you are not going fast enough

MARIO ANDRETTI

Contents

Dynamic systems are usually classified into two types of systems, continuous systems and discrete systems. However, there are certain systems, such as systems that combine analog and digital components such as a power converter, which can be classified into both groups. These types of systems are called hybrid systems [72].

One kind of this type of systems is the switched system that is a hybrid dynamical system consisting of several continuous-time subsystems and a rule that selects between

them [73, 74]. These systems present an interesting behavior. For example, it is possible to switch between asymptotically stable systems and obtain an unstable overall system, and on the other hand, to switch between unstable systems and obtain a stable overall switched system [75, 76]. A class of switched systems are the switched affine systems which are non-linear systems that are linear in the input [73, 77]. The control of this kind of systems presents a challenge since the different subsystems do not necessarily share a common equilibrium.

Many different works have been published proposing new control methods to get stabilization, like [78], where authors reformulate the stabilization of switched affine systems as a classical stabilization problem for nonlinear systems affine in the input, thus obtaining stability into a ball, or [77], where several control laws are designed in order to obtain stability in a set of equilibrium points. The objective of this last paper is to calculate the set and design the control law so that any system trajectory converges to the interior of the set. In these works, the equilibrium is achieved with infinite arbitrarily switching. In [79, 80], it is possible to find similar solutions for switched affine systems with dwell-time guarantees, ensuring a finite arbitrarily switching.

In many occasions it is necessary to control these kind of systems with periodic switching which are useful to describe periodic natural phenomena and also arise in linearisation of time-invariant dynamical systems around periodic orbits and when treating multi-rate systems where actuator and sensors operate at different frequencies [81]. This problem was dealt in [82], where simple criteria are given to optimize the choice of Lyapunov functions and a sampled-data switching control is designed to ensure robustness in switched affine systems. In that paper, the goal is to provide methods for the design of sampled-data switching laws that practically stabilize the system guaranteeing that the state converges to a compact set. This is first investigated for systems that admit a stable convex combination for the desired equilibrium and then is generalized to the rest of the systems using switched Lyapunov functions. The solution obtained in that paper turns out to be conservative due to the use of the Jensen inequality. In [79], robust stability for affine discrete systems using sampled-data controllers is investigated. In that paper, the different control strategies are also based on achieving convergence to a compact set. As can be seen, the solution is even more conservative than in [82].

In some applications, when discretizing these systems, if the sample time is very low, problems may appear to achieve convergence to the continuous solution, because of numerical issues. In [83], a comparison is made between the z operator (q in that work) and the δ operator to perform this discretization. There, it is possible to observe as the δ operator presents as advantages the natural convergence to a continuous system, while

avoiding numerical problems when the sampling period is very short. Thus, in [84] it is possible to observe that the delta operator is used to design the sliding mode fuzzy controller of a DC-DC buck converter due to the need for very fast sampling. Therefore, the use of the δ operator presents a great advantage in the design of controllers with very fast sampling times.

To address the control of systems with high-frequency sampling times, two controllers are presented in this thesis, inspired by [85], where δ operator is used taking into account the advantages of this operator mentioned previously. Therefore, due to the use of δ operator, less conservative results are obtained than those mentioned above for a non-linear affine system with a very fast switching frequency. Using all these resources, in section 5.1, a controller based on the Lyapunov function has been developed as well as another relaxed one in which the selection of the Lyapunov function and the design of the switching control law are decoupled.

For the cases when the sampling time is not excessively low and the z operator can be used without numerical problems, other two approaches are presented in section 5.2 without the need to use the δ operator. These control laws are based in the techniques presented in [86] to design periodic controllers for switching affine systems. These controllers guarantee the global asymptotic stabilization to a minimum invariant set including the origin, thanks to the solution of a simple optimization problem. It is also demonstrated that this relaxed control law includes Lyapunov matrix-based controllers as particular cases. In the controllers presented, the design is based on a quadratic Lyapunov function and guarantee global practical stabilization. The first one is based on a relaxed control law. The second one is a robust control that presents the possibility to apply the method to systems with parameter uncertainties. Although the δ operator has advantages over traditional discretization, it has not been used in these last controllers since they are designed for systems with low switching frequency, so that the traditional approach, based on [86], has very good results.

4.1 Problem Formulation for Systems with High-Frequency Sampling Time

This section focuses on a class of switched affine systems defined by

$$\dot{z} = A_\sigma z + a_\sigma, \tag{4.1}$$

where $z \in \mathbb{R}^n$ is the state and it is accessible and A_σ and a_σ present suited dimensions. The control action is performed through the high frequency switching signal $\sigma \in \mathbb{K}_N := \{1,2,...,N\}$, which may be only modified at sampling instants t_k, with $k \in \mathbb{N}$. The length of the sampling interval $t_{k+1} - t_k = T$ is assumed to be constant, known and very small.

Thus, this section focuses on the design problem of a feedback law for the high frequency periodic switching signal σ, in such a way to ensure suitable practical convergence properties of the plant state z to a operating equilibrium z_e, which is not necessarily an equilibrium for the continuous-time dynamics in (4.1), but can be obtained as an equilibrium for the switching system with arbitrary switching. A necessary and sufficient condition characterizing this equilibrium is then represented by the following standard assumption (see [74, 77]).

Assumption 1

There exists $\lambda = [\lambda_1,\lambda_2,...,\lambda_N]$ satisfying $\sum_{i\in\mathbb{K}} \lambda_i = 1$ and $0 \leq \lambda_i \leq 1$, such that the following convex combination holds:

$$\sum_{i\in\mathbb{K}} \lambda_i (A_i z_e + a_i) = A(\lambda) z_e + a(\lambda) = 0. \tag{4.2}$$

It is emphasized that Assumption 1 is both necessary and sufficient for the existence of a suitable switching signal ensuring forward invariance of the point z_e (namely inducing an equilibrium at z_e) when understanding solutions in the generalized sense of Krasovskii or Filippov. Indeed, under (4.2), we can conclude that the error equation of (4.1) is:

$$\dot{x} = A_\sigma x + B_\sigma, \tag{4.3}$$

where the error vector is denoted by $x := z - z_e$ and where the matrices B_σ are defined by $B_\sigma := A_\sigma z_e + a_\sigma$ and verify the following convex combination $\sum_{i\in\mathbb{K}} \lambda_i B_i = 0$. The objective is to ensure that the error state x converges to the equilibrium $x = 0$ in the Filippov sense.

In addition, the following property is assumed.

Assumption 2

The matrices A_i, for $i \in \mathbb{K}_N$ are non-singular and $A(\lambda)$ is Hurwitz.

4.1.1 Delta Operator for High-Frequency Switching Signals

In this subsection, a discrete-time model based on the δ operator [87] is proposed, which is suitable for high switching frequencies. The δ operator has been widely used in the literature to avoid numerical problems in the computation of discrete-time dynamics. This is based on the continuous ones in the situation where the sampling period T is potentially very small. The definition of the δ operator is as follows. For any function ξ from $\mathbb{R}^+$ to $\mathbb{R}^n$, the vector $\delta\xi_k$, at any sampling instant $t_k \in \mathbb{R}^+$, is defined as follows

$$\delta\xi_k := \frac{1}{T}(\xi_{k+1} - \xi_k), \qquad \forall k \geq 0,$$

where the convention $\xi_k = \xi(t_k)$ and $\delta\xi_k = \delta\xi(t_k)$ have been used, for all integer $k \geq 0$. Hence the dynamics of system (4.1) can be rewritten in the framework of the δ operator, which yields the following dynamics

$$\delta x_k = E_\sigma x_k + F_\sigma \tag{4.4}$$

where the matrices that defines the system dynamics are given by

$$E_\sigma = \tfrac{1}{T}(e^{A_\sigma T} - I), \qquad F_\sigma = \tfrac{1}{T}\int_0^T e^{A_\sigma(T-s)}dsB_\sigma. \tag{4.5}$$

The interest of this formulation compared to the usual discrete-time formulation comes from the fact that, when T goes to zero, matrices E_σ and F_σ converge to A_σ and B_σ, respectively. Another important issue is that matrices E_σ and F_σ depend explicitly on the switching period T. Indeed, considering small values of T, the usual discretization of (4.3) may lead to several numerical problems, which are avoided using the formulation (4.4).

Note that if matrix A_σ is non singular, then a simple expression of F_σ is provided by

$$F_\sigma = \frac{e^{A_\sigma T} - I}{T} A_\sigma^{-1} B_\sigma.$$

It is worth noting that model (4.4) does not account for the continuous evolution of (4.1) during the intersampling time. It is however possible to characterize the continuous solution by integrating the solution over a sampling interval, leading, for all $t \in [t_k, t_k + T]$

and for all $k \in \mathbb{N}$, to

$$x(t) = e^{A_\sigma(t-t_k)}x(t_k) + \int_{t_k}^{t} e^{A_\sigma(\tau-t_k)}d\tau a_\sigma$$

Since t belongs to the bound interval $[t_k, t_k + T]$, the solutions to the system are obviously bounded during the inter sampling time.

4.1.2 Control objectives

When considering switching affine system (4.3), its solutions do not necessarily converge to the origin but to a neighbourhood of it, generating a chattering effect around zero when employing sliding mode control [88]. Therefore, one has to relax the control objectives and to consider attractor sets, which are not necessarily reduced to the equilibrium set. In this way, an estimation of the attractive set is considered, which is of the following quadratic form

$$\mathcal{E} := \left\{ x \in \mathbb{R}^n, \quad x^\top S x \leq 1 \right\}. \tag{4.6}$$

where S is a symmetric positive definite matrix to be optimized. This formulation is quite usual and has been used in other contexts as in [80, 82, 85].

Therefore, the control objective is the design of a feedback law for the high frequency periodic switching signal σ, in such a way to ensure suitable practical convergence properties of the plant state x to zero, which is not necessarily an equilibrium for the continuous-time dynamics in (4.3), but can be obtained as an equilibrium for the switching system with arbitrary switching. A necessary and sufficient condition characterizing this equilibrium is then represented by the standard Assumption 2 (see [74, 77]). The problem can be summarized as follows

Problem 1

For any small sampling period T, the problem is to find a switching control law that selects, at each sampling time, the mode or subsystem among all possibilities that stabilizes system (4.1) with certain performance guarantees at its equilibrium.

4.2 Usual Discrete-Time Formulation for Switched Affine Systems

This section presents an alternative model to the formulation made in the previous section. In that section, an improvement in the results with respect to existing techniques has been shown, but it has a disadvantage. When using a Lyapunov function based on a matrix P different from the matrix that defines the attractor $\mathcal{E}$, there is a possibility that the evolution of the system reaches a point outside the level set that define $\Delta V < 0$ but remain within of the attractor. This fact can cause the system to become unstable. In this way, a new formulation has been used where the volume of the attractor depends directly on the matrix that defines the Lyapunov function. An improvement has also been included defining the center of the attractor at an optimal point that does not have to be the origin.

In this way, inspired by [86], we define again the system model as:

$$z^+ \quad = \quad A_\sigma z + a_\sigma \tag{4.7}$$

where $z \in \mathbb{R}^n$ is the state, z^+ represents the update of the system and matrices A_σ and a_σ present suited dimensions. The control action is performed through the switching signal $\sigma \in \mathbb{K} := \{1,2,...,N\}$, that selects at each instant of time one of the N subsystems.

Definition 1

Consider the set Ω_e given by

$$\Omega_e = \{z_e \in \mathbb{R}^n, \ \exists \lambda \in \Lambda_\mathbb{K}, \ (A_\lambda - I)z_e + a_\lambda = 0\} \tag{4.8}$$

where z_e is not necessarily an equilibrium for the continuous-time dynamics in (4.7), but can be obtained as equilibrium for the switching system with arbitrary switching, $\Lambda_\mathbb{K} := \left\{\lambda = (\lambda_1,\ldots,\lambda_N) \in [0,1]^N \,|\, \sum_{i\in\mathbb{K}} \lambda_i = 1\right\}$, $A_\lambda := \sum_{i\in\mathbb{K}} \lambda_i A_i$ and $a_\lambda := \sum_{i\in\mathbb{K}} \lambda_i a_i$.

Set Ω_e only characterizes some possible acceptable equilibriums for system (4.7). It is important to note that not all acceptable equilibriums belong to this set.

For a given z_e in Ω_e let us define the error variable $x := z - z_e$, where z is driven by system (4.7). Then, the error dynamics is governed by

$$x^+ = A_\sigma x + B_\sigma, \tag{4.9}$$

with $B_\sigma := (A_\sigma - I)z_e + a_\sigma$. Then, from Definition 1, the linear combination λ in $\Lambda_{\mathbb{K}}$ implies

$$B_\lambda := \sum_{i \in \mathbb{K}} \lambda_i B_i = 0 \text{ for } \lambda \in \Lambda_{\mathbb{K}}. \tag{4.10}$$

4.2.1 Control Objectives

As said in subsection 4.1.2, we will consider an estimation of an invariant set that includes the origin. Then, we introduce the set given by

$$\mathcal{A} := \{x \in \mathbb{R}^n, \quad V(x,x_c) \leq 1\}. \tag{4.11}$$

Which is defined by a level set of a Lyapunov function given by

$$V(x,x_c) = (x - x_c)^\top P (x - x_c), \tag{4.12}$$

where P is a positive definite matrix. In order to obtain less conservative results, the vector x_c will be used to shift the center of the level sets from the origin.

Thus, the objective is to design a robust control law for σ, which ensures that $\mathcal{A}$ is a neighbourhood of the origin and is globally asymptotically stable for system (4.9), which is also sought of minimum volume. This can be summarized as follows

(i) If x is not in $\mathcal{A}$, then $\Delta V(x,x_c) = V(x^+,x_c) - V(x,x_c)$ is negative definite.

(ii) The origin $x = 0$ belongs to $\mathcal{A}$.

(iii) If x belongs to $\mathcal{A}$, then x^+ also belongs to $\mathcal{A}$ under the dynamics of (4.9).

Asymptotic stability is a fundamental property of dynamical systems due to the fact that provides qualitative information about solutions, especially a characterization of the solutions' long-term trends [72]. As said before, the solution of a hybrid system often do not converge to an equilibrium point, so the asymptotic stability of a closed set is studied. Anyway, asymptotic stability of an equilibrium point is a particular case of the asymptotic stability of a closed set, since an equilibrium point is just a closed set formed with a single point.

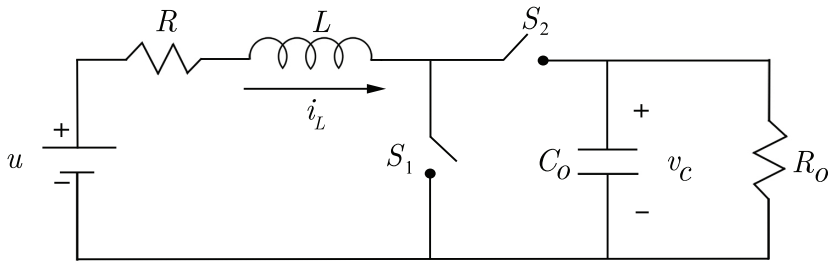

Figure 4.1 Schematic diagram of a boost converter.

4.2.2 Application to a DC-DC Converter

In order to use the expressions in (4.3) and (4.9) applied to a boost type DC-DC converter like the one shown in Fig. 4.1, it is possible to define the matrices A_σ and a_σ by

$$A_1 = \begin{bmatrix} -\frac{R}{L} & 0 \\ 0 & -\frac{1}{R_0 C_0} \end{bmatrix}, \quad a_1 = \begin{bmatrix} \frac{1}{L} \\ 0 \end{bmatrix} u$$

$$A_2 = \begin{bmatrix} -\frac{R}{L} & \frac{-1}{L} \\ \frac{1}{C_0} & -\frac{1}{R_0 C_0} \end{bmatrix}, \quad a_2 = \begin{bmatrix} \frac{1}{L} \\ 0 \end{bmatrix} u,$$

where S_1 and S_2 are the switches, u is the input voltage and R_0 is the load.

Due to the configuration of the converter, N is equal to 2, which are the two states defined by the possible positions of the switches. Thus, when σ is equal to 1, the switch S_1 is closed and the switch S_2 is open and when σ is equal to 2, the switch S_1 is open and the switch S_2 is closed. It must be remembered that the positions of the switches have to be the opposite each other, so when S_1 is open, S_2 must be closed and viceversa.

In this application, the error dynamics is defined by the state variable $x = [i_L \quad v_c]^\top$, where i_L denotes the inductor current and v_c the capacitor voltage.

This model will be used in the next chapter to show the numerical examples of the developed control design methods.

5 Control of Switched Affine Systems

If you want to find the secrets of the Universe, think in terms of energy, frequency, and vibration

NIKOLA TESLA

Contents

In the previous chapter, two models of switched affine systems were presented with application to a boost DC-DC converter. One model for systems with a high sampling frequency and on the other hand, a usual discrete-time formulation. In this chapter, different control laws for each of these models will be proposed. As mentioned in the introduction of this thesis, the objective is to minimize the chattering around the equilibrium point, reducing as much as possible the attractor set. Numerical results obtained in simulation will also be shown, where the advantages over an existing control law can be observed.

5.1 Control Laws for Systems with High-Frequency Sampling time

This section is dedicated to show the control laws developed for switched affine systems with high-frequency sampling time. Two laws will be shown as well as simulation results for each of them applied to a boost converter.

5.1.1 Lyapunov-Based Switching Control

Looking at the literature on switched affine systems, one can find the well-known min-projection control law for such a class of systems [82, 85, 89]. This type of control is used in this thesis to design all the controllers that will be presented in this chapter. The underlying idea of this control law is to select the mode of the system which minimizes the decrease of a quadratic Lyapunov function given by

$$V(x) := x^\top P x, \qquad \forall x \in \mathbb{R}^n \tag{5.1}$$

where $P \succ 0$ is a positive definite matrix of $\mathbb{R}^{n\times n}$. This idea is formalized in the first theorem developed in this chapter of the thesis.

Theorem 1

Consider Assumptions 1 and 2 in section 4.1 and matrices $P \succ 0$ and $S \succ 0$ of suited dimension that are solution to the feasibility problem

$$\Gamma_{ij}^{(1)} \prec 0, \quad \forall i,j \in \mathbb{K} \tag{5.2}$$

for any pair (i,j) in $\mathbb{K}^2$.

$$\begin{aligned} \Gamma_{ij}^{(1)} &= \Psi_i(P)+\mu_i \begin{bmatrix} S & 0 \\ 0 & -1 \end{bmatrix} + \gamma_i \left[\Psi_j(P)-\Psi_i(P)\right], \\ \Psi_i(P) &= \begin{bmatrix} PE_i+E_i^\top P+TE_i^\top PE_i & PF_i+TE_i^\top PF_i \\ F_i^\top P+TF_i^\top PE_i & TF_i^\top PF_i \end{bmatrix}, \end{aligned} \tag{5.3}$$

for some given parameters $\gamma_i > 0$ and $\mu_i > 0$. Then the switching control law (C1) defined by

$$\text{(C1)} \quad \sigma(x_k) = \underset{i\in\mathbb{K}_N}{\operatorname{argmin}} \begin{bmatrix} x_k \\ 1 \end{bmatrix}^\top \Psi_i(P) \begin{bmatrix} x_k \\ 1 \end{bmatrix} \tag{5.4}$$

guarantees ΔV<0 outside of set $\mathcal{E}$.

Proof. Consider the Lyapunov function given in (5.1), where $P \succ 0 \in \mathbb{R}^{n\times n}$. Let us first compute the expression of δV_k as follows

$$\begin{aligned} \delta V(x_k) &= \frac{1}{T}(V(x_{k+1})-V(x_k)) \\ &= \frac{1}{T}((x_k+T\delta x_k)^\top P(x_k+T\delta x_k)-x_k^\top P x_k) \\ &= 2\delta x_k^\top P x_k + T\delta x_k^\top P \delta x_k. \end{aligned} \tag{5.5}$$

Replacing δx_k by its expression given in (4.4), and using the definition of the matrix $\Psi_i(P)$ provided in (5.3) yields

$$\delta V(x_k) = \begin{bmatrix} x_k \\ 1 \end{bmatrix}^\top \Psi_\sigma(P) \begin{bmatrix} x_k \\ 1 \end{bmatrix}.$$

Using (5.3), the previous expression can be rewritten as follows, for any j in $\mathbb{K}$

$$\delta V(x_k) = \begin{bmatrix} x_k \\ 1 \end{bmatrix}^\top \left(\Gamma_{\sigma j}^{(1)} - \mu_\sigma \begin{bmatrix} S & 0 \\ 0 & -1 \end{bmatrix} - \gamma_\sigma \left[\Psi_j(P)-\Psi_\sigma(P)\right] \right) \begin{bmatrix} x_k \\ 1 \end{bmatrix}$$

Since the matrix inequalities $\Gamma_{i,j}^{(1)} \prec 0$ holds for any pair (i,j) in $\mathbb{K}^2$, we have

$$\delta V(x_k) \quad < \quad \mu_\sigma(1-x_k^\top S x_k) - \gamma_\sigma \begin{bmatrix} x_k \\ 1 \end{bmatrix}^\top \left[\Psi_j(P) - \Psi_\sigma(P)\right] \begin{bmatrix} x_k \\ 1 \end{bmatrix}$$

Note that the switching control law (5.4) ensures that the last term of the right hand side of the previous inequality is non positive, which guarantees that

$$\delta V(x_k) < \mu_\sigma(1-x_k^\top S x_k)$$

The previous inequality finally guarantees that for any values of x_k outside of $\mathcal{E}$ (i.e. $1-x_k^\top S x_k < 0$), the quantity $\delta V(x_k)$ is strictly negative, which concludes the proof. ■

5.1.2 Relaxed Switching Control

In the previous section, a Lyapunov-based switching control was proposed. This control was clearly inspired from the existing literature on switched affine systems such as [82, 85] but adapted to the δ operator modelling of DC-DC converters. The motivation of this section is to present a relaxed version of the previous control law. This relaxation considered here is related to the fact that the a priori intuition behind this Lyapunov-based control law might be too restrictive in the sense that the selection of the Lyapunov matrix P is done to verify two distinct purposes, namely, the definition of the Lyapunov function and the construction of the switching signal. Based on this comment, a relaxed control law can be provided by decoupling the two problems of selecting a Lyapunov function and of designing the switching control law.

The relaxed control law is based on the simple idea consisting of keeping the same structure of control law presented in (5.4). However, instead of using the Lyapunov matrix P, a new unconstrained matrix is introduced to define the switching law. This is formalized in the following theorem.

Theorem 2

Consider again Assumptions 1 and 2 in section 4.1, matrices $P \succ 0$ and $S \succ 0$ of suited dimension and a new matrix $N \in \mathbb{R}^{n\times n}$ that are solution to the feasibility problem

$$\Gamma_{ij}^{(2)} \prec 0, \quad \forall i,j \in \mathbb{K} \tag{5.6}$$

where, for any pair (i,j) in $\mathbb{K}^2$,

$$\Gamma_{ij}^{(2)} = \Psi_i(P) + \mu_i \begin{bmatrix} S & 0 \\ 0 & -1 \end{bmatrix} + \gamma_i \left[\Psi_j(N) - \Psi_i(N)\right], \tag{5.7}$$

where the matrices $\Psi_i(P)$ and $\Psi_i(N)$ are given in (5.3) and, again, for some given parameters $\gamma_i > 0$ and $\mu_i > 0$. Then the switching control law (C2) defined by

$$\text{(C2)} \quad \sigma(x_k) = \underset{i \in \mathbb{K}_N}{\operatorname{argmin}} \begin{bmatrix} x_k \\ 1 \end{bmatrix}^\top \Psi_i(N) \begin{bmatrix} x_k \\ 1 \end{bmatrix} \tag{5.8}$$

guarantees ΔV<0 outside of set $\mathcal{E}$.

Proof. The proof strictly follows the proof of Theorem 1, except that, now, the switching control law is not characterized by the Lyapunov matrix P but by an arbitrary matrix N, which only has to be a solution to the feasibility problem (5.6). ■

Remark 1

Compared to Theorem 1, there are two main advantages. The first one relies on the fact that matrix N is not required to be symmetric nor positive. The second one consists in the fact that the switching law is now completely decoupled from the definition of the Lyapunov function. Moreover, one can see that selection $N = P$ in Theorem 2 leads to the same statement as in Theorem 1. This ensures that the set of feasible solutions of (5.6) is greater than the ones of (5.2). It is then expected to derive relaxed solutions that will be presented in the example section where the optimization procedure presented later in Section 5.1.3 is included.

5.1.3 Optimisation Procedure

The feasibility problems proposed in Theorems 1 and 2, only ensure that there exists a switching control law that stabilizes the system to a bounded region around the equilibrium. Without an optimization process, the resulting regions might be too large to be relevant from the physical point of view. Indeed, considering a too large set $\mathcal{E}$ can possibly increase the chattering effects which are the main phenomena to avoid or limit in the control design of DC-DC converters. This chattering behavior can damage or even break the devices. Therefore, it is necessary to include an optimization procedure in these theorems, whose objective is to minimize the size of the set $\mathcal{E}$. Since this set is fully characterized by the symmetric positive definite matrix S, minimizing the size of $\mathcal{E}$ can be achieved by

maximizing the determinant of S. Based on the discussion above, the following proposition of stated dealing with the optimization of the solutions to the conditions of Theorems 1 and 2 is stated.

Proposition 1

For any a priori fixed scalar parameters μ_j and γ_i, the optimisation problem

$$\max_{S,P} \det(S), \quad \text{s.t.} \quad \Gamma_{ij}^{(c)} \prec 0, \quad \forall i,j \in \mathbb{K} \tag{5.9}$$

for any $c = \{1,2\}$, minimizes the size set (4.6) guaranteeing ΔV<0 outside of set $\mathcal{E}$.

Note that we do not optimize the chattering region, because it is constrained to an ellipse form and, the controller is also constrained for a given structure. Thus, it is expected that set $\mathcal{E}$ will be relaxed with the control given in Theorem 2, with respect to the control law C1.

Remark 2

This optimization process strongly depends on the selection of the scalar parameters γ_i and μ_j. Hence it is expected that an iterative procedure to selected the best parameters needs to be included.

Other optimization objectives can be considered such as the maximization of the eigenvalues of S, which can be done by maximizing a scalar τ such that $\tau I \leq S$.

5.1.4 Numerical Validations

The control laws introduced above are evaluated on a classical boost converter system. This converter switches at high frequency between two modes ($N = 2$) corresponding to two affine subsystems. The state variable is defined by $x = [i_L \quad v_c]^\top$, where i_L denotes the inductor current and v_c the capacitor voltage.

Parameters are taken from [77] for comparison with the switched control algorithm presented therein, which switches with arbitrary aperiodic switching in the steady-state. This type of switching tends to be complicated in physical applications. The considered nominal values are: $u = 100V$, $R = 2\Omega$, $L = 500\mu H$, $C_o = 470\mu F$ and $R_o = 50\Omega$. The

Table 5.1 Numerical values of μ_1,μ_2,γ_1 and γ_2.

Parameters	T_s	μ_1	μ_2	γ_1	γ_2
Th. 1	10^{-4}	9.84	9.86	0.948	0.0515
	10^{-5}	0.16	0.157	0.777	0.223
	10^{-6}	0.907	0.907	0.782	0.218
Th. 2	10^{-4}	3.16	3.16	0.916	0.327
	10^{-5}	1	1	0.349	0.1
	10^{-6}	0.313	0.313	10	2.793

switched system state space model (4.1) is defined by the following matrices for $i = 1,2$:

$$A_i = \begin{bmatrix} -\frac{R}{L} & \frac{(1-i)}{L} \\ \frac{(i-1)}{C_0} & -\frac{1}{R_0 C_0} \end{bmatrix}, \quad a_i = \begin{bmatrix} \frac{1}{L} \\ 0 \end{bmatrix} u.$$

The chosen simulation parameters are given by

$$z_e = \begin{bmatrix} 3 & 120 \end{bmatrix}^\top, \ \lambda = [0.22 \ \ 0.78]$$

for which simple calculations ensure the satisfaction of Assumption 2. The optimization problems given in Proposition 1 is solved using the CVX solver [90, 91]. The results obtained with this software illustrate our the efficiency of the new control law presented in Theorem 2 with respect to the Lyapunov-based controller employed in the literature, presented in Theorem 1.

As pointed out in Remark 2, the optimization scheme presented in Proposition 1 delivers different results for different values of γ_i and μ_j. Therefore, a random algorithm has been considered to obtain the best tuple of parameters. The values of these parameters μ_1,μ_2,γ_1 and γ_2, obtained for several values of the sampling period T_s are provided in Table 5.1.

Figure 5.1 shows the state trajectories, set $\mathcal{E}$ and $\delta V > 0$ surface in the state-plane for the different controllers given in Proposition 1, as well as for different sampling periods. Note that the $\delta V > 0$ surface is in the interior of the set $\mathcal{E}$ as is expected from Theorem 1 and 2. Remark also as $\mathcal{E}$ is reduced, as T_s decreases. We can see that set $\mathcal{E}$ is reduced with control law C2 with respect to C1, showing as the control law C2 provide reduced region of attraction with respect to C1. This is consistent with Remark 1. Another important remark concerns the fact that the region where $\delta V > 0$ is concentrated in a smaller area in control law C2 with respect to C1.

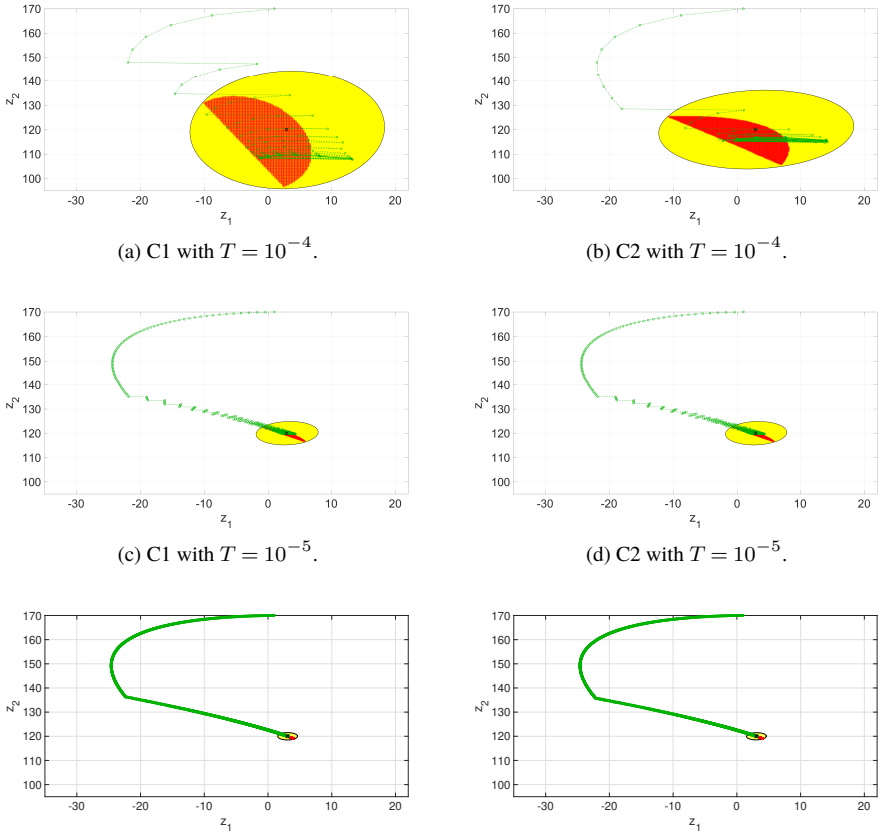

(a) C1 with $T = 10^{-4}$.

(b) C2 with $T = 10^{-4}$.

(c) C1 with $T = 10^{-5}$.

(d) C2 with $T = 10^{-5}$.

(e) C1 with $T = 10^{-6}$.

(f) C2 with $T = 10^{-6}$.

Figure 5.1 Numerical results of Proposition 1. Time trajectories (green), set $\mathcal{E}$ (yellow) and $\delta V > 0$ (red).

These simulations demonstrate the advantages of the relaxed control law over the existing Lyapunov-based one. Indeed, the proposed controller C2 allows to control efficiently the DC-DC converter under study even with relatively high sampling period with a notable reduction of the switches of the system, which ensures an increase of the lifespan and the reduction of the dissipated energy.

5.2 Control Laws for the Usual Discrete-Time Formulation of Switched Affine Systems

In this section two design methods will be presented, the first one is for nominal systems while the second is aimed to obtain robustness against model parameter variations of the usual discrete-time formulation of switched affine systems presented in section 4.2. Also a control design method already existing in the literature will be presented, which will serve to perform a comparison in terms of robustness and optimization.

5.2.1 Basic Switching control

In this section, a novel stabilization theorem based on a relaxed control law is proposed. This theorem notably differs from the classical Lyapunov matrix-based min-projection control law developed in [82, 86, 89], for instance. This type of control law implies that the controller corresponding to the smallest Lyapunov function should be selected.

The first theorem proposed is formalized as follows

Theorem 3

For a given z_e in Ω_e, assume that there exist $P \in \mathbb{R}^{n\times n} \succ 0$, $h \in \mathbb{R}^n$, $N_i = N_i^\top \in \mathbb{R}^{(n+1)\times(n+1)}$ and $\mu \in (0,1)$, solution to the optimization problem

$$\min_{P,h,N_i,\mu} \quad -\log\left(\det(P)\right), \tag{5.10}$$

$$\text{s.t. } P \succ 0, \tag{5.11}$$

$$\begin{bmatrix} \Psi_i + N_\lambda - N_i - \begin{bmatrix} 0 & 0 \\ * & \mu \end{bmatrix} & \mu \begin{bmatrix} P \\ h^\top \end{bmatrix} \\ * & -\mu P \end{bmatrix} \prec 0, \forall i \in \mathbb{K}, \tag{5.12}$$

where λ is the linear combination related to z_e in Definition 1 (Section 4.2) and

$$\Psi_i := \begin{bmatrix} A_i & B_i \\ 0 & 1 \end{bmatrix}^\top \begin{bmatrix} P & h \\ * & 0 \end{bmatrix} \begin{bmatrix} A_i & B_i \\ 0 & 1 \end{bmatrix} - \begin{bmatrix} P & h \\ * & 0 \end{bmatrix}. \tag{5.13}$$

$$N_\lambda := \sum_{i \in \mathbb{K}} \lambda_i N_i. \tag{5.14}$$

Then, the switching control law, given by

$$\sigma \in \underset{i \in \mathbb{K}}{\operatorname{argmin}} \begin{bmatrix} z - z_e \\ 1 \end{bmatrix}^\top N_i \begin{bmatrix} z - z_e \\ 1 \end{bmatrix}, \tag{5.15}$$

ensures that set $\mathcal{A}$, with $x = z - z_e$, fulfills properties (i), (ii) and (iii) of Problem 1 for system (4.7).

It should be note that control law σ in (5.15) is defined as an inclusion to allow the possibility of having several modes resulting from the min-projection control law. This is an important issue for the well-posedness of the system.

The minimization problem presented in Theorem 3 is similar to the one presented in [86]. The main motivation of minimizing $-\log(\det(P))$ is related to the minimization of the volume of set $\mathcal{A}$ through the maximization of eigenvalues of the positive definite matrix P. Indeed, the volume of the ellipsoid characterized by $V(x,x_c) \leq 1$ is proportional to $(\det(P))^{-1/2}$. In this section, the evaluation of performance will be based on the minimum value of $(\det(P))^{-1/2}$, obtained in several situations. This represents another improvement respect to the formulation made in the section before.

Remark 3

The non-convex optimization problem (5.10)-(5.12) can be reformulated as a Linear Matrix Inequality (LMI), and consequently into a convex problem, by fixing parameter μ in $(0,1)$. Then, a line-search routine on $\mu \in (0,1)$ allows finding the optimum.

In the next proof, it will be demonstrated that the controller designed fulfills (i), (ii) and (iii).

Proof. Proof of (i): Assume that there exist a positive definite matrix P, a vector h and symmetric matrices N_i, $i \in \mathbb{K}$ that are solution to (5.10)-(5.12) for a given positive parameter $\mu \in (0,1)$, following Remark 3. Then, consider Lyapunov function $V(x,x_c) = (x-x_c)^\top P(x-x_c)$, defined in (4.12), with $x = z - z_e$ and $x_c = -P^{-1}h$ given by

$$V(x,-P^{-1}h) := (x+P^{-1}h)^\top P(x+P^{-1}h). \tag{5.16}$$

It is clear that the assumption on the positive definiteness of matrix P ensures the positive definiteness of V. The computation of the forward increment of the Lyapunov function is given by

$$\begin{aligned} \Delta V(x,-P^{-1}h) &= V(x^+,-P^{-1}h) - V(x,-P^{-1}h) \\ &= (x^+ + P^{-1}h)^\top P(x^+ + P^{-1}h) \\ &\quad -(x+P^{-1}h)^\top P(x+P^{-1}h) \\ &= {x^+}^\top P x^+ - x^\top P x + 2(x^+ - x)^\top h. \end{aligned}$$

Replacing x^+ by its expression $x^+ = A_\sigma x + B_\sigma$, the forward increment of the Lyapunov function can be rewritten as follows

$$\Delta V(x,-P^{-1}h) = \begin{bmatrix} x \\ 1 \end{bmatrix}^\top \Psi_\sigma \begin{bmatrix} x \\ 1 \end{bmatrix},$$

where $\sigma \in \mathbb{K}$, corresponds to the active mode at the current time and where Ψ_σ is defined in (5.13) with $i = \sigma$. In order to include the selection of the control law (5.15) and the fact that $x \notin \mathcal{A}$, two additional steps are required. First, the switching control law (5.15) ensures

$$\begin{aligned} \sigma \in \underset{i\in\mathbb{K}}{\operatorname{argmin}} \begin{bmatrix} x \\ 1 \end{bmatrix}^\top N_i \begin{bmatrix} x \\ 1 \end{bmatrix} \quad &\Rightarrow \quad \begin{bmatrix} x \\ 1 \end{bmatrix}^\top (N_i - N_\sigma) \begin{bmatrix} x \\ 1 \end{bmatrix} \geq 0, \forall i \in \mathbb{K}, \\ &\Rightarrow \quad \begin{bmatrix} x \\ 1 \end{bmatrix}^\top (N_\lambda - N_\sigma) \begin{bmatrix} x \\ 1 \end{bmatrix} \geq 0, \forall \lambda \in \Lambda_{\mathbb{K}}. \end{aligned} \tag{5.17}$$

The second step is related to the fact that the negative definiteness of ΔV is only required outside $\mathcal{A}$, i.e. for any $x \in \mathbb{R}^n$, such that $V(x,P^{-1}h) \geq 1$, which can be easily rewritten as follows

$$\forall x \notin \mathcal{A}, \quad \begin{bmatrix} x \\ 1 \end{bmatrix}^\top \begin{bmatrix} P & h \\ * & h^\top P^{-1} h - 1 \end{bmatrix} \begin{bmatrix} x \\ 1 \end{bmatrix} \geq 0.$$

Hence, to summarize the previous computations, (i) holds if, for a given parameter $\mu \in (0,1)$ and λ satisfying Definition 1, there exist matrices P, h and N_i such that

$$\begin{bmatrix} x \\ 1 \end{bmatrix}^\top \Psi_\sigma \begin{bmatrix} x \\ 1 \end{bmatrix} < 0$$

holds for all (x,σ) in $\mathbb{R}^n \times \mathbb{K}$ that verify

$$\begin{bmatrix} x \\ 1 \end{bmatrix}^\top \begin{bmatrix} P & h \\ * & h^\top P^{-1} h - 1 \end{bmatrix} \begin{bmatrix} x \\ 1 \end{bmatrix} \geq 0, \quad \begin{bmatrix} x \\ 1 \end{bmatrix}^\top (N_\lambda - N_\sigma) \begin{bmatrix} x \\ 1 \end{bmatrix} \geq 0.$$

Using two successive S-procedures as in [86], which introduces unavoidably some conservatism, this problem is recast into the existence of a parameter $\mu > 0$ such that

$$\Psi_\sigma + N_\lambda - N_\sigma + \mu \begin{bmatrix} P & h \\ * & h^\top P^{-1} h - 1 \end{bmatrix} \prec 0, \ \sigma \in \mathbb{K}. \tag{5.18}$$

The proof is concluded by noting that matrix $\left[\begin{smallmatrix} P & h \\ * & h^\top P^{-1} h \end{smallmatrix}\right]$ can be rewritten as $\left[\begin{smallmatrix} P \\ h^\top \end{smallmatrix}\right] P^{-1} \left[\begin{smallmatrix} P \\ h^\top \end{smallmatrix}\right]^\top$, so that the application of the Schur complement leads to condition (5.12).

Proof of (ii): The objective is here to prove that LMI (5.12) ensures that the origin belongs to $\mathcal{A}$. Formally, this means

$$V(0, -P^{-1}h) = h^\top P^{-1} h \leq 1. \tag{5.19}$$

To proceed with this proof, let us compute the linear combination of (5.18), weighted by λ. This yields

$$\sum_{i \in \mathbb{K}} \lambda_i \left(\Psi_i + N_\lambda - N_i + \mu \begin{bmatrix} P & h \\ * & h^\top P^{-1} h - 1 \end{bmatrix} \right) \prec 0.$$

Noting that $\sum_{i \in \mathbb{K}} \lambda_i = 1$ and $\sum_{i \in \mathbb{K}} \lambda_i N_i = N_\lambda$, the previous inequality reduces to

$$\Psi_\lambda + \mu \begin{bmatrix} P & h \\ * & h^\top P^{-1} h - 1 \end{bmatrix} \prec 0, \tag{5.20}$$

where $\Psi_\lambda = \sum_{i\in\mathbb{K}} \lambda_i \Psi_i$, and is given by

$$\Psi_\lambda = \begin{bmatrix} \sum_{i\in\mathbb{K}} \lambda_i A_i^\top P A_i - P & \sum_{i\in\mathbb{K}} \lambda_i A_i^\top P B_i - (I - A_\lambda^\top)h \\ * & \sum_{i\in\mathbb{K}} \lambda_i B_i^\top P B_i \end{bmatrix}, \tag{5.21}$$

where $B_\lambda = 0$ have been used . A necessary condition for this inequality is that the last diagonal term located at position $(n+1,n+1)$ is negative definite, which corresponds to $\sum_{i\in\mathbb{K}} \lambda_i B_i^\top P B_i + h^\top P^{-1} h - 1 < 0$, which ensures (5.19) since the first term is positive.

Proof of (iii): Let us assume that x is in set $\mathcal{A}$. From (5.12), we know that

$$\begin{aligned} V(x^+, -P^{-1}h) - V(x, -P^{-1}h) \\ + \mu \big(V(x, -P^{-1}h) - 1\big) + C_\sigma < 0, \end{aligned}$$

where $C_\sigma = [\begin{smallmatrix} x \\ 1 \end{smallmatrix}]^\top (N_\lambda - N_\sigma) [\begin{smallmatrix} x \\ 1 \end{smallmatrix}]$ is known to be positive according to (5.17). Hence, we have

$$\begin{aligned} V(x^+, -P^{-1}h) &\leq (1-\mu) V(x, -P^{-1}h) + \mu - C_\sigma \\ &\leq (1-\mu) V(x, -P^{-1}h) + \mu. \end{aligned}$$

Since x belongs to $\mathcal{A}$, we know, by definition, that $V(x, -P^{-1}h) \leq 1$. Since the parameter μ has been selected in $(0,1)$, $1-\mu$ is positive, so that we have

$$V(x^+, -P^{-1}h) \leq (1-\mu) + \mu = 1,$$

which means that x^+ also belongs to $\mathcal{A}$.
The optimization regarding parameter μ has to be performed using a line-search routine on $(0,1)$, c.f. Remark 3, which concludes the proof. ■

Remark 4

As mentioned in this proof, condition (5.12) imply inequality (5.20). Another necessary condition of (5.12) apart from $0 \in \mathcal{A}$, is obtained from the definition of matrices Ψ_i, which leads to inequality $\sum_{i\in\mathbb{K}} \lambda_i A_i^\top P A_i - (1-\mu) P \prec 0$. This necessary condition will be commented in the next section.

Comparison with the optimal control design of [86]

In this section, it is shown as the solution given in [86] for system (4.7) is included in the solutions given in Theorem 3. First of all, the statement of [86, Theorem 3] is recalled. This theorem has been reformulated in order to be consistent with the presentation of this thesis.

Theorem 4 [86]

For a given z_e in Ω_e, and the associated linear combination λ related to Definition 1, assume that matrices P,$W \in \mathbb{R}^{n\times n} \succ 0$ and parameter $\beta > 0$ are the solution to the optimization problem

$$\min_{P,W,\beta} \quad -\log\left(\det(P)\right), \tag{5.22}$$

$$\text{s.t. } P \succ 0, \tag{5.23}$$

$$\sum_{i\in\mathbb{K}} \lambda_i A_i^\top P A_i - P < -W \tag{5.24}$$

$$\sum_{i\in\mathbb{K}} \lambda_i \begin{bmatrix} \beta W & 0 & -P \\ * & 1-\beta B_i^\top P B_i & -h_*^\top \\ * & * & P \end{bmatrix} > 0, \tag{5.25}$$

where $h_* = (1 - A_\lambda^\top)^{-1} \sum_{i\in\mathbb{K}} \lambda_i A_i^\top P B_i$.

Then, the switching control law, given by

$$\sigma^* \in \underset{i\in\mathbb{K}}{\operatorname{argmin}}\, V(A_i(z - z_e) + B_i, -P^{-1}h_*), \tag{5.26}$$

where V corresponds to the Lyapunov function (4.12), ensures that $\mathcal{A}$, with $x = z - z_e$, fulfills properties (i), (ii) and (iii) of Problem 1 for system (4.7).

Remark 5

The interest of this theorem relies on the optimality of a min-max problem that provides the smallest upper bound of the decrement of V. This optimal value of the shifting vector h is given by the expression $h_* = (1 - A_\lambda^\top)^{-1} \sum_{i\in\mathbb{K}} \lambda_i A_i^\top P B_i$. However, this selection of h_* is performed regardless the minimization of volume of the invariant set $\mathcal{A}$.

In order to validate the potential of Theorem 3 over Theorem 4, there is a need to

understand if the optimal solution to Theorem 4 is also a solution provided in Theorem 3. This property is summarized in the following proposition.

Proposition 2

Solution (P_*,h_*,β) of Theorem 4 is also solution to the minimization problem of Theorem 3.

Proof. Note that the control law (5.26) provided in [86] can be expressed as the control law (5.15) provided in Theorem 3 using the Ψ_i matrices defined in (5.13), with $P = P_*$, since

$$\sigma^* \in \underset{i\in\mathbb{K}}{\operatorname{argmin}} \begin{bmatrix} x \\ 1 \end{bmatrix}^\top \left(\Psi_i + \begin{bmatrix} P_* & h_* \\ * & 0 \end{bmatrix} \right) \begin{bmatrix} x \\ 1 \end{bmatrix}, \tag{5.27}$$

where $x = z - z_e$ and the free matrices N_i are given by $\Psi_i + \left[\begin{smallmatrix} P_* & h_* \\ * & 0 \end{smallmatrix}\right]$. Hence, re-injecting this expression into (5.12) yields

$$\begin{aligned} \Gamma_i &:= \begin{bmatrix} \Psi_i + \Psi_\lambda - \Psi_i - \begin{bmatrix} 0 & 0 \\ * & \mu \end{bmatrix} & \mu \begin{bmatrix} P_* \\ h_*^\top \end{bmatrix} \\ * & -\mu P_* \end{bmatrix}, \quad i \in \mathbb{K} \\ &:= \begin{bmatrix} \Psi_\lambda - \begin{bmatrix} 0 & 0 \\ * & \mu \end{bmatrix} & \mu \begin{bmatrix} P_* \\ h_*^\top \end{bmatrix} \\ * & -\mu P_* \end{bmatrix}, \quad i \in \mathbb{K}, \end{aligned} \tag{5.28}$$

where $\Psi_\lambda = \sum_{i\in\mathbb{K}} \lambda_i \Psi_i$. Already note from the previous expression, that the definition of Γ_i does not depend on the mode i. Therefore, it is possible to omit the subscript i and only consider $\Gamma_i = \Gamma$, for all i in $\mathbb{K}$.

It can be note from the definition of h_* ensures that the non diagonal entry of (5.21), verifies

$$\sum_{i\in\mathbb{K}} \lambda_i A_i^\top P_* B_i - (I - A_\lambda^\top) h_* = 0.$$

Therefore, from (5.21) and (5.24), the following upper bound of Γ is derived

$$\Gamma \prec -\mu \underbrace{\begin{bmatrix} \mu^{-1}W & 0 & -P_* \\ * & 1-\mu^{-1}\sum_{i\in\mathbb{K}} \lambda_i B_i^\top P_* B_i & -h_*^\top \\ * & * & P_* \end{bmatrix}}_{\succ 0 \text{ with } \mu=\beta^{-1}.} \prec 0.$$

In order to be complete, it remains to prove that parameter $\mu = \beta^{-1}$ belongs to the interval $(0,1)$. To do that, notice that a necessary condition for constrain (5.25) to hold is that matrix $\left[\begin{smallmatrix} \beta W & -P_* \\ -P_* & P_* \end{smallmatrix}\right]$ is positive definite or, equivalently, $W \succ \beta^{-1} P_*$, which together with (5.24) requires the satisfaction of $\sum_{i\in\mathbb{K}} \lambda_i A_i^\top P_* A_i - (1-\beta^{-1}) P_* \prec 0$. This inequality cannot be satisfied unless $\mu = \beta^{-1}$ belongs to $(0,1)$, which concludes the proof. ■

The previous proposition demonstrates that the optimal solution presented in [86] is also a solution of the optimization problem (5.10)–(5.12). This means that Theorem 3 provides, at least, the same optimal solution as Theorem 4. Moreover, since the control law defined in Theorem 3 has more degrees of freedom, one may expect that it may even relax some constraints and provides less conservative solutions. Another advantage of the unstructured control matrices N_i's over the Lyapunov matrix-based control law relies on the fact that they are decoupled from the Lyapunov matrix P. This means that there is no need to introduce an additional parameter to the LMI when applying the S-procedure to account for control law (5.15), which generally introduces additional conservatism.

It is possible to see that both Theorems 3 and 4 include the same necessary condition given in Remark 4. This means, again, that both theorems have the same limitations. However, in light of Proposition 2, Theorem 3 can provide a smaller estimation of the set $\mathcal{A}$, thanks to the relaxed control law (5.15).

It is worth noting that the conditions of Theorem 4 are computationally less demanding than those of Theorem 3. Indeed, Theorem 3 introduces the control matrices N_i as decisions variables of the minimization problem and the number of LMIs to be verified increases linearly with the number of modes.

5.2.2 Robust controlled system

Another interest of the presented approach over [86] concerns the design of a robust switching control law for uncertain switched affine systems. In this situation, matrices A_i and B_i may be subject to parameter uncertainties. Therefore, it is not possible to define a

control law as in (5.26), which depends explicitly on the precise knowledge of the model. However, the conditions of Theorem 3 can be straightforwardly extended to the robust stabilization of switched affine systems as provided below.

Let us now assume that the matrices A_i,B_i are subject to parameter uncertainties, that are, for the sake of simplicity, expressed as polytopic uncertainties. This means that

$$\begin{bmatrix} A_i, & a_i \end{bmatrix} \in \mathrm{Co}\left(\begin{bmatrix} A_i^j, & a_i^j \end{bmatrix} \right)_{j \in \mathbb{D}}, \quad \forall i \in \mathbb{K}, \tag{5.29}$$

where $\mathbb{D}$ is a bounded subset of $\mathbb{N}$, and where matrices A_i^j and a_i^j, for (i,j) in $\mathbb{K} \times \mathbb{D}$, are constant and known. The uncertainties in model (4.7) can be alternatively rewritten for model (4.9) by defining $B_i^j := (A_i^j - I)z_e + a_i^j$, for (i,j) in $\mathbb{K} \times \mathbb{D}$. Note that other types of uncertainties can be easily undertaken, as norm-bounded ones. Indeed, since the condition of Theorem 3 is convex respect to A_i and B_i several manipulations would allow one to derive a robust stabilization theorem dedicated to this situation. The motivation for considering polytopic-type uncertainties arises from the fact that it requires less technical manipulations.

It also has to be noted that the equilibrium and the convex combination parameters λ are defined for a given nominal system included in the polytope. In other words, let us consider given so-called nominal matrices $\begin{bmatrix} A_{i0}, & B_{i0} \end{bmatrix} \in \mathrm{Co}\left(\begin{bmatrix} A_i^j, & B_i^j \end{bmatrix} \right)_{j \in \mathbb{D}}$, for all $i \in \mathbb{K}$. In this context, the following theorem holds.

Theorem 5

For a given z_e in Ω_e associated to some nominal matrices $[A_{i0},B_{i0}]$, assume that there exist $P \in \mathbb{R}^{n \times n} \succ 0$, $h \in \mathbb{R}^n$, $N_i = N_i^\top \in \mathbb{R}^{(n+1)\times(n+1)}$ and $\mu \in (0,1)$, solution to the optimization problem

$$\min_{P,h,N_i,\mu} \quad -\log\left(\det(P)\right), \tag{5.30}$$

$$\text{s.t. } P \succ 0, \tag{5.31}$$

$$\begin{bmatrix} \Psi_i^j + N_\lambda - N_i - \begin{bmatrix} 0 & 0 \\ * & \mu \end{bmatrix} & \mu \begin{bmatrix} P \\ h^\top \end{bmatrix} \\ * & -\mu P \end{bmatrix} \prec 0, \tag{5.32}$$

for any $(i,j) \in \mathbb{K} \times \mathbb{D}$, where λ is the linear combination related to z_e in Definition 1 and

$$\Psi_i^j := \begin{bmatrix} A_i^j & B_i^j \\ 0 & 1 \end{bmatrix}^\top \begin{bmatrix} P & h \\ * & 0 \end{bmatrix} \begin{bmatrix} A_i^j & B_i^j \\ 0 & 1 \end{bmatrix} - \begin{bmatrix} P & h \\ * & 0 \end{bmatrix}. \tag{5.33}$$

Then, the switching control law given by

$$\sigma \in \underset{i \in \mathbb{K}}{\operatorname{argmin}} \begin{bmatrix} z - z_e \\ 1 \end{bmatrix}^\top N_i \begin{bmatrix} z - z_e \\ 1 \end{bmatrix}, \tag{5.34}$$

ensures that $\mathcal{A}$, with $x = z - z_e$, fulfills properties (i), (ii) and (iii) of Problem 1 for system (4.7) with (5.29).

Proof. Following Remark 3, parameter μ results from a line-search optimization, and therefore can be considered in the proof as a given scalar in $(0,1)$. The proof of Theorem 5 is based on the convexity of the quadratic term (5.33), which can be summarized, as follows

$$\begin{bmatrix} A_i & B_i \\ 0 & 1 \end{bmatrix}^\top \begin{bmatrix} P & h \\ * & 0 \end{bmatrix} \begin{bmatrix} A_i & B_i \\ 0 & 1 \end{bmatrix} - \begin{bmatrix} P & h \\ * & 0 \end{bmatrix} \leq \sum_{j \in \mathbb{D}} \bar{\lambda}_j \Psi_i^j \ ,$$

where the fact that matrices $[A_i \ B_i]$ can be rewritten as $\sum_{j \in \mathbb{D}} \bar{\lambda}_j [A_i^j \ B_i^j]$ have been used, for some positive scalar coefficients $\bar{\lambda}_j$, that verify $\sum_{j \in \mathbb{D}} \bar{\lambda}_j = 1$. The remainder of the proof directly follows the lines of the proof of Theorem 3. ■

Remark 6

Note that LMI (5.12) with matrices A_i and B_i fulfilling (5.29) is more constrained than the nominal one. Consequently the volume of $\mathcal{A}$ computed with Theorem 3 will be equal or smaller than with Theorem 5.

Remark 7

Note that the solutions to Theorem 5 constrained by the structured Lyapunov matrix-based control matrices $N_i = \Psi_i + \left[\begin{smallmatrix} P_* & h_* \\ * & 0 \end{smallmatrix}\right]$, for any i in $\mathbb{K}$, with the nominal matrices, corresponding to the control law (5.26) given in [86] are again included in the solutions of the original conditions of Theorem 5. Therefore, the relaxed control law employed in Theorem 5 can only improve the performance compared with Lyapunov matrix based-controllers.

5.2.3 Numerical validations

In this section the numerical results, obtained in simulations carried out with the control laws developed above, will be shown. The first two examples shown in this section are generic mathematical examples to show the effectiveness of the presented control laws compared with an existing method. The last example shows the validation for a DC-DC converter.

Basic controller and comparison with [86]

Consider system (4.7) taken from [86] and composed by two unstable subsystems, defined by

$$A_i = e^{F_i T}, \quad a_i = \int_0^T e^{F_i \tau} d\tau \; g_i, \quad i = 1,2,$$

$$F_1 = \begin{bmatrix} 0 & 1 & 0 \\ 0 & 0 & 1 \\ -1 & -1 & -1 \end{bmatrix}, \; F_2 = \begin{bmatrix} 0 & 1 & 0 \\ 0 & 0 & 1 \\ 0 & -1 & -1 \end{bmatrix}, g_1 = \begin{bmatrix} 1 \\ 0 \\ 0 \end{bmatrix}, \; g_2 = \begin{bmatrix} 0 \\ 1 \\ 0 \end{bmatrix},$$

and where parameter T is equal to 1.

The desired equilibrium is $z_e = [5/3 \;\; -0.6 \;\; -0.4]^\top$, which satisfies Definition 1 under $\lambda = [0.6 \;\; 0.4]$.

Table 5.2 presents the numerical results obtained by solving the conditions of Theorem 3. These values were computed by using a line-search routine together with CVX (LMI solver in MATLAB), as mentioned in Remark 3. These values have to be regarded in comparison with the ones issued from the application of the performances of the controller developed in [86] for a given value of μ, corresponding to β^{-1} in that paper. This table shows the value of parameter μ, that minimizes the volume of the invariant set $\mathcal{A}$, which is characterized by Lyapunov matrix P, more precisely, by $(\det(P))^{-\frac{1}{2}}$, as mentioned in section 5.2.1. Then the associated control matrices N_1 and N_2 are presented.

It is worth noting that the Lyapunov matrix P provided by Theorem 3 generates a notably smaller volume, referring to the quantity $(\det(P))^{-\frac{1}{2}}$ than the one proposed in [86] with a reduction of 32.07%. It also has to be noted that the centre x_c of the invariant set $\mathcal{A}$ provided in both cases are close to each other. In addition, the resulting values of h obtained by Theorem 3 and in Remark 5 are $h = [0.0840 \;\; 0.0891 \;\; 0.0871]^\top$ and $h^* = [0.0599 \;\; 0.0614 \;\; 0.0560]^\top$, respectively. These values of h are quite similar but

sufficiently different, so that it is possible to conclude that the one provided in this thesis does not follow the optimality criteria given in [86].

Table 5.2 Comparison of the numerical results of Theorem 3 and [86]. For the optimal value of μ, this table reports, the Lyapunov matrix, P and the inverse of the square root of its determinant, the center of the invariant set $\mathcal{A}$ and the control matrices N_1 and N_2.

Theorem	[86]	Theorem 3
μ	0.0833	0.0977
$10^2 \cdot P$	$\begin{bmatrix} 7.77 & 5.80 & 4.99 \\ 5.80 & 10.44 & 6.25 \\ 4.99 & 6.25 & 10.10 \end{bmatrix}$	$\begin{bmatrix} 10.32 & 7.72 & 6.53 \\ 7.72 & 13.95 & 8.31 \\ 6.53 & 8.31 & 13.46 \end{bmatrix}$
$(\det(P))^{-\frac{1}{2}}$	59.9697	38.7049
x_c	$\begin{bmatrix} -0.4930 \\ -0.1930 \\ -0.1771 \end{bmatrix}$	$\begin{bmatrix} -0.4804 \\ -0.1993 \\ -0.2914 \end{bmatrix}$
$10^2 \cdot N_1$	$\begin{bmatrix} 4.00 & 3.49 & -0.12 & 2.40 \\ 3.49 & 8.22 & 4.47 & 1.26 \\ -0.12 & 4.47 & 5.85 & -0.18 \\ 2.40 & 1.26 & -0.18 & -3.21 \end{bmatrix}$	$-\begin{bmatrix} 2.88 & 2.90 & 4.89 & 6.20 \\ 2.90 & 1.81 & 2.09 & 8.13 \\ 4.89 & 2.09 & 1.82 & 9.42 \\ 6.20 & 8.13 & 9.42 & 18.78 \end{bmatrix}$
$10^2 \cdot N_2$	$\begin{bmatrix} 7.77 & 7.95 & 6.37 & 10.99 \\ 7.95 & 10.98 & 7.70 & 13.07 \\ 6.37 & 7.70 & 7.41 & 13.91 \\ 10.99 & 13.07 & 13.91 & 21.84 \end{bmatrix}$	$-N_1$

Another advantage of the unstructured control law (5.15) over the one developed in [86] expressed in (5.26) or in (5.27), is that, on the one hand, it does not depend on the system matrices and on the other hand it only requires the computation of a single matrix N_1 since $N_1 = -N_2$. This simple structure is particular to the case of two modes since, in this situation, $\lambda_2 = 1 - \lambda_1$ and, consequently, in LMI (5.12), we note that $N_\lambda - N_1 =$

$(1-\lambda_1)(N_2-N_1)$ and $N_\lambda - N_2 = \lambda_1(N_2-N_1)$, which means that matrices N_1 and N_2 are linked.

Robust switching control of affine systems

Consider now the uncertain system driven by (4.7) composed by three functioning modes:

$$A_1 = \begin{bmatrix} 0 & 0.15+\delta \\ -0.35 & -1 \end{bmatrix}, \quad a_1 = \begin{bmatrix} 1 \\ 0.35 \end{bmatrix},$$

$$A_2 = \begin{bmatrix} 0.24 & 0.15+\delta \\ -2.35 & -1 \end{bmatrix}, \quad a_2 = \begin{bmatrix} -1 \\ -0.35 \end{bmatrix}, \tag{5.35}$$

$$A_3 = \begin{bmatrix} -0.24 & 0.15+\delta \\ -2.35 & -0.5 \end{bmatrix}, \quad a_3 = \begin{bmatrix} 0.05 \\ 1.5 \end{bmatrix},$$

where δ is an unknown, possibly time-varying perturbation to the system, which is only assumed to be bounded by a known parameter $\bar{\delta}$, such that $|\delta| \leq \bar{\delta}$. The desired equilibrium is $z_e = [0.1 \;\; 0.2]^T$ with $\lambda = [0.36 \;\; 0.3 \;\; 0.34]$. The nominal matrices A_{i0} and B_{i0} to be employed to define Ω_e correspond to $\delta = 0$.

From Theorem 5, we compute the corresponding matrices P, N_i with $i = 1,2,3$ and μ, for several values of $\bar{\delta} \in [0,\, 0.2]$. Figure 5.2 depicts three simulations of uncertain system (4.7), (5.35) in the situation where the uncertainty δ is taken constant and equal to the upper bounds $\bar{\delta} = 0, 0.1, 0.2$, respectively. The figure exposes the state and σ evolutions, and the set $\mathcal{A}$ in the state plane. Note that the states converge to a point close to the origin, which is inside the invariant set. The plot of the Lyapunov function enhances that once the system reaches $\mathcal{A}$, (i.e. $V \leq 1$) it never leaves. Likewise, note that the size of $\mathcal{A}$ increases when $\bar{\delta}$ increases, as is stated in Remark 6. Therefore, global asymptotic stability of $\mathcal{A}$ established by Theorems 3 and 5 holds.

As a final comment, Fig. 5.3, shows the evolution of the volume of $\mathcal{A}$ with respect to $\bar{\delta}$ implementing control (5.34) and the control given in [86], summarized in (5.27). It can be seen first that increasing upper bound of the uncertainty $\bar{\delta}$ implies a natural increase of the size of $(\det(P))^{-\frac{1}{2}}$, which, again represents the volume of the invariant set $\mathcal{A}$. Moreover, it can be seen that the use of the relaxed and unstructured control matrices N_i provides a lower volume than the one of the Lyapunov matrix-based controller. This demonstrates again the potential of the presented approach and validates both Proposition 2 and Remark 7.

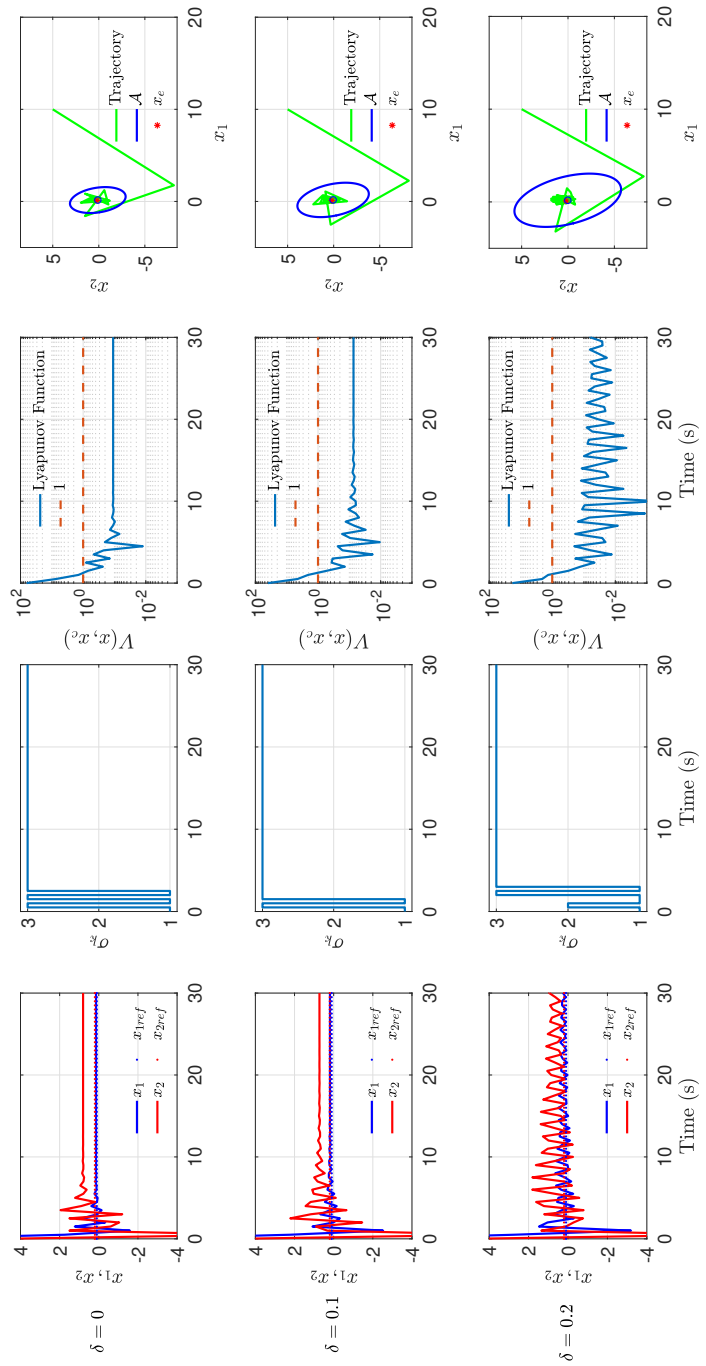

Figure 5.2 Simulation results of uncertain switched affine system (4.7), (5.35) for three different values of $\bar{\delta}$, from top to bottom. From left to right, the figure shows the evolution of the state variables (x_1,x_2), the control input σ and the Lyapunov function $V(x,x_c)$ (in a logarithmic scale), with respect to time. The last column shows the trajectories of the state in the phase portrait.

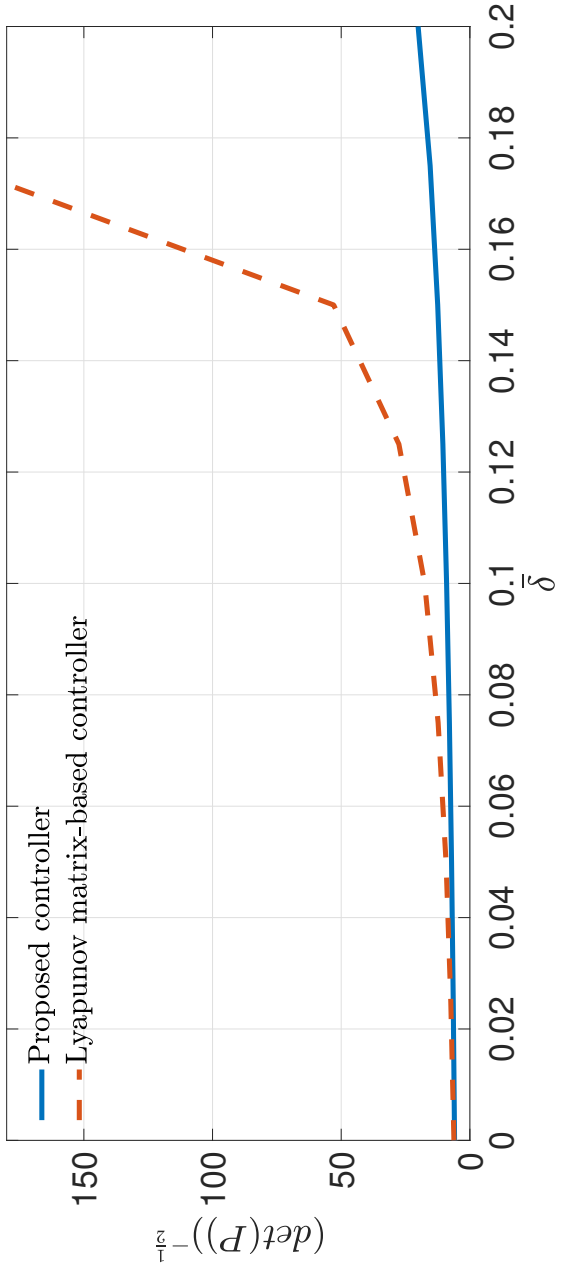

Figure 5.3 Evolution of $(\det(P))^{-\frac{1}{2}}$ with unstructured matrices N_i's (solid) in (5.34), and with the Lyapunov matrix-based control law (5.27) (dashed).

Application to a Boost Converter

A possible application of the control laws presented in section 5.2 is a boost converter like the one showed in 4.2.2. In that section, the state variable is defined by $x = [i_L \quad v_c]^\top$, where i_L denotes the inductor current and v_c the capacitor voltage.

In order to compare the efficiency with the other control laws presented in section 5.1 and in [77], the considered nominal values of the parameters of the converter are: $u = 100V$, $R = 2\Omega$, $L = 500\mu H$, $C_o = 470\mu F$ and $R_o = 50\Omega$. This parameters define the switched system state space models (4.3) and (4.9) by the following matrices for $i = 1,2$:

$$A_i = \begin{bmatrix} -\frac{R}{L} & \frac{(1-i)}{L} \\ \frac{(i-1)}{C_0} & -\frac{1}{R_0 C_0} \end{bmatrix}, \quad a_i = \begin{bmatrix} \frac{1}{L} \\ 0 \end{bmatrix} u.$$

The chosen simulation parameters are given by

$$z_e = \begin{bmatrix} 3 & 120 \end{bmatrix}^\top, \ \lambda = [0.22 \ \ 0.78] \text{ and T} = 10^{-4} s$$

With this parameters and the value of μ=0.1137 for an example with the values showed before and μ=0.1180 for an example with a variation of 10% less in the value of the resistor R, the Table 5.3 is obtained.

Table 5.3 Results from simulation of the application to a DC-DC converter.

Control law	mu	Volume ($det^{-1/2}$)
Nominal case	0.1137	393.4204
10% less R variation	0.1180	394.6410

In this table it is possible to observe that the volume, expressed in term of $det(P)^{-1/2}$, of the set $\mathcal{A}$ is practically the same in the nominal case and with variations.

The evolution of the error trajectory x and the set $\mathcal{A}$ is showed in Fig. 5.4.

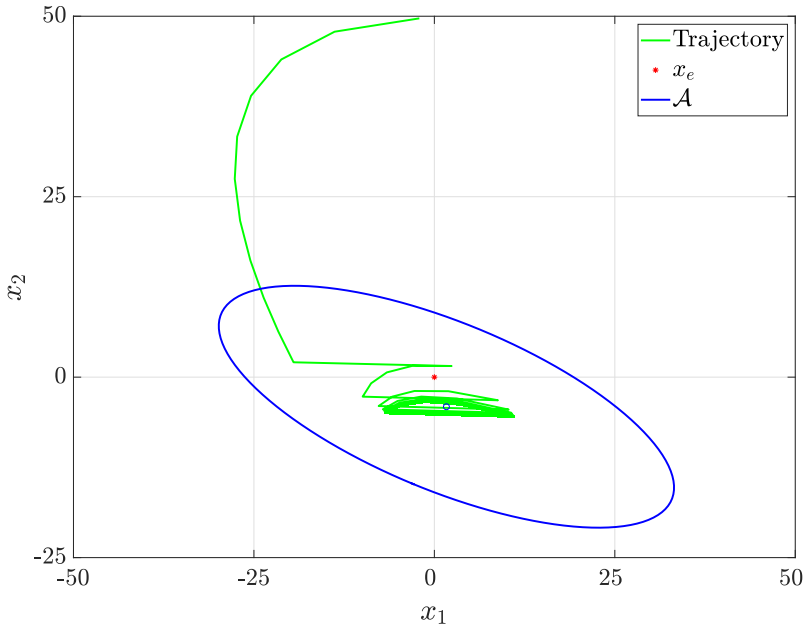

Figure 5.4 Evolution of the error trajectory and the set $\mathcal{A}$.

5.3 Conclusions

In this chapter, several controllers for switched affine systems have been presented. Two for systems with high-frequency sampling time and two for an usual discrete-time formulation made to improve the previous formulation.

Therefore, in the first instance two main contributions have been presented to control switched affine systems with high-frequency sampling time. The first one deals with the definition of accurate discrete-time model for high-frequency sampling DC-DC converters. The second contribution consists in the extension of the usual Lyapunov-based control laws employed in this domain to a less restrictive control law that encompass this first formulation. This new control law delivers notable improvements with respect to the Lyapunov-based control law in terms when comparing the estimate of the set $\mathcal{E}$ of the switched affine system.

An usual discrete-time formulation has been proposed, as alternative to the previous formulation, that have some advantages. In this way, the matrix is the same to define the attractor set and the used in the control law, avoiding some possible situations of instability. In this new formulation, the centre of the ellipsoid that define this attractor do not have to be the origin, reducing its volume. Another improve respect to the previous formulation is in the iterative process to search the optimal value of the parameters μ and γ due to that the new formulation only use the value of one parameter (μ). The main result presented provides a relaxed control which is not based on the computation of the Lyapunov function as usually considered in the literature. It is demonstrated, by theoretical and numerical validations, that the solution of the optimization problem provided in [86] is included in this proposed solution. Numerical applications even show a notable improvement of the guarantees on an example. Even so, the results in comparison with the control laws presented for high frequency sample time do not show an improvement due to numerical problems when the parameters of the converter are used. This fact can be observed in the Table 5.4, where the value of $det(P)^{-1/2}$ is shown for the proposed control laws. In this table it is also possible to observe that the control method of (5.15) does not have solution for T=10^{-5} and T=10^{-6} showing the difficulty to solve the LMI for high frequency systems due to numerical problems. A possible solution to this may be the use of δ operator in conjunction with the usual discrete-time formulation.

Besides, the potential of this last method compared with the existing solution from the literature is the possibility to apply the same control design methodology in the case of uncertain systems, which is not straightforward using Lyapunov matrix-based control laws

because it requires the exact knowledge of the system matrices. The "relative simplicity" of the proposed analysis has, indeed, the price of introducing some degree of conservatism.

Table 5.4 Comparison results from the application to a DC-DC converter.

	Volume ($det(P)^{-1/2}$)		
Period	C1 (5.4)	C2 (5.8)	Nominal Case (5.15)
T=10^{-4}	369.9298	245.9012	393.4204
T=10^{-5}	23.7921	23.5335	-
T=10^{-6}	2.3222	2.2996	-

6 Conclusions and Future Work

One approaches the journey's end. But the end is a goal, not a catastrophe.

GEORGE SAND

Contents

This thesis has addressed the control of power electronic converters. On the one hand, the first goal has been the control of the voltage balance in the capacitors of a three-level NPC. In the other hand, two design methods are presented for control the output voltage of a DC-DC converter. The next section explain the thesis contributions and the methods used to reach the objectives. At the end of the chapter some future works are proposed.

6.1 Thesis contributions and conclusions

In the first part of this thesis, the model of a three-level NPC converter has been revisited. This model is an average model where the control signals have been expressed as averaged

duty ratios of each level in each phase. This model is not a contribution of this thesis but it has been used to design several new control laws. The main objective of all of this control laws is the voltage balance in the capacitors of the dc-link, taking into account the power or current controllers and the total dc-link voltage control. Thus, three approaches have been presented and compared with the existing technique mVSVPWM. It is important to remember that the first approach (ICM1) was theoretically proposed in a previous work [44] and in this thesis it has been implemented experimentally. The results of the comparison allow to observe that the THD values obtained in the three proposed variants are similar or better to the mVSVPWM technique. The first two variants improve in simplicity, expressed in the reduction of computational burden, at the cost of a higher number of commutations. This fact is solved in the third variant, where although the computational burden does not decrease so much, the number of commutations is reduced considerably. Regarding the balancing time, again the first two variants are a bit slow achieving the voltage balance in the capacitors, being the third one even faster than mVSVPWM. It should be remembered that the first two variants present a trade-off between balancing speed and transient behaviour, expressed in the modification of some control parameters, which could improve the speed of the voltage balance. As result of the comparison between all the techniques implemented, it can be seen that the first proposed variant (ICM1), even though it is the simplest one, the worsening of THD, number of commutations and balance time is not compensated by the improvement in computational load. However, the modifications made from this technique in the second variant (ICM2) and the proposal of the third one (Variant 3), show very promising results with respect to the rest of the techniques.

In the second part of the thesis, the DC-DC converter is modelled as switched affine system due to its hybrid behaviour. In this type of systems, stability to a desired equilibrium point is not possible and the chattering around that point is an effect to mitigate, decreasing the attractor set where the system converges to. Several control design methods have been presented to achieve this objective. Two for systems with high frequency sampling time and two for an usual discrete-time formulation considered for improving the previous ones.

Therefore, in the first instance two main contributions have been presented to control switched affine systems with high frequency sampling time using the δ operator. The first one deals with the definition of accurate discrete-time model for high frequency sampling DC-DC converters where the control is based in the Lyapunov function. The second contribution consists in the extension of the usual Lyapunov-based control laws to a less restrictive control law that encompass this first formulation. This new control law delivers notable improvements with respect to the Lyapunov-based control law when comparing the estimate of the attractive set $\mathcal{E}$ of the system.

In the case of the usual discrete-time formulation, the main result presented provides a relaxed control which is not based on the computation of the Lyapunov function as usually considered in the literature. It is demonstrated, by theoretical and numerical validations, that the solution of the optimization problem provided in [86] is included in this proposed solution. Numerical applications show the improvement of this methods on the examples. Even so, the results in comparison with the control laws presented for high frequency sample time do not show an improvement due to numerical problems when the parameters of the converter are used. A possible solution to this is outlined in the next section as a future work to do. Besides, the potential of this last method compared with the existing solution from the literature is the possibility to apply the same control design methodology in the case of uncertain systems, which is not straightforward using Lyapunov matrix-based control laws because it requires the exact knowledge of the system matrices. The "relative simplicity" of the proposed analysis has, indeed, the price of introducing some degree of conservatism.

6.2 Future work

Some challenging reach lines are still able to be addressed:

- Multilevel Converters

  The control laws presented in the first part of this thesis have been developed for three-level converters, however, it is possible to adapt them to more level systems. In fact, some of them are already been studied and experimentally implemented in a five-level NPC converter [92]. This is a challenge from the point of view of the control of this type of converters. In fact, due to the difficulty presented to design controllers in more than three levels, another methods could to be used. In this sense, a new control method would compute the on-off values of the switching devices as a mixed-integer linear optimization problem. This optimal switching sequence is computed offline based on normalized values for a given operation point at steady state. A grid period is simulated and the resulting optimal switching sequence is stored in a table. Afterwards, the modulator can look for the more similar situation to the stored ones in the table and apply its switching criteria. In this way, an optimal modulation is computed offline and integrated with very low computational burden.

  Alternatively, instead of focusing on one operation point, an optimal modulation law can be derived from the data obtained for several operational points. To do

so, different operation points are simulated and their resulting switching sequences are obtained. Several normalized state variables are used as inputs to distinguish the different switching sequences obtained as outputs. Thus, classification and regression trees are trained with this data, resulting in a simpler way to implement the optimal sequences from the state variables.

- Switched Affine Systems In section 5.2.3 it has been shown as the usual discrete-time formulation present numerical problems in the DC-DC converter application when using high-frequency sampling times. It has even been seen that for very small values of the sampling time, the designed method does not find a solution to the LMI. A possible solution to these numerical problems is the use of the δ operator in conjunction with this model formulation. With this new alternative, it is expected to improve the volume of the attractor set $\mathcal{A}$ of the application example.

  All the control design methods developed to switched affine systems have been applied to DC-DC converters in this thesis. A possible future work in this sense is to extend this methods to other type of converters like the three-level NPC. This future work will surely present the same difficulty that the DC-DC converters respect to numerical problems mentioned before since the sampling time must be very small. To avoid these problems, the same solution indicated above could be used.

Appendix A

Design and Construction of a Experimental Prototype Power Converter

A.1 Introduction

In this appendix the design and assembly of a five-level diode-clamped converter operating in rectifier mode will be presented. This prototype, can be used as a three-level converter and has been employed to perform the experimental test of the approaches presented in this thesis. The proposed approaches, as well as others in development, are intended to be used in five-level converters, so although the experiments in this thesis are performed for three levels, a five-level converter has been designed. Due to the complexity to achieve good control results with five-level converters, this type is so far mainly used for research, where it is a challenge from the point of view of the total dc-link voltage control and the balance of the voltage in the capacitors.

In this way, a five-level diode-clamped converter has been designed, whose circuit can be seen in Fig. A.1. The specifications for this design are a 220 volts three-phase grid as supply voltage and a 800 volts of continuous voltage as the nominal output, thus obtaining a converter of about 11 kW of power. Although the converter is designed to work in

rectifier mode, it is possible to use it both in this mode and in inverter mode. Another particularity of this converter is that it can also be used as a three-level converter. As said befroe, this option is the one that has been used to perform the experiments of Section 3.6 in this thesis.

For the design of this converter has been used a real-time control equipment of the trademark $Speedgoat$, whose characteristics will be explained later.

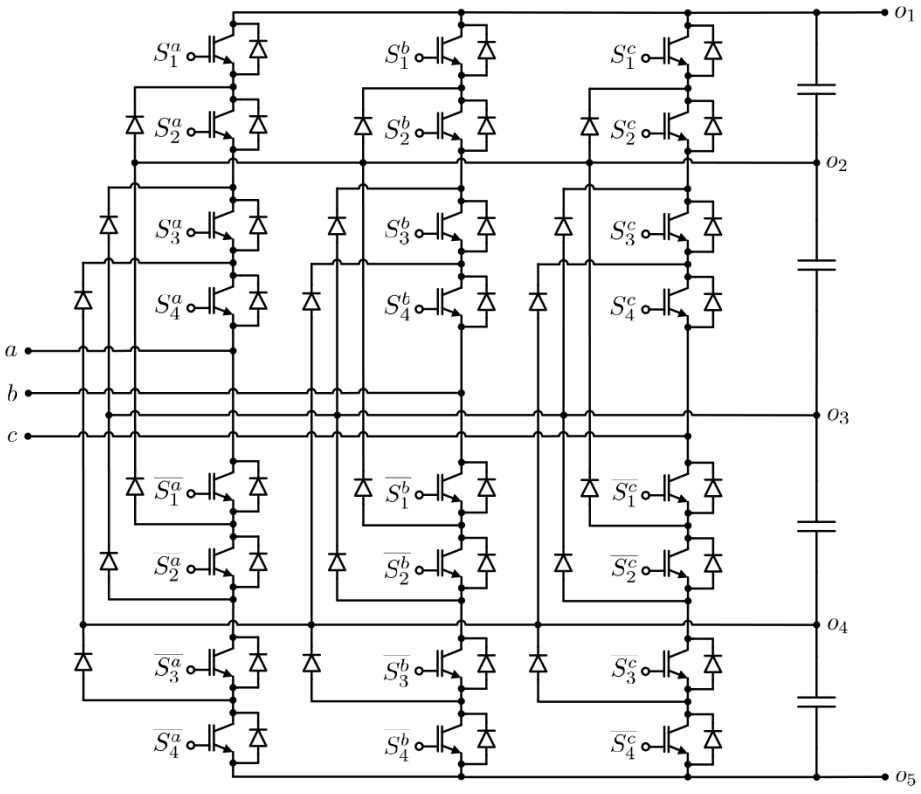

Figure A.1 Circuit of the five-level diode-clamped.

A.2 Schematic and Model

Figure A.2 shows the schematic of the five-level diode-clamped converter operating in rectifier mode, which is the configuration that has been considered when designing the

converter.

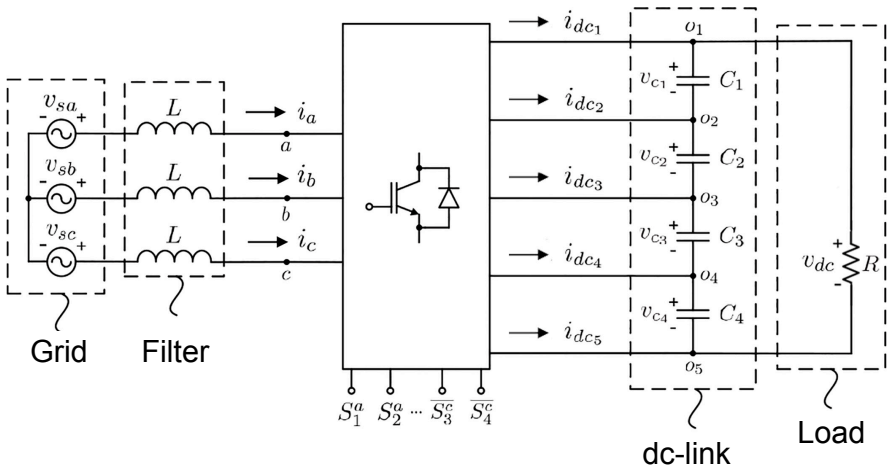

Figure A.2 Schematic of the five-level diode-clamped converter in rectifier mode.

As can be seen, the converter is connected to the grid through a filter where the inductances are considered of equal value L. $v_{sa}, v_{sb}, v_{sc}, i_a, i_b$ and i_c represent the phase voltages and currents respectively.

The dc-link is composed of four capacitors C_1, C_2, C_3 and C_4, all of the same value C. Their respective voltages are represented by v_{c1}, v_{c2}, v_{c3} and v_{c4}. The sum of these voltages represents the total dc-link voltage v_{dc}. This side is connected to a purely resistive load R.

The dynamic model of the five-level converter was presented in [93]. In this way, the dynamics of the phase currents, expressed in $\alpha\beta\gamma$ coordinates, and the voltage differences in the capacitors can be expressed as,

$$L\frac{di_\alpha}{dt} = v_\alpha - u_1\frac{v_{dc}}{4} - (3u_3 - u_5 + 2u_7)\frac{v_{d_1}}{4} + (u_3 - 3u_5 + 2u_7)\frac{v_{d_2}}{4} + (u_3 - u_5 + 2u_7)\frac{v_{d_3}}{2} \quad \text{(A.1)}$$

$$L\frac{di_\beta}{dt} = v_\beta - u_2\frac{v_{dc}}{4} - (3u_4 - u_6 + 2u_8)\frac{v_{d_1}}{4} + (u_4 - 3u_6 + 2u_8)\frac{v_{d_2}}{4} + (u_3 - u_5 + 2u_8)\frac{v_{d_3}}{2} \quad \text{(A.2)}$$

$$C\frac{dv_{d_1}}{dt} = u_3 i_\alpha + u_4 i_\beta \tag{A.3}$$

$$C\frac{dv_{d_2}}{dt} = u_5 i_\alpha + u_6 i_\beta \tag{A.4}$$

$$C\frac{dv_{d_3}}{dt} = -u_7 i_\alpha - u_8 i_\beta, \tag{A.5}$$

where u_1 to u_8 are the control signals, and the voltage differences are defined by,

$$v_{d_1} = v_{c_1} - v_{c_4} \tag{A.6}$$

$$v_{d_2} = v_{c_2} - v_{c_3} \tag{A.7}$$

$$v_{d_3} = v_{c_3} - v_{c_4}. \tag{A.8}$$

The control objectives of the converter are to:

- Reach the voltage reference on the dc-link.
- Achieve the voltage balance in the capacitors, so that the equations (A.6) - (A.8) are equal to zero.
- Obtain a shape of currents i_a, i_b and i_c as sinusoidal as possible, which means a low THD value.

A.3 Design and Assembly

A.3.1 Components

Based on simulations performed in the laboratory, the following components have been selected to build the converter.

Capacitors

The capacitors chosen are the model MAL210217332E3 by the trademark Vishay. These electrolytic capacitors have a capacity of 3300 μF and support a voltage of 450V.

Filter

As can be seen in Fig. A.2, three coils, one per phase, are arranged at the input of the equipment to filter the current. The value of its inductance is 2 mH each. These coils were manufactured by the electronic components company Clarkia S.L.

Sensors

The converter has two types of sensors necessary for control tasks:

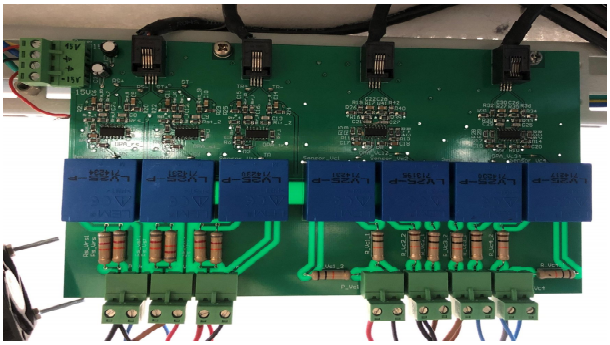

Figure A.3 Measuring circuit and adaptation of voltage sensors.

Voltage Sensors The sensors used for voltage measurement are of the brand LEM, model LV25-800. These sensors can measure both alternating and continuous voltages, so they can be used to measure the grid voltages at the input and the voltage of the dc-link at the output of the converter. Being Hall effect sensors, the output is a signal that varies its current, so it is necessary a circuit to adapt it to a voltage from 0 to 5 V in order that the control system can process the voltage measurement. This circuit with the voltage sensors can be seen in Fig. A.3.

Current Sensors For the measurement of current at the input of the converter, Hall effect sensors of the brand LEM, model LA 55-P, are used due to their immunity against

electromagnetic noise. The measuring range of this sensor is up to 70 amps, since maximum values of 40 amps have been obtained by simulation. These sensors also need an adaptation circuit like the one shown in the figure A.4 since they also generate current variation in the output.

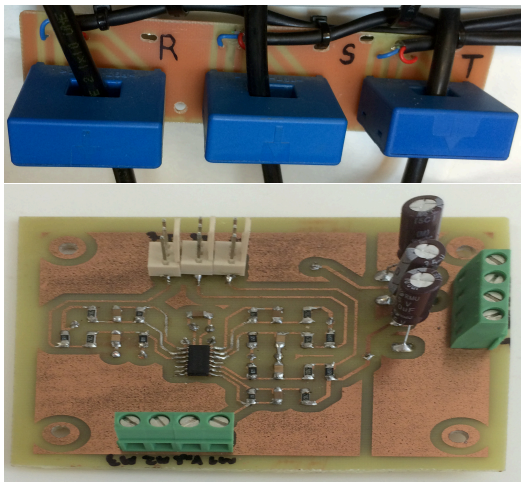

Figure A.4 Current sensors and adaptation circuit.

Processor

Figure A.5 Speedgoat real time machine.

To carry out the control tasks, a processor of the trademark *Speedgoat* has been used, which is a machine to perform real-time experiments using the simulation program Matlab-Simulink. The characteristics of the processor, which justify its use in this

converter are several:

- The possibility of creating the converter model and its control strategy using Simulink.
- The option to build and automatically download an application in real time from Simulink to the processor.
- Adjust controller parameters, monitor the process and store data in real time during the execution of an experiment.
- Work at high sampling frequencies, which is important when working with power electronics applications.

The processor is configured with an Intel Core i7 3.5 Ghz processor and a 75 MHz FPGA module that has 128 inputs/outputs. 24 of these outputs will be used to send the control signals to the actuators and 6 inputs will be used to send possible error signals to the processor.

In Fig. A.5, the real-time machine is shown.

To transmit the control signals from the processor, optical fiber have been used. In power converters, common mode voltages can produce enough noise to affect the control signals. For this reason the optical fiber has been used, which is immune to this noise. In this way, the control signal calculated by the processor reaches the conversion board through the Sub-D terminal in a range of 0 to 5 volts and is transformed into a light signal that reaches the actuators through the optical fiber cable. In Fig. A.6 it is possible to see the conversion circuit.

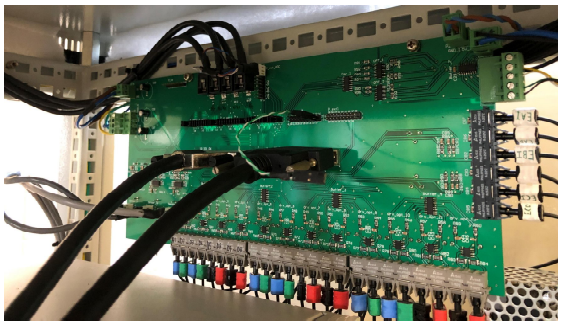

Figure A.6 Circuit to adapt votlage signal to optical fiber.

Switching elements

As switching element, IGBT transistors have been used. These transistors are semiconductor devices that act as a switch controlled by a control signal. The model used in the converter is the SKM100GB12V of the brand Semikron.These IGBTs that support a maximum voltage of 1200 volts have been selected due to the fact that the working voltage in the dc-link will be about 800 volts. The IGBTs are encapsulated in pairs as shown in Fig. A.7.

Figure A.7 IBGT by Semikron.

Inside these IGBT modules are also switching diodes, which are of vital importance since they are responsible for setting the block voltages of the switches at a fraction of the dc-link voltage. These diodes have fast recovery and must support the nominal voltage of the converter, so modules that support up to 100 amps have been chosen.

Once the control signal has been sent, calculated by the Speedgoat, through optical fiber, it is necessary to perform another adaptation of the signal when reaches the IGBT. This new adaptation is made in the circuit shown in Fig. A.8. In this circuit, the signal coming from the optical fiber is read and the IGBTs are triggered through the drivers. These drivers of the brand Semikron and model Skyper 32 PRO R, have the characteristic of switching each IGBT module independently. In addition, they incorporate protection against shortcircuit and soft shutdown. An important characteristic is that they do not introduce dead times between commutations, so in order to avoid shortcircuits in the commutations it will be necessary to produce these dead times from the real-time computer.

Snubber Capacitors

They are high frequency response capacitor devices. These devices are in parallel with the IGBTs and serve to reduce the electrical stress of these elements, avoiding voltage peaks when performing the commutations.

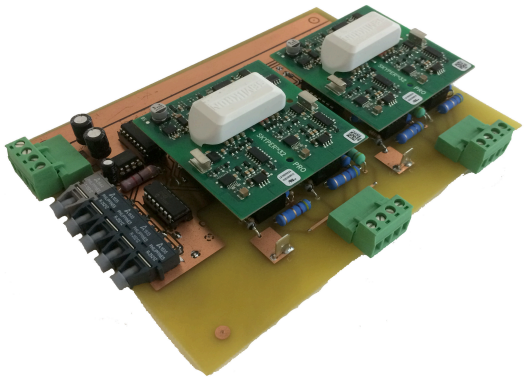

Figure A.8 Circuit to adapt the signal from optical fiber cable to the IGBT module.

Fans and Heatsinks

After carrying out a thermal study on the converter, maximum temperatures were obtained in the IGBT modules of 147 ° C, for a simulation with test currents of 15 A and reference voltage in the dc-link of 800 V.

For the chosen models of IGBT modules and diodes, the maximum working temperature is 150 ° C. In order to make the converter work with favorable thermal conditions or in the case of working with higher currents or voltages, it was decided to include heatsinks for every three IGBT modules. The heatsink P3 / 300B of the brand Semikron was selected with an axial fan at one of its ends. This heatsink is specially designed for the assembly of the IGBT modules.

As a result of the simulation including these heatsinks and for an ambient temperature of 40 ° C, a maximum sink temperature of 95.75 ° C was obtained, with the final temperature in the IGBT module of 114.55 ° C.

Contactor

For security reasons, a contactor has been placed at the input of the converter. In this way it is possible to disconnect the power supply if necessary. This contactor of the brand Lovato, supports a power of 15 KW.

In addition to that contactor, another one with the same characteristics has been placed to switch to a converter preload circuit. The installed capacitors must not be subjected to sudden voltage changes, so before establishing a high voltage reference, a controlled preload is made by an external circuit to the converter at the beginning of the experiments.

Once this preload is done, the contactor connects the converter directly to the grid and disconnects the external circuit.

A.3.2 Assembly

Figure A.9 Five-level converter.

In Fig. A.9, the five-level converter with all its elements is shown.

The structure in which the converter has been assembled has a height of 1.8 meters, 60 cm wide and 60 cm deep. This structure has metal panels on all sides as well as a door on the front. For security, a methacrylate structure surrounding the converter has also been installed.

The converter has been assembled so that each of the three central trays of the structure correspond to each of the phases of the supply a, b and c shown in the figures A.1 and A.2.

In Fig. A.10, the construction of each tray can be observed in detail. It can be seen

that the connections of the capacitors and IGBTs have been established, using aluminum plates, in three different planes separated by an insulating layer. In this figure you can also see the arrangement of different elements described in previous sections.

The filter coils in the supply have been placed in the lower tray next to the current sensors, while the Speedgoat and the voltage sensors have been placed in the upper tray next to the power supplies of the electronics parts.

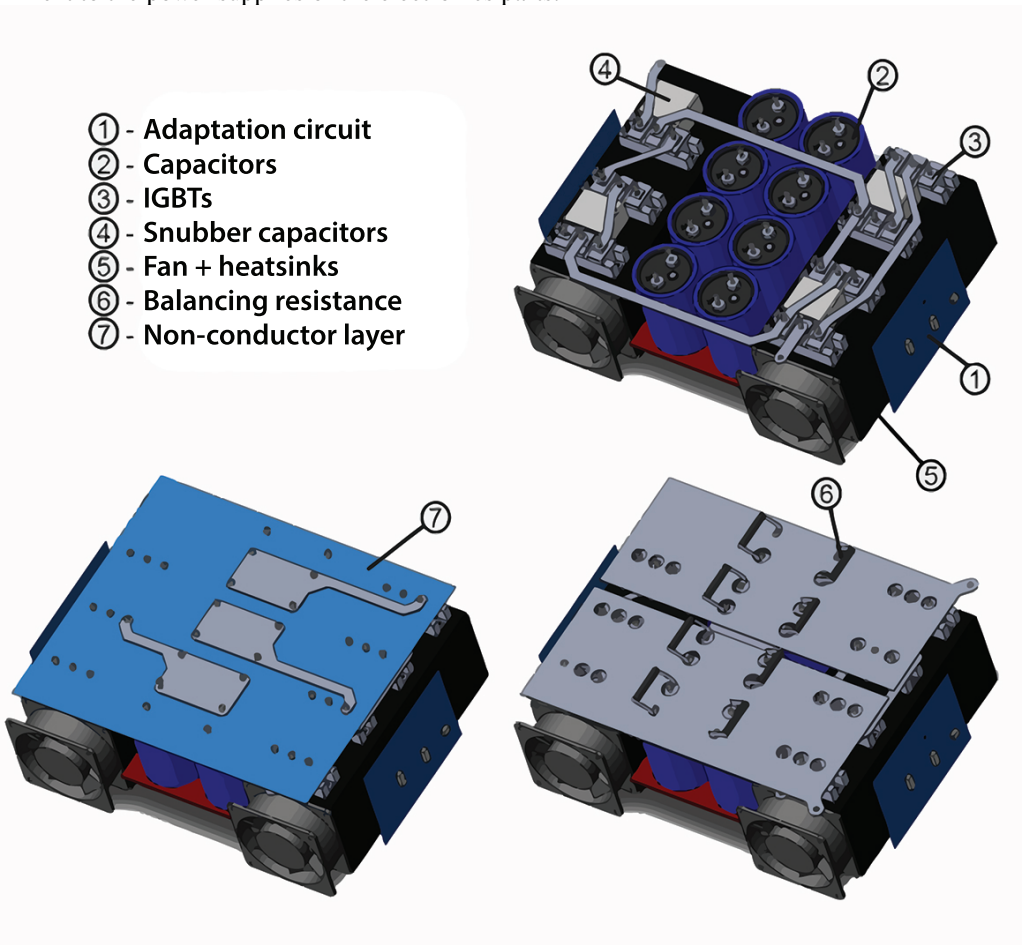

Figure A.10 Tray of components in detail.

A.3.3 Future Work

In the future, it is planned to install a network of contactors so that the converter can be switched quickly and automatically between rectifier and inverter mode. For this, a circuit formed by 10 contactors has already been designed. This network of contactors will be controlled by the digital outputs of the real-time machine.

Future extensions include the use of photovoltaic panels emulators and a three-phase motor as power supply of the converter in inverter mode, as well as the use of a non-linear load.

List of Figures

List of Tables

Bibliography

[1] J. Rodríguez, M. P. Kazmierkowski, J. R. Espinoza, P. Zanchetta, H. Abu-Rub, H. A. Young, and C. A. Rojas, "State of the art of finite control set model predictive control in power electronics," *IEEE Transactions on Industrial Informatics*, vol. 9, no. 2, pp. 1003–1016, 2013.

[2] P. Karamanakos, T. Geyer, and S. Manias, "Direct Voltage Control of DC-DC Boost Converters Using Model Predictive Control Based on Enumeration," in *EPE-PEMC 2012 ECCE*, Novi Sad, 2012.

[3] R. Teichmann and S. Bernet, "A comparison of three-level converters versus two-level converters for low-voltage drives, traction, and utility applications," *IEEE Transactions on Industry Applications*, vol. 41, no. 3, pp. 855–865, 2005.

[4] S. Kouro, M. Malinowski, K. Gopakumar, J. Pou, L. Franquelo, B. W. B. Wu, J. Rodriguez, M. Perez, and J. Leon, "Recent Advances and Industrial Applications of Multilevel Converters," *IEEE Transactions on Industrial Electronics*, vol. 57, no. 8, pp. 2553–2580, 2010.

[5] S. Aurtenechea, M. A. Rodriguez, E. Oyarbide, and J. R. Torrealday, "Predictive direct power control of MV-grid-connected two-level and three-level NPC converters: Experimental results," in *2007 European Conference on Power Electronics and Applications, EPE*, 2007.

[6] W. McMurray, "Fast response stepped-wave switching power converter circuit," may 1971. [Online]. Available: https://patents.google.com/patent/US3581212A/en

[7] J. A. Dickerson and G. Ottaway, "Transformerless power supply with line to load isolation," aug 1971. [Online]. Available: https://patents.google.com/patent/US3596369A/en

[8] R. H. Baker, "High-voltage converter circuit," 1981.

[9] A. Nabae, I. Takahashi, and H. Akagi, "A New Neutral-Point-Clamped PWM Inverter," *IEEE Transactions on Industry Applications*, vol. IA-17, no. 5, pp. 518–523, 1981.

[10] P. Steimer, "High power electronics, trends of technology and applications," in *PCIM'07*, Nuremberg, 2007.

[11] N. Zargari and S. Rizzo, "Medium Voltage Drives in Industrial Applications," Rockwell Automation, Tech. Rep., 2004.

[12] Y. Cheng, C. Qian, M. L. Crow, S. Pekarek, and S. Atcitty, "A comparison of diode-clamped and cascaded multilevel converters for a STATCOM with energy storage," *IEEE Transactions on Industrial Electronics*, vol. 53, no. 5, pp. 1512–1521, 2006.

[13] J. Wang and F. Z. Peng, "Unified power flow controller using the cascade multilevel inverter," *IEEE Trans. Power Electron.*, vol. 19, no. 4, pp. 1077–1084, 2004.

[14] J. C. Clare, "Advanced power converters for universal and flexible power management in future electricity networks," *2009 13th European Conference on Power Electronics and Applications*, pp. 1–29, 2009.

[15] M. Carpita, D. Moser, M. Marchesoni, and M. Pellerin, "Multilevel converter for traction applications: Small-scale prototype tests results," *IEEE Transactions on Industrial Electronics*, vol. 55, no. 5, pp. 2203–2212, 2008.

[16] O. Anaya-Lara, N. Jenkins, J. Ekanayake, P. Cartwright, and M. Hughes, *Wind energy generation : modelling and control*. Wiley, 2009, vol. 54, no. 2. [Online]. Available: http://strathprints.strath.ac.uk/14944/

[17] J. Suul, K. Uhlen, and T. Undeland, "Variable speed pumped storage hydropower for integration of wind energy in isolated grids: case description and control strategies," in *Nordic Workshop on Power and Industrial Electronics*, 2008. [Online]. Available: https://aaltodoc.aalto.fi/handle/123456789/800

[18] J. Guerrero, L. De Vicuna, and J. Uceda, "Uninterruptible power supply systems provide protection," *IEEE Industrial Electronics Magazine*, vol. 1, no. 1, pp. 28–38,

2007. [Online]. Available: http://ieeexplore.ieee.org/document/4154605/

[19] A. J. Forsyth and S. V. Mollov, "Modelling and control of DC-DC converters," *Power Engineering Journal*, vol. 12, no. 5, pp. 229–236, 1998.

[20] A. Bubovich, "The comparison of different types of DC-DC converters in terms of low-voltage implementation," in *Proceedings of the 5th IEEE Workshop on Advances in Information, Electronic and Electrical Engineering, AIEEE 2017*, vol. 2018-Janua, 2018, pp. 1–4.

[21] S. Verma, S. K. Singh, and A. G. Rao, "Overview of control Techniques for DC-DC converters," Tech. Rep. 8, 2013. [Online]. Available: www.isca.in

[22] H. Zhu, "New Multi-Pulse Diode Rectifier Average Models for AC and DC Power Systems Studies," Ph.D. dissertation, Virginia Tech, 2005.

[23] A. Ventosa-Cutillas, P. Montero-Robina, F. Umbría, F. Cuesta, and F. Gordillo, "Integrated Control and Modulation for Three-Level NPC Rectifiers," *Energies*, vol. 12, no. 9, p. 1641, apr 2019. [Online]. Available: https://www.mdpi.com/1996-1073/12/9/1641

[24] A. Ventosa-Cutillas, P. Montero-Robina, F. Umbria, F. Cuesta, and F. Gordillo, "A Simplified and Integrated Control and Modulation for Three-Level NPC Rectifiers," *Energy (Under revision)*, 2019.

[25] C. Albea Sánchez, A. Ventosa-Cutillas, A. Seuret, and F. Gordillo, "Robust switching control design for uncertain discrete-time switched affine systems," *International Journal of Robust and Nonlinear Control (Under revision)*, 2019.

[26] A. Ventosa-Cutillas, M. Gómez-Correa, F. Gordillo, and F. Cuesta, "Diseño, construcción y control de un convertidor de potencia de cinco niveles," in *XXXVII Jornadas de Automática*, Madrid, 2016.

[27] A. Ventosa-Cutillas, C. Albea Sanchez, A. Seuret, and F. Gordillo, "Relaxed periodic switching controllers of high-frequency DC-DC converters using the delta-operator formulation," in *57th IEEE Conference on Decision and Control (CDC'18)*, Miami, USA, 2018.

[28] A. Ventosa-Cutillas, F. Gordillo, and F. Salas, "Contributions to Control of Electronic Power Converters," in *XVII Simposio CEA de Ingeniería de Control y V Seminario de Innovación Docente en Automática*, Sevilla, 2019.

[29] L. G. Franquelo, J. Rodriguez, J. I. Leon, S. Kouro, R. Portillo, and M. A. M. Prats, "The Age of Multilevel Converters Arrives," *IEEE Industrial Electronics Magazine*, vol. 2, no. 2, pp. 28–39, jun 2008.

[30] J. Rodríguez, S. Bernet, B. Wu, J. O. Pontt, and S. Kouro, "Multilevel Voltage-Source-Converter Topologies for Industrial Medium-Voltage Drives," *IEEE Trans. Ind. Electron.*, vol. 54, no. 6, pp. 2930–2945, dec 2007.

[31] I. Staudt, "3L NPC & TNPC Topology," *Topology*, pp. 1–12, 2011.

[32] S. Busquets-Monge, J. Ortega, J. Bordonau, J. Beristain, and J. Rocabert, "Closed-Loop Control of a Three-Phase Neutral-Point-Clamped Inverter Using an Optimized Virtual-Vector-Based Pulsewidth Modulation," *IEEE Transactions on Industrial Electronics*, vol. 55, no. 5, pp. 2061–2071, may 2008.

[33] D. G. Holmes and T. A. Lipo, *Pulse Width Modulation for Power Converters: Principles and Practice*. Wiley, 2003.

[34] J. I. Leon, S. Kouro, L. G. Franquelo, J. Rodriguez, and B. Wu, "The Essential Role and the Continuous Evolution of Modulation Techniques for Voltage-Source Inverters in the Past, Present, and Future Power Electronics," *IEEE Transactions on Industrial Electronics*, vol. 63, no. 5, pp. 2688–2701, may 2016.

[35] J. Rodriguez, L. Moran, C. Silva, and P. Correa, "A high performance vector control of a 11-level inverter," in *Proceedings - IPEMC 2000: 3rd International Power Electronics and Motion Control Conference*, vol. 3, 2000, pp. 1116–1121.

[36] T. Noguchi, H. Tomiki, S. Kondo, and I. Takahashi, "Direct power control of PWM converter without power-source voltage sensors," *IEEE Trans. Ind. Appl.*, vol. 34, no. 3, pp. 473–479, may 1998.

[37] S. Kouro, P. Cortes, R. Vargas, U. Ammann, and J. Rodriguez, "Model Predictive Control-A Simple and Powerful Method to Control Power Converters," *Industrial Electronics, IEEE Transactions on*, vol. 56, no. 6, pp. 1826–1838, jun 2009.

[38] S. Vazquez, J. I. Leon, L. G. Franquelo, J. Rodriguez, H. A. Young, A. Marquez, and P. Zanchetta, "Model predictive control: A review of its applications in power electronics," pp. 16–31, 2014.

[39] J. Holtz, "Pulse width Modulation-A Survey," *IEEE Trans. Ind. Electron.*, vol. 39, no. 5, pp. 410–420, dec 1992.

[40] Z. Pan and F. Z. Peng, "A sinusoidal PWM method with voltage balancing capability for diode-clamped five-level converters," *IEEE Transactions on Industry Applications*, vol. 45, no. 3, pp. 1028–1034, 2009.

[41] S. L. Capitaneanu, B. De Fornel, M. Fadel, J. Faucher, and A. Almeida, "Graphical and algebraic synthesis for PWM methods," *EPE Journal (European Power Electronics and Drives Journal)*, 2001.

[42] L. M. D. Jimena, C. M. G. Alberto, D. C. J. Oscar, and G. L. C. Alberto, "Modulación PWM aplicada a inversores trifásicos dentro del esquema de accionamientos eléctricos AC," *DEIC-FIET*, 2007.

[43] Z. B. Mahmoud, M. Hamouda, and A. Khedher, "A comparative study between the Nearest Three Vectors and two-level hexagons based space vector modulation algorithms for three-level NPC inverters," *International Journal of Renewable Energy Research*, vol. 7, no. 3, pp. 1074–1084, 2017.

[44] F. Umbria, F. Gordillo, and F. Salas, "Model-based NPC Converter Regulation for Synchronous Rectifier Applications," *Proceedings, IECON 2014 - 40th Annual Conference of the IEEE Industrial Electronics Society*, pp. 4669–4675, oct 2014.

[45] S. Alepuz, S. Busquets-Monge, J. Bordonau, J. Gago, D. González, and J. Balcells, "Interfacing Renewable Energy Sources to the Utility Grid Using a Three-Level Inverter," *IEEE Trans. Ind. Electron.*, vol. 53, no. 5, pp. 1504–1511, oct 2006.

[46] Q. Yan, Kai and Wang, Wei and Zhu, Zhongni and lu, "Study on neutral-point balancing for three-level space voltage vector pulse-width modulation inverter," in *2008 International Conference on Electrical Machines and Systems*, 2008, pp. 1571–1576.

[47] R. Krishna, D. E. Soman, S. K. Kottayil, and M. Leijon, "Pulse delay control for capacitor voltage balancing in a three-level boost neutral point clamped inverter," *IET Power Electronics*, vol. 8, no. 2, pp. 268–277, 2015.

[48] A. Von Jouanne, S. Dai, and H. Zhang, "A multilevel inverter approach providing DC-link balancing, ride-through enhancement, and common-mode voltage elimination," *IEEE Transactions on Industrial Electronics*, vol. 49, no. 4, pp. 739–745, 2002.

[49] S. Gauthier and F. Okou, "Transformer-less five-level diode-clamped converter based active power filter with auxiliary balancing circuit," in *CCECE 2010*. IEEE, may 2010, pp. 1–5.

[50] H. Hotait, A. Massoud, S. Finney, and B. Williams, "Capacitor voltage balancing using redundant states of space vector modulation for five-level diode clamped inverters," *IET Power Electronics*, vol. 3, no. 2, p. 292, 2010.

[51] B. Omri, K. Ammous, and A. Ammous, "New Method for Balancing Capacitors Voltages in NPC Inverter without DC-link Voltages Sensors," *International Journal of Computer Applications*, vol. 65, no. 22, pp. 17–24, 2013.

[52] A. Choudhury, P. Pillay, and S. S. Williamson, "DC-Bus Voltage Balancing Algorithm for Three-Level Neutral-Point-Clamped (NPC) Traction Inverter Drive With Modified Virtual Space Vector," *IEEE Transactions on Industry Applications*, vol. 52, no. 5, pp. 3958–3967, sep 2016.

[53] S. Busquets-Monge, J. Bordonau, D. Boroyevich, and S. Somavilla, "The Nearest Three Virtual Space Vector PWM - a Modulation for the Comprehensive Neutral-Point Balancing in the Three-Level NPC Inverter," *IEEE Power Electron. Lett.*, vol. 2, no. 1, pp. 11–15, mar 2004.

[54] S. R. Pulikanti, M. S. A. Dahidah, and V. G. Agelidis, "Voltage Balancing Control of Three-Level Active NPC Converter Using SHE-PWM," *IEEE Transactions on Power Delivery*, vol. 26, no. 1, pp. 258–267, jan 2011.

[55] F. Umbría, S. Vazquez, F. Gordillo, and F. Gómez-Estern, "Observer-based Direct Power Control for three-level NPC rectifiers," *undefined*, 2009.

[56] F. Grimm, Z. Zhang, M. Abdelrahem, and R. Kennel, "Computationally efficient predictive control of three-level NPC converters with DC-link voltage balancing: A priori state selection approach," in *2017 IEEE International Symposium on Predictive Control of Electrical Drives and Power Electronics (PRECEDE)*. IEEE, sep 2017, pp. 72–77. [Online]. Available: http://ieeexplore.ieee.org/document/8071271/

[57] N. Celanovic and D. Boroyevich, "A Fast Space-Vector Modulation Algorithm for Multilevel Three-Phase Converters," *IEEE Transactions on Industry Applications*, vol. 37, no. 2, pp. 637–641, 2001.

[58] W. Yao, H. Hu, and Z. Lu, "Comparisons of Space-Vector Modulation and Carrier-Based Modulation of Multilevel Inverter," *IEEE Transactions on Power Electronics*, vol. 23, no. 1, pp. 45–51, 2008.

[59] Sanmin Wei, Bin Wu, Fahai Li, and Congwei Liu, "A general space vector PWM control algorithm for multilevel inverters," in *Eighteenth Annual IEEE Applied*

Power Electronics Conference and Exposition, 2003. APEC '03., vol. 1. IEEE, 2003, pp. 562–568. [Online]. Available: http://ieeexplore.ieee.org/document/1179268/

[60] F. Umbría, F. Gordillo, and F. Salas, "Modeling and Full Decoupling Control of a Grid-Connected Five-Level Diode-Clamped Converter," *Electric Power Components and Systems*, 2016.

[61] R. Teodorescu, F. Blaabjerg, M. Liserre, and P. Loh, "Proportional-resonant controllers and filters for grid-connected voltage-source converters," *IEE Proceedings - Electric Power Applications*, vol. 153, no. 5, p. 750, 2006.

[62] J. Rodriguez, S. Bernet, P. K. Steimer, and I. E. Lizama, "A Survey on Neutral-Point-Clamped Inverters," *IEEE Transactions on Industrial Electronics*, vol. 57, no. 7, pp. 2219–2230, jul 2010.

[63] S. Vazquez, J. a. Sanchez, J. M. Carrasco, J. I. Leon, and E. Galvan, "A Model-Based Direct Power Control for Three-Phase Power Converters," *IEEE Transactions on Industrial Electronics*, vol. 55, no. 4, pp. 1647–1657, apr 2008.

[64] M. Malinowski, M. Jasin, and M. P. Kazmierkowski, "Simple Direct Power Control of Three-Phase PWM Rectifier Using Space-Vector," *IEEE Transactions on Industrial Electronics*, vol. 51, no. 2, pp. 447–454, apr 2004.

[65] P. Antoniewicz and M. Kazmierkowski, "Virtual-Flux-Based Predictive Direct Power Control of AC/DC Converters With Online Inductance Estimation," *IEEE Transactions on Industrial Electronics*, vol. 55, no. 12, pp. 4381–4390, dec 2008.

[66] J. Steinke, "Switching frequency optimal PWM control of a three-level inverter," *IEEE Transactions on Power Electronics*, vol. 7, no. 3, pp. 487–496, jul 1992.

[67] A. Videt, P. Le Moigne, N. Idir, P. Baudesson, and X. Cimetière, "A new carrier-based PWM providing common-mode-current reduction and DC-bus balancing for three-level inverters," *IEEE Transactions on Industrial Electronics*, 2007.

[68] C. B. Jacobina, A. M. N. Lima, E. R. C. Da Silva, R. N. C. Alves, and P. F. Seixas, "Digital scalar pulse-width modulation: A simple approach to introduce non-sinusoidal modulating waveforms," *IEEE Transactions on Power Electronics*, 2001.

[69] I. Lopez, S. Ceballos, J. Pou, J. Zaragoza, J. Andreu, I. Kortabarria, and V. G. Agelidis, "Modulation Strategy for Multiphase Neutral-Point-Clamped Converters," *IEEE Transactions on Power Electronics*, 2016.

[70] R. Maheshwari, S. Munk-Nielsen, and S. Busquets-Monge, "Neutral-Point Current Modeling and Control for Neutral-Point Clamped Three-Level Converter Drive with Small DC-link Capacitors," in *2011 IEEE Energy Conversion Congress and Exposition*. IEEE, 2011, pp. 2087–2094.

[71] G. Escobar, A. Stankovic, J. Carrasco, E. Galvan, and R. Ortega, "Analysis and design of direct power control (DPC) for a three phase synchronous rectifier via output regulation subspaces," *IEEE Transactions on Power Electronics*, vol. 18, no. 3, pp. 823–830, 2003.

[72] R. Goebel, R. G. Sanfelice, and A. R. Teel, "Hybrid dynamical systems," *IEEE Control Systems*, vol. 29, no. 2, pp. 28–93, 2009. [Online]. Available: https://ieeexplore.ieee.org/document/4806347/

[73] C. Albea, G. Garcia, and L. Zaccarian, "Hybrid dynamic modeling and control of switched affine systems : application to DC-DC converters," in *54th IEEE Conference on Decision and Control*, 2015, pp. 2264–2269.

[74] D. Liberzon and A. S. Morse, "Basic Problems in Stability and Design of Switched Systems," *IEEE Control Systems*, vol. 19, no. 5, pp. 59–70, 1999.

[75] R. A. Decarlo, M. S. Branicky, S. Pettersson, and B. Lennartson, "Perspectives and results on the stability and stabilizability of hybrid systems," *Proceedings of the IEEE*, vol. 88, no. 7, pp. 1069–1082, 2000.

[76] D. Liberzon, *Switching in systems and control*. Birkhauser, 2003.

[77] G. S. Deaecto, J. C. Geromel, F. S. Garcia, and J. A. Pomilio, "Switched affine systems control design with application to DC-DC converters," pp. 1201–1210, 2010.

[78] L. Hetel and E. Bernuau, "Local Stabilization of Switched Affine Systems," *IEEE Transactions on Automatic Control*, vol. 60, no. 4, pp. 1158–1163, 2015.

[79] P. Hauroigne, P. Riedinger, and C. Iung, "Switched affine systems using sampled-data controllers: Robust and guaranteed stabilization," *IEEE Transactions on Automatic Control*, vol. 56, no. 12, pp. 2929–2935, 2011.

[80] C. Albea Sanchez, G. Garcia, H. Sabrina, W. Heemels, and L. Zaccarian, "Practical stabilisation of switched affine systems with dwell-time guarantees," *IEEE Transactions on Automatic Control*, pp. 1–1, 2019.

[81] P. Bolzern and P. Colaneri, "Switched periodic systems in discrete time: Stability and input-output norms," *International Journal of Control*, vol. 86, no. 7, pp. 1258–1268, 2013.

[82] L. Hetel and E. Fridman, "Robust sampled-data control of switched affine systems," *IEEE Transactions on Automatic Control*, vol. 58, no. 11, pp. 2922–2928, 2013.

[83] B. L. Eidson, J. Y. Hung, and R. M. Nelms, "An experimental evaluation of the PID controller represented by the delta operator," in *Conference Proceedings - IEEE SOUTHEASTCON*, 2012.

[84] K. Viji, A. Kumar, and R. Nagaraj, "Improved Delta Operator based Discrete Sliding Mode Fuzzy Controller for Buck Converter," *Indian Journal of Science and Technology*, vol. 10, no. 25, pp. 1–11, 2017.

[85] G. S. Deaecto, M. Souza, and J. C. Geromel, "Discrete-time switched linear systems state feedback design with application to networked control," *IEEE Trans. on Automatic Control*, vol. 60, no. 3, pp. 877–881, 2015.

[86] G. S. Deaecto and J. C. Geromel, "Stability Analysis and Control Design of Discrete-Time Switched Affine Systems," *IEEE Transactions on Automatic Control*, 2017.

[87] R. Middleton and G. Goodwin, "Improved finite word length characteristics in digital control using delta operators," *IEEE Transactions on Automatic Control*, vol. 31, no. 11, pp. 1015–1021, nov 1986. [Online]. Available: http://ieeexplore.ieee.org/document/1104162/

[88] C. Edwards and S. K. Spurgeon, *Sliding mode control : theory and applications*.

[89] S. Pettersson and B. Lennartson, "Stabilization of hybrid systems using a min-projection strategy," in *Proceedings of the 2001 American Control Conference*, 2001, pp. 223–228 vol.1. [Online]. Available: http://ieeexplore.ieee.org/document/945546/

[90] M. C. Grant and S. P. Boyd, "Graph Implementations for Nonsmooth Convex Programs," in *Recent Advances in Learning and Control*. London: Springer London, 2008, pp. 95–110. [Online]. Available: http://link.springer.com/10.1007/978-1-84800-155-8{_}7

[91] M. Grant and S. Boyd, "CVX: Matlab software for disciplined convex programming, version 2.1," 2014.

[92] P. Montero-Robina, F. Umbria, F. Salas, and F. Gordillo, "Integrated Control of

Five-Level Diode-Clamped Rectifiers," *IEEE Transactions on Industrial Electronics*, vol. 66, no. 9, pp. 6628–6636, 2019.

[93] F. Umbría, F. Gordillo, and F. Salas, "A controller for practical stability of capacitor voltages in a five-level diode-clamped converter," *European Journal of Control*, vol. 28, pp. 56–68, mar 2016.